

CRANFIELD UNIVERSITY

Boris Dorian TANE KEGNE

**Flight Dynamics Modelling and
System Identification of a Light
Fixed Wing UAV**

SCHOOL OF AEROSPACE, TRANSPORT
AND MANUFACTURING
MSc Aerospace Dynamics

Master of Science
Academic Year: 2014 - 2015

Supervisors: Dr. Mudassir Lone and Dr. Alastair Cooke
August 2015

CRANFIELD UNIVERSITY

**SCHOOL OF AEROSPACE, TRANSPORT
AND MANUFACTURING**

MSc Aerospace Dynamics

Master of Science
Academic Year: 2014 - 2015

Boris Dorian TANE KEGNE

**Flight Dynamics Modelling and System
Identification of a Light Fixed Wing UAV**

Supervisors: Dr. Mudassir Lone and Dr. Alastair Cooke

August 2015

This thesis is submitted in partial fulfilment of the requirements for
the degree of MSc Aerospace Dynamics

© Cranfield University, 2015. All rights reserved. No part of this
publication may be reproduced without the written permission of the
copyright owner.

Abstract

Low cost instrumentation, flight dynamics modelling, flight testing, and system identification of a fixed wing Unmanned Aerial Vehicle (UAV) is accomplished in this thesis. This is achieved by providing a framework for both developing simulation models and implementing system identification for current and future work in flight dynamics studies.

The modelling consists of building an aerodynamic model of the aircraft based on Vortex Lattice Method (VLM) results. The model has been implemented in MATLAB/Simulink and completed with various other blocks including the equations of motion and the atmosphere blocks in order to build a full 6 Degrees of Freedom (6DoF) model of the aircraft. This model has been linearised and decoupled. The effects of the centre of gravity position and the airspeed on the dynamic modes of the linearised model have been investigated.

The system identification consists of firstly instrumenting the aircraft, followed by developing a flight test routine. Next, a state space representation of the aircraft has been introduced and a parameter estimation procedure based on the Maximum Likelihood Estimation (MLE) technique developed. After the completion of the flight tests, the aircraft state space parameters have been estimated and an identified model built for its dynamic modes. The effects of the centre of gravity position and the airspeed on the dynamic modes of both the identified model and the full 6DoF model have been investigated and compared with flight test results.

The two models have been validated making use of independent data sets with regards to their dynamic modes. The validation focuses on not only the modal characteristics of the modes (frequency, damping ratio and time ratio) but on the probability distribution of their innovations too.

Acknowledgements

First and foremost, I would like to thank my supervisors, Dr. Mudassir Lone and Dr. Alastair Cooke not only for offering me the opportunity to work on such an interesting and stimulating project, but also for their support, guidance and patience throughout the project.

I would also like to express my gratitude to my classmate and friend Adnan Asif with who I worked on this project. Ioannis Katsoulis, has played a critical role as our flight test pilot and further helped us with the aircraft instrumentation.

Last but not least, I will never be able to express my gratitude sufficiently to my parents for supporting me throughout my studies, and without whom I would not have gone so far.

Contents

Abstract	iii
Acknowledgements	v
List of Figures	xiii
List of Tables	xv
Nomenclature	xvii
1 Introduction	1
1.1 Introduction and Motivation	1
1.2 Aim and Objectives	2
1.2.1 General Aim	2
1.2.2 Objectives	3
1.2.3 Instrumentation Objectives	3
1.2.4 Modelling Objectives	3
1.2.5 System Identification Objectives	4
1.2.6 Validation Objectives	4
2 Literature Review	5
2.1 Instrumentation Assembly and Programming	5
2.1.1 Electronic Board	6
2.1.1.1 Intel® Edison	6
2.1.1.2 3DR® Pixhawk	7
2.1.2 Inertial Measurement Unit (IMU)	8
2.1.3 Air-Ground Data Link Module	10
2.1.3.1 MaxStream® XBee-PRO TM	10
2.1.3.2 3DR Radio Set	10
2.1.4 Airspeed Sensor	11
2.1.5 Data Logging Device	12
2.2 Dynamic Wind Tunnel Testing	12
2.2.1 Testing Techniques	14
2.3 Modelling and Validation Techniques	15

2.3.1	Modelling Techniques	15
2.3.2	Validation Techniques	15
2.4	Aerodynamic Modelling	16
2.4.1	The Vortex Lattice Method (VLM)	16
2.4.1.1	Theory	16
2.4.1.2	Limitations	17
2.4.1.3	Methodology	17
2.4.2	Available Computational Tools	19
2.4.2.1	AVL (Athena Vortex Lattice)	19
2.4.2.2	Tornado	20
2.4.2.3	XFLR5	20
2.5	Mass Properties Estimation	21
2.5.1	Experimental Techniques for Mass Properties Estimation of UAVs	21
2.5.1.1	Pendulum Method	21
2.5.1.2	Mass Properties Statistical Estimation	24
2.5.2	Mass Properties Estimation with XFLR5	26
2.6	System Identification	26
2.6.1	System Identification for Aircraft Applications	27
2.6.2	Parameter Estimation Techniques	31
2.6.2.1	Ordinary Least Square Method	32
2.6.2.2	Maximum Likelihood Method	33
2.6.3	Maximum Likelihood Estimation for Aircraft Application	34
2.7	Kalman Filtering for Aircraft Applications	35
2.7.1	Extended Kalman Filter	36
2.7.2	Background Theory	36
2.8	Relevance of the Literature Review in Respect to the Work Presented in the Thesis	36
2.8.1	Previous Research at Cranfield University	36
2.8.2	Choices and Limitations	37
3	Aircraft & Instrumentation Description	39
3.1	General Specifications	39
3.2	Airframe Geometry	40
3.2.1	Lifting Surfaces Geometry	41
3.2.2	Fuselage	42
3.2.3	Control Surfaces	42
3.3	Instrumentation	42
3.3.1	3DR Pixhawk autopilot	43
3.3.2	RC Receiver	45
3.3.3	Airspeed Sensor	47
3.3.4	Telemetry Module	47
3.3.5	Data Logging	47
3.3.6	Ground Station Software	48

3.4	Mass Properties	48
3.4.1	Airframe Mass Properties	48
3.4.2	Instrumentation Mass Properties	49
4	6 Degrees of Freedom Model Development & Description	51
4.1	Equations of Motion Sub-Model	51
4.1.1	Axes and Orientation	51
4.1.1.1	Earth Axes System	51
4.1.1.2	Body Axes System	52
4.1.1.3	Euler Angles	52
4.1.1.4	Stability Axes and Wind Axes	53
4.1.2	6 DoF Equations of Motion of a Rigid Aircraft	54
4.1.2.1	Translational and Rotational Dynamics	54
4.1.2.2	Rotational Kinematics	56
4.1.2.3	Navigation Equations	56
4.1.2.4	Gravitational Equations	56
4.2	6 DoF Model Development	57
4.2.1	Methodology	57
4.2.1.1	Aerodynamic Forces and Moments	57
4.2.1.2	Air Data	60
4.2.1.3	Atmosphere	61
4.2.1.4	Gravitational Forces and Moments	61
4.2.1.5	Mass Properties	61
4.2.2	Model Assumptions and Simplifications	62
4.2.2.1	Aerodynamic Block Assumptions and Simplifications	62
4.2.2.2	Other Assumptions and Simplifications	62
4.2.3	Model Testing	63
4.3	Model Trimming	64
4.4	Model Linearisation	67
4.4.1	Linearisation and Decoupling Methodology	68
4.4.2	Linear Model Modal Analysis	70
4.4.2.1	Short Period Pitching Oscillations (SPPO)	70
4.4.2.2	Phugoid	72
4.4.2.3	Dutch Roll	72
4.4.2.4	Roll Mode	73
5	System Identification Methodology	75
5.1	Model Postulation and Structure Determination	75
5.1.1	Longitudinal Dynamics	77
5.1.1.1	Short Period Pitching Oscillations (SPPO)	78
5.1.2	Lateral/Directional Dynamics	79
5.1.2.1	Dutch Roll	80
5.1.2.2	Roll Mode	81
5.2	Experiment Design	82

5.2.1	Experimental Set-up	82
5.2.2	Test Procedure	83
5.2.2.1	Pre-Flight Check	83
5.2.2.2	Flight/Wind Tunnel Test	84
5.2.3	Flight Test	85
5.2.3.1	Longitudinal Dynamic Stability	85
5.2.3.2	Lateral/Directional Dynamic Stability	86
5.2.3.3	Timescale	87
5.2.4	Dynamic Wind Tunnel Test	87
5.2.4.1	Longitudinal Dynamic Stability	87
5.2.4.2	Lateral/Directional Dynamic Stability	88
5.2.4.3	Timescale	88
5.2.5	Input Design	89
5.2.5.1	Longitudinal Dynamics	89
5.2.5.2	Lateral/Directional Dynamics	90
5.3	Data Analysis Methodology	91
5.3.1	Butterworth Filter Principle	91
5.3.2	Butterworth Filter Implementation	92
5.4	Maximum Likelihood Estimation Methodology	92
5.4.1	Aircraft Model	92
5.4.2	Maximum Likelihood Cost Function	94
5.4.3	Optimisation Algorithm: Output Error Approach	97
5.4.4	Quality of the Estimates	100
5.4.5	Summary	102
5.5	Model Validation	103
5.5.1	Modal Characteristics Validation	104
5.5.2	Statistical Validation	104
6	Flight Test and Parameters Estimation	105
6.1	Flight Test	105
6.2	Parameters Estimation	108
6.2.1	Short Period Pitching Oscillations (SPPO)	109
6.2.2	Full Longitudinal Model (3-2-1-1 δ_e)	113
6.2.3	Dutch Roll	117
6.2.4	Roll Mode	120
6.2.5	Full Lateral Model (3-2-1-1 δ_a)	123
7	Models Validation	125
7.1	Short Period Pitching Oscillations (SPPO)	125
7.2	Dutch Roll	127
7.3	Roll Mode	130
7.4	Phugoid	132
8	Conclusion & Suggestions	137
8.1	Aim and Objectives Achievement	137

8.1.1	Aim Achievement	137
8.1.2	Instrumentation Objectives Achievement	137
8.1.3	Modelling Objectives Achievement	138
8.1.4	System Identification Objectives Achievement	138
8.1.5	Validation Objectives Achievement	139
8.2	Personal Research Outcomes	139
8.3	Main Difficulties	140
8.4	Improvements and Suggestions for Future Work	141
8.4.1	Instrumentation Improvements	141
8.4.2	Modelling Improvements	141
8.4.3	System Identification Improvements	141
8.4.4	Validation Improvements	142
A	6DoF Model SIMULINK Blocks	143
A.1	Overall Equations of Motion Subsystem	144
A.2	Overall 6 DoF Simulation Model	145
B	Graphical User Interfaces	147
C	System Identification Results	151
	Bibliography	159

List of Figures

2.1	Intel Edison with Ardruiino Expansion Board[1]	6
2.2	3DR Pixhawk[2]	7
2.3	XBee Pro Connection[3]	10
2.4	3DR Radio Set[2]	11
2.5	Model of a Boeing 777 Mounted to a Sting Support System	12
2.6	Dynamic free-flight model tests of the X-29 advanced technology demonstrator	13
2.7	UAV and Sting Mount[4]	14
2.8	Wind Tunnel Test Setup[4]	15
2.9	Vortex Lattice Method.	18
2.10	Various Compound Pendulum Configurations - [5]	23
2.11	At left: small rotorcraft UAV with steel rods and IMU, suspended at a pivot point. At right: detail of the pivot.[6]	25
2.12	System Identification for Aircraft Applications Process.	29
2.13	Maximum Likelihood Estimation for Aircraft Applications	35
3.1	Multiplex EasyStar II	40
3.2	Tail and Fin aerofoil section.	41
3.3	Wing Aerofoil Section.	41
3.4	Instrumentation bloc diagram.	44
3.5	Control Deflections and Throttle PWM signals map.	46
4.1	Earth Axes System[7].	52
4.2	Body Axes System[7].	52
4.3	Euler Angles[7].	53
4.4	Stability and Wind Axes Systems[8]	54
4.5	Equations of Motion Sub-System.	55
4.6	6 DoF Model Data Flow Chart[9].	58
4.7	Aerodynamic and Engines Loads Subsystem[9].	58
4.8	Air Data Subsystem[9].	60
4.9	Atmosphere Subsystem[9].	61
4.10	Gravitational Forces and Moments Subsystem[9].	61
4.11	Test Model Flight Trajectory.	64
4.12	Earth Axes Reference Test Position.	64
4.13	Earth Axes Reference Trimmed Position.	66
4.14	Trimmed Model Body Axes Reference Velocities.	67

4.15 Trimmed Model Euler Angles	67
5.1 SPPO Illustration[7].	78
5.2 Dutch Roll Illustration.	81
5.3 Roll Mode illustration.	81
5.4 Flight/Wind Tunnel Test Process.	85
5.5 Dynamic Stability Analysis Inputs Representation.	90
5.6 Lateral/Directional Dynamic Stability Analysis Inputs Representation.	91
5.7 Output Error Optimisation Algorithm	99
6.1 Damaged Aircraft after Crash on 09 th July 2015.	106
6.2 SPPO Flight Test data and Identified Model q-response.	111
6.3 Effect of CG position on SPPO Characteristics - All models.	112
6.4 Full Longitudinal Flight Test data and Identified Model Response. .	116
6.5 Dutch Roll Flight Test data and Identified Model r-response. . . .	119
6.6 Effect of Airspeed on Dutch Roll Characteristics - All models. . .	120
6.7 Roll mode Flight Test data and Identified Model p-response. . . .	122
7.1 SPPO Validation q-Response.	126
7.2 SPPO q-Innovations Histograms.	127
7.3 Dutch Roll Validation r-Response.	128
7.4 Dutch Roll r-Innovations Histograms.	129
7.5 Roll Mode Validation p-Response.	130
7.6 Roll Mode r-Innovations Histograms.	132
7.7 Phugoid Validation q-Response.	133
7.8 Phugoid q-Innovations Histograms.	134
A.1 Equations of Motion Subsystem.	144
A.2 Overall 6 DoF Simulation Model.	145
B.1 Data Analysis Graphic User Interface.	148
B.2 MLE Parameter Estimation Graphic User Interface.	149
C.1 SPPO - CG = cg_2 ; EAS = 5m/s	151
C.2 SPPO - CG = cg_0 ; EAS = 4m/s	152
C.3 SPPO - CG = cg_1 ; EAS = 4m/s	152
C.4 SPPO - CG = cg_1 ; EAS = 4m/s	153
C.5 Full Longitudinal - CG = cg_1 ; EAS = 4m/s	153
C.6 Full Longitudinal - CG = cg_0 ; EAS = 5m/s	154
C.7 Full Longitudinal - CG = cg_0 ; EAS = 6m/s	154
C.8 Dutch Roll - CG = cg_3 ; EAS = 14m/s	155
C.9 Dutch Roll - CG = cg_0 ; EAS = 5m/s	155
C.10 Dutch Roll - CG = cg_0 ; EAS = 4m/s	156
C.11 Roll Mode - CG = cg_0 ; EAS = 4m/s	156
C.12 Roll Mode - CG = cg_3 ; EAS = 18m/s	157

List of Tables

2.1	Inertial Measurement Units Comparison.[10][11]	9
3.1	Aircraft BAC Position relative to Nose Tip.	40
3.2	Lifting Surfaces Geometrical Characteristics.	42
3.3	Control Surfaces Geometrical Characteristics.	42
3.4	Data Logging Frequencies.	48
3.5	Airframe Mass Properties Relative to BAC.	49
3.6	Instrumentation Mass and Position Relative to BAC.	49
3.7	Aircraft Mass Properties Relative to BAC.	50
4.1	Aerodynamic Coefficients Definition.	58
4.2	Model Testing Initial Flight Conditions.	63
4.3	MATLAB trim Function Trimming Results.	66
4.4	MATLAB trim Function States Results.	66
4.5	SPPO Airspeed Effects of the Linearised Model	71
4.6	SPPO CG Position Effects of the Linearised Model	71
4.7	Phugoid Airspeed Effects of the Linearised Model.	72
4.8	Dutch Roll Airspeed Effects of the Linearised Model.	73
4.9	Roll Mode Airspeed Effects of the Linearised Model.	74
5.1	Longitudinal Parameters.	79
5.2	Lateral/Directional Parameters.	82
5.3	Longitudinal Dynamic Stability Analysis Flight Test Matrix.	86
5.4	Lateral/Directional Dynamic Stability Analysis Flight Test Matrix.	86
5.5	Dynamic Stability Analysis Flight Test Time-scale.	87
5.6	Longitudinal Dynamic Stability Analysis Test Matrix.	88
5.7	Lateral/Directional Dynamic Stability Analysis Test Matrix.	88
5.8	Dynamic Stability Analysis Testing Time-scale.	88
6.1	Tested Centre of Gravity Positions.	107
6.2	Flight Test Conditions.	107
6.3	Flight Tests.	108
6.4	Valid Flight Tests.	109
6.5	SPPO Parameter Estimates.	110
6.6	Effect of CG position on SPPO Characteristics - All models.	112
6.7	Full Longitudinal Parameter Estimates.	115
6.8	Effect of CG position on Phugoid Characteristics - All models.	115

6.9	Dutch Roll Parameter Estimates.	118
6.10	Effect of Airspeed on Dutch Roll Characteristics - All models.	118
6.11	Roll mode Parameter Estimates.	121
6.12	Effect of Airspeed on Roll mode Characteristics - All models.	121
7.1	SPPO q-Innovations Statistical Characteristics.	126
7.2	Dutch Roll Validation Modal Characteristics.	128
7.3	Dutch Roll r-Innovations Statistical Characteristics.	129
7.4	Roll Mode Validation Modal Characteristics.	131
7.5	Roll Model p-Innovations Statistical Characteristics.	131
7.6	Phugoid Validation Modal Characteristics.	133
7.7	Phugoid q-Innovations Statistical Characteristics.	134
C.1	Centre of Gravity Positions.	151

Nomenclature

List of Abbreviations

	Signification	SI Unit
AR	Aspect Ratio	
AVL	Athena Vortex Lattice	
BAC	Body Axes Centre	
CAD	Computer Aided Design	
CFD	Computer Fluid Dynamics	
CG	Centre of Gravity	
DCM	Direction Cosine Matrix	
DoF	Degree of Freedom	
EAS	Equivalent Airspeed	$[m.s^{-1}]$
ESC	Electronic Speed Controllers	
GPS	Global Positioning System	
IMU	Inertial Measurement Unit	
ISA	International Standard Atmosphere	
MAC	Mean Aerodynamic Chord	$[m]$
MEMS	Micro Electro-Mechanical Systems	
MLE	Maximum Likelihood Estimation	
PWM	Pulse Width Modulation	
SPPO	Short Period Pitching Oscillations	
TAS	True Airspeed	$[m.s^{-1}]$
UAV	Unmanned Aerial Vehicle	
VLM	Vortex Lattice Method	

List of Symbols

Global Constants

	Signification	SI Unit	Value
g	Gravity Constant	[$m.s^{-2}$]	9.81

Roman Letters

	Signification	SI Unit
a_x	Longitudinal BAC Acceleration	[$m.s^{-2}$]
a_y	Lateral BAC Acceleration	[$m.s^{-2}$]
a_z	Vertical BAC Acceleration	[$m.s^{-2}$]
A	System Matrix	
b	Wing Span	[m]
B	Input Matrix	
B_w	Process Noise Matrix	
\mathcal{B}	Covariance Matrix of the Innovation	
\bar{c}	Mean Aerodynamic Chord	[m]
C	Output Matrix	
C_D	Drag Coefficient	
C_L	Lift Coefficient	
C_l	Rolling Moment Coefficient	
C_m	Pitching Moment Coefficient	
C_n	Yawing Moment Coefficient	
C_Y	Side Force Coefficient	
d_x	Longitudinal Position of the CG in Body Axes, from BAC	[m]
d_y	Lateral Position of the CG in Body Axes, from BAC	[m]
d_z	Vertical Position of the CG in Body Axes, from BAC	[m]
D	Feedthrough Matrix	
\mathcal{D}	Drag Force in Body Axes Reference	[N]
e	Oswald Efficiency Coefficient	
h	Down Position in Earth Axes Reference	[m]
H_p	Pressure Altitude	[m]
I_{xx}	Inertia around the Body Axes Horizontal Axis	[$kg.m^2$]
I_{yy}	Inertia around the Body Axes Lateral Axis	[$kg.m^2$]

I_{zz}	Inertia around the Body Axes Vertical Axis	$[kg.m^2]$
I_{xz}	Product of Inertia from the xz-plane in Body Axes	$[kg.m^2]$
J	Maximum Likelihood Cost Function	
$l_{\ }$	Rolling Moment Concise Derivative due to <i>subscript</i>	
L	Lift Force in Body Axes Reference	$[N]$
\mathcal{L}	Rolling Moment in Body Axes Reference, at BAC	$[N.m]$
\mathbb{L}	Likelihood Function	
m	Mass	$[kg]$
$m_{\ }$	Pitching Moment Concise Derivative due to <i>subscript</i>	
M	Pitching Moment in Body Axes Reference, at BAC	$[N.m]$
$M_{\theta=\theta_0}$	Fisher Information Matrix	
$n_{\ }$	Yawing Moment Concise Derivative due to <i>subscript</i>	
N	Yawing Moment in Body Axes Reference, at BAC	$[N.m]$
P, p	Roll Angular Rate in Body Axes Reference	$[rad.s^{-1}]$
P_E	East Position in Earth Axes Reference	$[m]$
P_N	North Position in Earth Axes Reference	$[m]$
\mathcal{P}	State Vector Covariance	
\bar{q}	Dynamic Pressure	$[Pa]$
Q, q	Pitch Angular Rate in Body Axes Reference	$[rad.s^{-1}]$
\mathcal{Q}	Process Noise Covariance Matrix	
R, r	Yaw Angular Rate in Body Axes Reference	$[rad.s^{-1}]$
\mathcal{R}	Measurement Noise Covariance Matrix	
S	Output Sensitivity Matrix	
S_w	Wing Reference Area	$[m^2]$
t	Time	$[s]$
T_r	Time constant	$[s]$
u	Longitudinal BAC velocity disturbance	$[m.s^{-1}]$
\mathbf{u}	Input Vector	
U	Longitudinal BAC velocity	$[m.s^{-1}]$
v	Lateral BAC velocity disturbance	$[m.s^{-1}]$
v_e	Disturbance in Equivalent Airspeed	$[m.s^{-1}]$
V	Lateral BAC velocity	$[m.s^{-1}]$
V_0	Initial True Airspeed	$[m.s^{-1}]$
V_D	Down Velocity in Earth Axes Reference	$[m.s^{-1}]$
V_e	Initial Equivalent Airspeed	$[m.s^{-1}]$
V_E	East Velocity in Earth Axes Reference	$[m.s^{-1}]$

V_N	North Velocity in Earth Axes Reference	$[m.s^{-1}]$
w	Vertical BAC velocity disturbance	$[m.s^{-1}]$
\mathbf{w}	Process Noise	
W	Vertical BAC velocity	$[m.s^{-1}]$
x_{\parallel}	Longitudinal Force Concise Derivative due to <i>subscript</i>	
\mathbf{x}	State Vector	
X	Longitudinal Force in Body Axes Reference	$[N]$
y_{\parallel}	Side Force Concise Derivative due to <i>subscript</i>	
\mathbf{y}	Output Vector	
Y	Lateral Force in Body Axes Reference	$[N]$
z_{\parallel}	Vertical Force Concise Derivative due to <i>subscript</i>	
\mathbf{z}	Measurement Vector	
Z	Vertical Force in Body Axes Reference	$[N]$
Z_N	Sequence of N measurements	

Greek Letters

	Signification	SI Unit
α	Body Angle of Attack	$[rad]$
β	Sideslip Angle	$[rad]$
γ	Flight Path Angle	$[rad]$
Γ	Discrete Input Matrix	
δ_a	Aileron Angle	$[rad]$
δ_e	Elevator Angle	$[rad]$
δ_{ij}	Dirac Delta	
δ_r	Rudder Angle	$[rad]$
ζ	Damping Ratio	
θ	Euler Pitch Angle	$[rad]$
$\boldsymbol{\theta}$	Parameter Vector	
$\boldsymbol{\nu}$	Measurement Noise	
ρ_a	Air Density	$[kg.m^{-3}]$
τ	Throttle	$[\%]$
\boldsymbol{v}	Innovation Vector	
ϕ	Euler Bank Angle	$[rad]$
ψ	Euler Yaw Angle	$[rad]$

Ψ	Discrete System Matrix
ω	Frequency of Oscillations [rad.s ⁻¹]

List of Subscripts

Signification	
$[\cdot]_0$	Initial Value
$[\cdot]_{aero}$	Aerodynamic
$[\cdot]_b$	Body Axes Reference
$[\cdot]_d$	Dutch Roll
$[\cdot]_E$	Earth Axis System
$[\cdot]_{grav}$	Gravitational
$[\cdot]_k$	Discrete element at time k
$[\cdot]_p$	Phugoid OR Roll Rate
$[\cdot]_q$	Pitch Rate
$[\cdot]_r$	Roll Mode OR Yaw Rate
$[\cdot]_s$	Stability Axes Reference OR Short Period Pitching Oscillations
$[\cdot]_u$	Forward Speed
$[\cdot]_v$	Wind Axes Reference OR Vertical Speed
$[\cdot]_w$	Wind Axes Reference OR Vertical Speed
$[\cdot]_{\delta_a}$	Aileron Angle
$[\cdot]_{\delta_e}$	Elevator Angle
$[\cdot]_{\delta_r}$	Rudder Angle
$[\cdot]_\theta$	Pitch Angle
$[\cdot]_\tau$	Throttle
$[\cdot]_\phi$	Roll angle
$[\cdot]_\psi$	Yaw angle

List of Superscripts

Signification	
$\dot{[\cdot]}$	Time Derivative
$\bar{[\cdot]}$	Mean Value
$\hat{[\cdot]}$	Estimate
$[\cdot]^T$	Matrix Transpose

Chapter 1

Introduction

1.1 Introduction and Motivation

Unmanned Aerial Vehicles (UAVs) represent a viable alternative to manned aircrafts and satellites for a numbers of applications both for the military and the civil applications. This includes environmental monitoring, agriculture, and surveying and strategic aerial presence. UAVs offer not only a greater precision but a much lower operating costs than traditional methods. The recent growth of the UAV industry for civil application is largely due to the ever increasing performance of electronics, from computing boards to Inertial Measurement Units (IMU) and Micro Electro-Mechanical Systems (MEMS). A critical part of any autonomous vehicle however is the autopilot design.

The ability to have a virtual environment to test and validate autopilots and control systems in a safe manner is significant in the development of Unmanned Aerial Vehicles. While providing repeatability in testing schemes, flight dynamics model allow engineers and researchers to improve the dynamic characteristics of aircraft with reduced dependence on expensive field trials. Numerical flight dynamics models are common in the aerospace industry and are used in the development of a great majority of modern aircraft and satellites. However the accuracy of a model is based on a good understanding of the original vehicle inner dynamics. For such a model to be of real use, its development process necessary includes implementation, verification and validation. As the UAV industry aspire to provide more solutions to end users, the requirement for rapid, reliable and safe means to

development flight algorithms is critical. This makes this project highly relevant and appropriate with the current industrial environment.

On the other hand, system identification is the inverse approach to engineering where a mathematical model of a physical system is built against observation of the system's response. The process is widely used in biology or economy and is based on statistical procedures: parameter estimation. For aircraft flight dynamics, the mathematical model is generally in the form of its equations of motions and the parameters are its stability and control derivatives. During the test, the aircraft is flown in manoeuvres designed to excite its dynamics and the recorded data is used to estimate the parameters. Thus in order to perform successful parameter estimation, several steps have to be conducted:

- Instrumentation: The aircraft should be accordingly instrumented in order to be able to record data capturing its dynamics airborne.
- Input Design: The manoeuvre should be designed to be able to excite the dynamics of the aircraft.
- Model Structure Definition: The structure of the mathematical model should be carefully designed, based on the type of vehicle under testing.
- Parameter Estimation: The parameters should be estimated making use of the right statistical method.

This process is usually followed by model validation.

1.2 Aim and Objectives

1.2.1 General Aim

The aim of this research project is to instrument, develop a flight dynamics model, develop a testing scheme and perform System Identification of the Easystar II fixed wing UAV. All the developed models should be validated.

Ultimately, a system identification framework for fixed wing air vehicles will be implemented. This will allow rapid system identification of similar vehicles for current and future research work.

1.2.2 Objectives

The first step in any research work is to carry out a literature review. This investigates the hardware assembly and programming required for the UAV data acquisition system, the testing techniques, the system identification procedure and the modelling and validation techniques of UAVs. It ultimately presents limitations and choices made for the both the 6DoF modelling and the System Identification.

1.2.3 Instrumentation Objectives

These objectives are developed in Chapter 3.

- Hardware Selection: The different components of the hardware making the instrumentation are selected.
- Assembly and Calibration: All components are put together and calibrated if required.
- Data Logging and Analysis: Required data is logged airborne and a ground station tool is developed for data analysis.

1.2.4 Modelling Objectives

These objectives are developed in Chapters 3 and 4.

- Geometrical Properties: The geometry of the aircraft is obtained and modelled.
- Mass Properties: The mass properties of the aircraft are obtained and modelled.
- 6 DoF Model Development: A 6DoF model of the aircraft is developed, trimmed, linearised and decoupled.
- Model Discussion: A discussion on the model characteristics is performed.

1.2.5 System Identification Objectives

These objectives are developed in Chapters 5 and 6.

- Model Structure Definition.
- Experimental Framework Definition: The required experiments and manoeuvres are defined and performed.
- Parameter Estimation: The aircraft control and stability derivatives are estimated and the identified model built.
- Model Discussion: A discussion on the model characteristics is performed.

1.2.6 Validation Objectives

These objectives are developed in Chapter 7.

- Models Validation: Both models are validated.
- Validation Discussion: Both models validations are discussed.

Chapter 2

Literature Review

Due to the wide range of topics encompassed by the work presented in this thesis, the literature covers a significant number of areas divided in a coherent manner. First, the electronics and hardware assembly and programming has been studied. The resources for this part of the work were mostly found on online forums and manufacturers websites. Next a detailed study of dynamic wind tunnel testing methods has been carried out. From testing schemes to data filtering and system identification, various methods have been studied and similarities and differences are presented. The next step was to study the modelling and validation techniques of UAVs. The Vortex Lattice Method (VLM) has been chosen to perform the aerodynamic modelling. Description of available computational tools is studied as well as a comparison of their main features. The mass properties of the airframe estimation methodology is studied and a summary of the various assumptions and limitations taken into account when building the 6 DoF model is presented.

2.1 Instrumentation Assembly and Programming

As the first part of the project is to design and implement a Data Acquisition System for the EasyStar II UAV, a study of the various components of such a device was performed. It consists of:

1. An electronic board;
2. An Inertial Measurement Unit (IMU);

3. An Air-Ground Data Link Module;
4. An Airspeed sensor;
5. A data logging device.

2.1.1 Electronic Board

2.1.1.1 Intel® Edison

An electronic board is needed to perform all calculations related to the telemetry, data logging, and sensors data filtering. Cranfield University purchased an Intel® Edison board illustrated in Figure 2.1. The Intel® Edison is a tiny computer designed by Intel® to provide solution to the fast growing new technology industry demanding high computational power. It features an Intel® Atom™ 22nm SoC with a dual-core CPU at 500Mhz and a MCU at 100Mhz. This allows the product to collect and preprocess data via the MCU in a low power state and hand the filtered data off to the CPU for analytics. The Intel® Edison board includes 1GB of memory, 4GB of storage and dual-band Wi-Fi and Bluetooth* 4.0 for communications. It supports 40 general-purpose input/output pins with multiple configuration options[1].

The Intel® Edison presents interests thanks to its high computational power, its size and weight, its large community and its flexibility in terms of computing technique and operating system. However, its lack of sensors and its programming complexity are downsides.

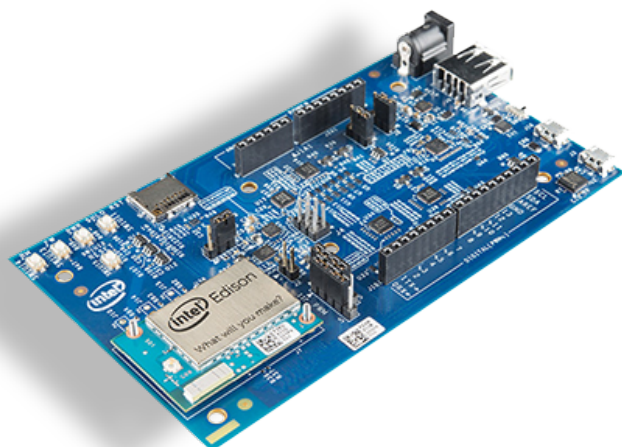


FIGURE 2.1: Intel Edison with Arduini Expansion Board[1]

2.1.1.2 3DR® Pixhawk

The Pixhawk, as illustrated in Figure 2.2 is a flight controller developed by 3DR and working with the Ardupilot firmwares. The system includes various sensors, including but not limited to a GPS, a combo accelerometer, magnetometer and gyroscope, and a barometer. The Pixhawk features integrated multithreading, and a Unix/Linux-like programming environment. These advanced capabilities ensure integration to any autonomous flight vehicle.

The Pixhawk features a 32-bit Cortex M4 core FPU with 168 MHz/256 KB RAM/2 MB Flash and a 32 bit failsafe co-processor. This computational power allows the implementation of an autonomous autopilot, control of servos, data logging on an SD-card or I²C connection to other instrumentation. Additionally, the Pixhawk module is accompanied by various peripheral options, including a digital airspeed sensor, support for an external multi-color LED indicator and an external magnetometer[2].

The 3DR Pixhawk presents as main advantages its readiness for airborne systems and its inherent compatibility with the Ardupilot firmwares.



FIGURE 2.2: 3DR Pixhawk[2]

2.1.2 Inertial Measurement Unit (IMU)

An Inertial Measurement Unit is required to gather flight data such as velocity, orientation, and gravitational forces, using a combination of accelerometers and gyroscopes, sometimes also magnetometers. Some IMUs are capable of using GPS and Pressure Altimeters to take measurements on Altitude and position which are consolidated with conventional data in order to improve the accuracy and precision of the measurements. Several IMUs have been considered for the data acquisition based on the Intel® Edison board, and compared with the IMU included with the 3DR Pixhawk and they are summarised in Table 2.1.

IMU	Gyro Full Scale Range	Gyro Rate Noise	Accel Full Scale Range	Compass Full Scale Range	Digital Output	Supply Voltage	Operating Voltage Supply	Sampling Rate
Intel Edison								
MPU - 9250	±250 ±500 ±1000 ±2000	0.01	±4 ±8 ±16	±2 ±4 ±8 ±16	I ² C or SPI ±4800	1.7V to VDD	2.4V to 3.6V	
MPU - 9150	±250 ±500 ±1000 ±2000	0.005	±4 ±8 ±16	±2 ±4 ±8 ±16	I ² C ±1200	1.8V ±5%	2.4V to 3.6V	
LSM - 9DS0	±245 ±500 ±2000	N/A	±4 ±6 ±8 ±16	±2 ±4 ±6 ±8 ±16	I ² C or SPI ±1200	N/A	N/A	
3DR Pixhawk								
MPU - 6000	±250 ±500 ±1000	0.005	±4 ±8 ±16	±2 ±4 ±8 ±16	I ² C or SPI ±1200	1.7V to VDD	2.4V to 3.5V	50 Hz

TABLE 2.1: Inertial Measurement Units Comparison. [10][11]

2.1.3 Air-Ground Data Link Module

2.1.3.1 MaxStream® XBee-PROTM

An Air-Ground Data Link Module is required as it is necessary to monitor essential flight data from the UAV on ground during the test. This can be performed using a MaxStream® XBee-PROTM OEM RF Module illustrated on Figure 2.3. This is an embedded device providing wireless connectivity between devices. It uses an IEEE 802.15.4 networking protocol for fast point-to-multipoint or peer-to-peer networking. The MaxStream® XBee-PROTM is operational worldwide since it uses a 2.4 GHz frequency for data linkage[3]. In addition, the Air-Ground data link module could be used to send control inputs to the UAV via predetermined signal from the ground station rather than a RF controller.

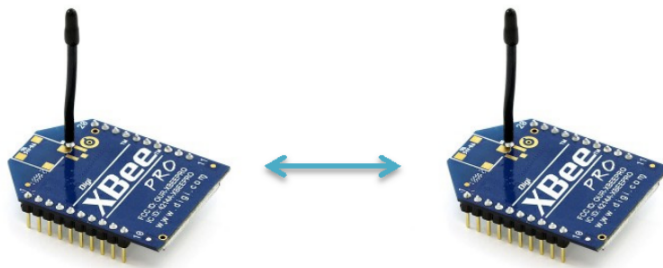


FIGURE 2.3: XBee Pro Connection[3]

2.1.3.2 3DR Radio Set

The 3DR Radio Set as illustrated in Figure 2.4 allows the ground station computer to communicate with the aerial vehicle wirelessly, providing monitoring of flight data and various other in flight settings. It works at a frequency of 433 MHz for Europe and is fully compatible with the 3DR Pixhawk. This module has been selected for this project.



FIGURE 2.4: 3DR Radio Set[2]

2.1.4 Airspeed Sensor

Although the Data Acquisition System is designed for wind tunnel testing purpose, it is required to include an airspeed sensor. In fact, the airspeed is not always constant in the wind tunnel testing section and it is necessary to have accurate measure of airspeed when developing aerospace vehicle models and performing system identification. Several airspeed sensors have been considered for this project application and here is presented a short-list of the selected ones.

1. Pixhawk Airspeed Sensor Kit:[12]

- Measurement Specialties 4525DO sensor, one psi measurement range (roughly up to 100 m/s or 360 km/h or 223 mp/h);
- Resolution of 0.84 Pa;
- Data delivered at 14 bits from a 24 bit delta-sigma ADC;
- M3/6-32 mounting holes

2. N2 Industries Airspeed FrSky Smart Port Sensor:[13]

- Airspeed Range: 7mph to 225mph (11 to 360kph equivalent);
- Pitot Tube: Pitot-Static Tube (Prandtl) type, weighing 3gm with a length of 80mm and diameter 4mm.

2.1.5 Data Logging Device

The data logging will be done airborne using a simple micro-SD card.

2.2 Dynamic Wind Tunnel Testing

The state of the art in aerospace engineering has been continually accelerated by the development of advanced wind tunnel testing techniques. Static wind tunnel models of aerospace vehicles are designed to obtain high-quality, detailed aerodynamic data for analysis of their corresponding full-scale model at specified flight conditions. Static tests as illustrated on Figure 2.5 are typically conducted with the model fixed to an internally mounted, force-measuring device known as an electrical strain-gauge, which is in turn mounted to a sting support system. The orientation of the model and its support system relative to the wind tunnel flow is controlled by the test engineer as required for specified aerodynamic test conditions. This allows to variate angle of incidence and sideslip angle. The static experiment focuses on obtaining aerodynamic data for combinations of airspeed, model attitudes, and configuration variables such as wing-flap or control surface deflections. The instrumentation here aims to measure aerodynamic parameters, which may include forces and moments, static and dynamic pressure acting on the surfaces or even flow visualisation. These static techniques do not require any motion of the model or free flight capability.

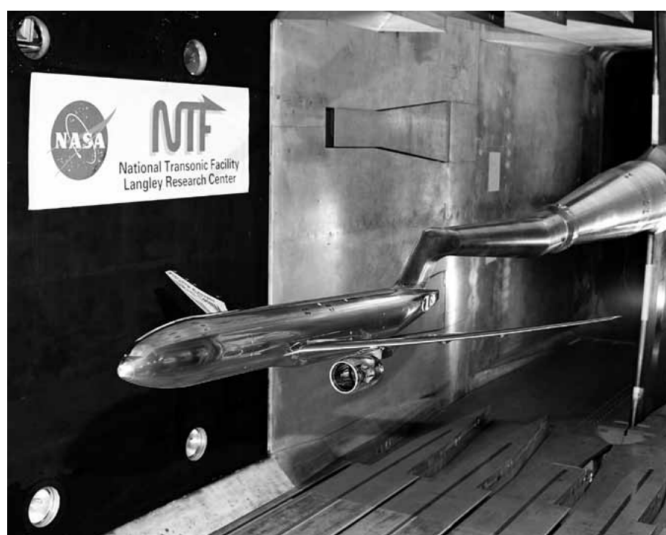


FIGURE 2.5: Model of a Boeing 777 Mounted to a Sting Support System¹

¹nasa.gov

Dynamic free flight model testing as illustrated on Figure 2.6 enhances the objectives of conventional static tests to include the effects of vehicle motions. Dynamic wind tunnel testing for the most part assesses the inherent flight motions of a model and its response to control inputs. The results of free flight model tests can be readily observed by the motions of the model in response to forcing functions by the wind tunnel or control deflections by pilots. Dynamic tests focus on critical characteristics such as stability, controllability, and safety during flight within and outside the conventional flight envelope. The principal interest in system identification of dynamic testing is the ability to set the control inputs to the system during the test, within a controlled environment. However, particular safety issues should be taken into account when designing the scheme. The most critical applications of free flight models include evaluations of unconventional aerodynamic designs for which no experience base exists, and the analysis of aircraft behaviour for flight conditions that are not easily studied with static testing techniques, or are not accurately modelled by computational techniques. Such conditions include high angles of attack flights, stalls, where non linearity have a significant impact on the aerodynamic behaviour of the vehicle.

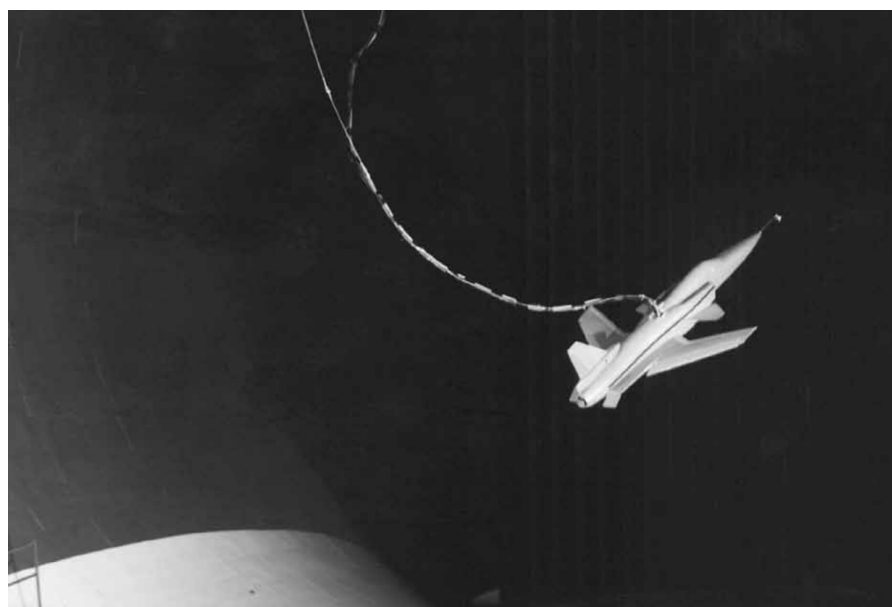


FIGURE 2.6: Dynamic free-flight model tests of the X-29 advanced technology demonstrator²

²nasa.gov

2.2.1 Testing Techniques

In 2009, Wong et Al.[\[4\]](#) performed a pseudo-dynamic wind tunnel testing scheme on a UAV in order to extract its aerodynamic properties. The testing set up consisted of a large open wind tunnel which was used with a relatively large model. One significant source of inaccuracy when using such a configuration is the the wind tunnel airflow speed is not constant throughout the test, and this had to be considered when analysing the results.

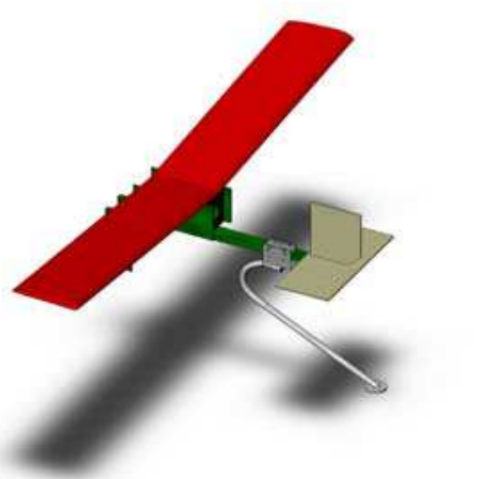


FIGURE 2.7: UAV and Sting Mount[\[4\]](#).

A sting mount set up for mounting the UAV model was designed with a commercial CAD software, as shown in Figure 2.7. The mount was based on an existing sting (used in a previous wind tunnel experiments) which was fastened to a U-shaped clamp with a bolt. The UAV was clamped to the sting and the sting was bolted to a force plate using a series of screws in order to minimise the damage to the force plate. The force place measured the forces and moments that the sting was subjected to during testing using a series of strain gauges. The wind tunnel set up and the UAV under test are shown in Figure 2.8.



FIGURE 2.8: Wind Tunnel Test Setup[4]

2.3 Modelling and Validation Techniques

2.3.1 Modelling Techniques

As presented by X.Q. Chen[14], flight dynamics modelling presents numbers of advantages. It not only reduces the number of costly real flight tests but also allows a high degree of repeatability. In addition, flight dynamics models are suitable when designing flight control laws, autopilots or when performing initial static and dynamic stability analysis, in a safe environment. The development of flight dynamics models is usually highly dependent on the degree of fidelity and details required by the project. Non linearities, fluid-structure interaction or unsteady aerodynamics could be implemented but when considering Unmanned Aerial Vehicles under small input perturbations, a linear model is generally good enough.

2.3.2 Validation Techniques

The validation process of a flight dynamics model consist in carrying out either flight testing or wind tunnel testing at specific flight conditions and controls input and perform a comparative analysis between the experiments data and the simulation one. It therefore requires extensive airborne instrumentation and sensors in order to gather he experimental data. In the case of small fixed wing Unmanned Aerial Vehicles, common Data Acquisition Systems are suitable for most flight parameters except for the angle of attack and sideslip angle. However, when performing wind tunnel testing, these are known before hand. The comparative

analysis could be performed either with parameter estimation techniques such as the least square method or the maximum likelihood estimations as described by J.R. Raol in 2004[15] or using graphical methods.

2.4 Aerodynamic Modelling

One of the crucial aspects of any flight dynamics modelling is the estimation of aerodynamic characteristics of the airframe. A vast amount of theories is available, ranging from simple lifting line to high order Navier- Stokes CFD solvers. Kier[16] presented a comparison of Aerodynamic modelling methodologies with respect to flight loads analysis on flexible aircraft structures. He claimed that classical methods derived from potential theory, such as the Vortex Lattice Method (VLM) are generally employed. This quasi-steady method results in an aerodynamic influence coefficient (AIC) matrix, thus calculation of the aerodynamic forces and moments reduces to a common matrix multiplication.

2.4.1 The Vortex Lattice Method (VLM)

The Vortex Lattice Method (VLM) is a CFD method mainly used in the aircraft early design stages and for educational purposes. It models lifting surfaces as infinitely thin sheets of distinct vortices in order to compute the lift and the induced drag. The influence of thickness, viscosity and compressibility is generally neglected.

The VLM modelling approach is best suited for aerodynamic configurations that primarily consists of thin lifting surfaces at small angles of attack and sideslip. Volumetric bodies are to be modelled with caution and are generally idealized with a cruciform shapes.

2.4.1.1 Theory

The Vortex Lattice Method (VLM) relies on potential flow theory. Ideal flow assumption is made; Viscosity, turbulence, dissipation, boundary layer and unsteady aerodynamics are not solved when carrying out computation. The lifting surfaces

and their trailing wakes are pictured as single-layer vortex sheets, discretised into horseshoe vortex filaments (Fig. 2.9).

When implementing the VLM, one can assess the lift, induced drag and pitching moment coefficients of lifting surfaces. In some restricted cases and with special considerations, stall phenomena can be modelled.

2.4.1.2 Limitations

As any CFD method, the Vortex Lattice Method has limitations in its possibilities. These limitations have to be kept in mind when carrying out any analysis.

- The flow field is assumed to be inviscid, irrotational and incompressible. Yet, taking advantage of the Prandtl-Glauert transformation, subsonic incompressible flow can be modelled.
- No unsteady aerodynamics phenomenon is modelled.
- The influence of thickness is neglected.
- Small angle approximation. Both the angle of attack and the sideslip angle are small.

2.4.1.3 Methodology

According to the potential flow theory the flow field is a conservative flow field, and there exists a velocity potential such as,

$$\mathbf{v} = \nabla\phi \quad (2.1)$$

where

\mathbf{v} is the flow velocity

∇ is the nabla operator

ϕ is the velocity potential

and the Laplace's equation, Eq. 2.2 hold.

$$\nabla^2 \phi = 0 \quad (2.2)$$

The Laplace's equation is a second order differential equation and follows the principle of superposition. Assuming y_1 and y_2 are two distinct solutions of the Laplace's equation, then the linear combination $Y = c_1y_1 + c_2y_2$ is also a solution of the Laplace's equation, where c_1 and c_2 are any real constant numbers. Anderson[17] states "A complicated flow pattern for an irrotational, incompressible flow can be synthesized by adding together a number of elementary flows, which are also irrotational and incompressible.". Such elementary flows can be sources, sinks, doublets and in the particular case of the VLM, vortex lines, all solutions of the Laplace's equation. Those vortex lines are therefore combined to form the vortex sheets modelling the lifting surface.

Practically, the lifting surface is divided into several panels. On each of these panels, a box control point is defined. It is located at a 1/4 chord of the panel and the collocation point is placed at 3/4 chord as illustrated in Figure 2.9. A horseshoe vortex is applied at the box control point and the induced velocity vector is evaluated.

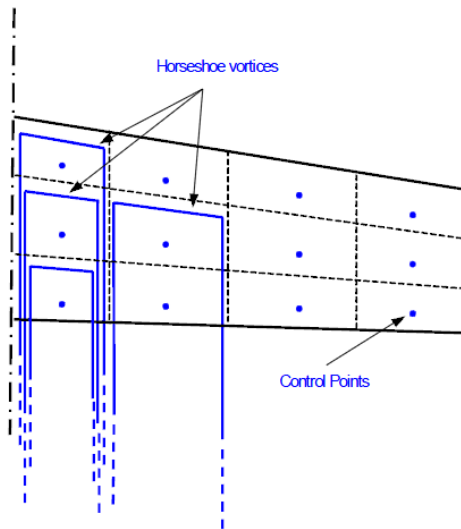


FIGURE 2.9: Vortex Lattice Method.

By applying the Neumann boundary conditions, prescribing that the normal velocity at the boundary is zero, and considering that the flow must be parallel to the lifting surface, the Biot-Savart-Law as in Equation 2.3[16] yields,

$$w_i = A_{ii}\Gamma_i \quad (2.3)$$

where

w_i is the induced velocity at the box control point of panel i .

A_{ii} is the panel i induced downwash matrix.

Γ_i is the circulation of the panel i .

The induced downwash matrix A_{ii} , relates the circulation strength of each horseshoe vortice to the induced velocities at the control points.

Finally, using the Kutta-Joukowski theorem[18], the pressure distribution is computed:

$$p_i = \rho_a U_\infty \Gamma_i l_i \quad (2.4)$$

where

p_i is the aerodynamic pressure acting on the panel i .

ρ_a is the air density.

U_∞ is the free stream velocity.

l_i is the panel i length.

2.4.2 Available Computational Tools

The subsequent software tools based on the VLM are accessible for aerodynamic analysis.

2.4.2.1 AVL (Athena Vortex Lattice)

AVL³ is a program developed by the MIT for the aerodynamic and flight dynamics analysis of rigid aircraft of arbitrary configuration. It employs an extended Vortex

³<http://web.mit.edu/drela/Public/web/avl/>

Lattice Model for the lifting surfaces, together with a slender-body model for fuselages and nacelles. AVL assumes quasi-steady flow fields. Any unsteady vorticity shedding is neglected. It employs the Prandtl-Glauert (PG) transformation for modelling compressible flows, and the forces and moments are computed using the Kutta-Joukowski theorem to each vortex. AVL should be used at small local angles of attack and sideslip to stay within the operating range of the implemented VLM.

2.4.2.2 Tornado

Tornado⁴ is a program developed as a collaboration between KTH, the Royal Institute of Technology Stockholm in Sweden, the University of Bristol in the UK and the University of Linkoping in Sweden. It implements a VLM and assumes linear aerodynamics. Tornado has been developed in MATLAB and can provide the aerodynamic and control derivatives for a wide range of aircraft configurations.

2.4.2.3 XFLR5

XFLR5⁵ is an aerodynamics and flight dynamics analysis tool suitable airfoils, wings and planes operating at low Reynolds Numbers. It includes wing design and analysis capabilities based on the Lifting Line Theory, the Vortex Lattice Method, and a 3D Panel Method. It has been developed by André Deperrois and can be used to design and analyse aerofoils too.

XFLR5 implements three different 3-D numerical methods:

- Non Linear Lifting Line Theory

This method should be used for medium to high aspect ratio wings as it assumes 2-D wing surface. It is best suited for wing with no dihedral and no sweep.

- Vortex Lattice Method

The VLM as presented before is suitable for low aspect ratio lifting surfaces and can deal with dihedral and wing sweep. It takes advantage of the foil design capability of XFLR5 to predict and model viscous drag.

⁴<http://tornado.redhammer.se/>

⁵<http://www.xflr5.com/xflr5.htm>

- 3-D Panels Method

The 3-D panel method is an extension of the two previous methods as it takes into account the thickness of the lifting surface and provides a 3-D pressure distribution around the wing.

XFLR5 also provides stability analysis capabilities. It can estimate aerodynamic and control derivatives of an aircraft for a given trimmed flight condition based on its mass properties. However, this analysis does not take viscous effects into account. Furthermore, fuselage (bluff bodies) modelling is not recommended within XFLR5 just as with AVL.

2.5 Mass Properties Estimation

Determining with accuracy the mass properties of the air vehicle when developing its flight dynamics model is critical as they are part of the gravitational forces and play an important role in the equation of motions definition. A full Computer Aided Design (CAD) model would be ideal to determine the mass properties of the aircraft, however it presents numbers of difficulties and is time consuming. Moreover it is out of the scope of the work presented in this thesis.

Three approaches to mass properties estimation have been studied: two based on experimental procedure and the other based on the XFLR5 software.

2.5.1 Experimental Techniques for Mass Properties Estimation of UAVs

The experimental approach is advantageous as it allows to determine the mass properties of the aircraft in a lab, prior to flight or wind tunnel testing. This simplifies the flight/wind tunnel testing parameter estimation as the later concentrates on the aerodynamic and control derivatives.

2.5.1.1 Pendulum Method

In 2008, Halder, A. et al developed a method to determine the mass properties of high wing unmanned aerial vehicles[19].

The method consists various theoretical concepts:

- **Effective mass**

The relative mass of the UAV is its apparent mass when considering gravity, aerodynamic effects and the buoyancy force acting on it. It is defined as:

$$m_{eff} = m + m_a + \rho V \quad (2.5)$$

where

m is the true mass of the aircraft.

m_a is the equivalent mass of the aircraft resulting from aerodynamic effects.

ρ is the air density.

V is the aircraft volume.

- **Pendulum Equation**

A compound pendulum as when considering only gravitational forces is described by Equation 2.6:

$$I \frac{d^2\theta}{dt^2} + WL\theta = 0 \quad (2.6)$$

where

I is the Inertia of the pendulum about its axis of oscillation.

W is the weight of the pendulum.

L The distance between the centre of gravity of the pendulum and its axis of oscillation.

θ is the attitude of the pendulum.

The period of such a pendulum is thus obtained as:

$$T = 2\pi \sqrt{\frac{I}{WL}} \quad (2.7)$$

The experimental set-up is as illustrated on Figure 2.10.

The estimation of the mass properties is thus performed:

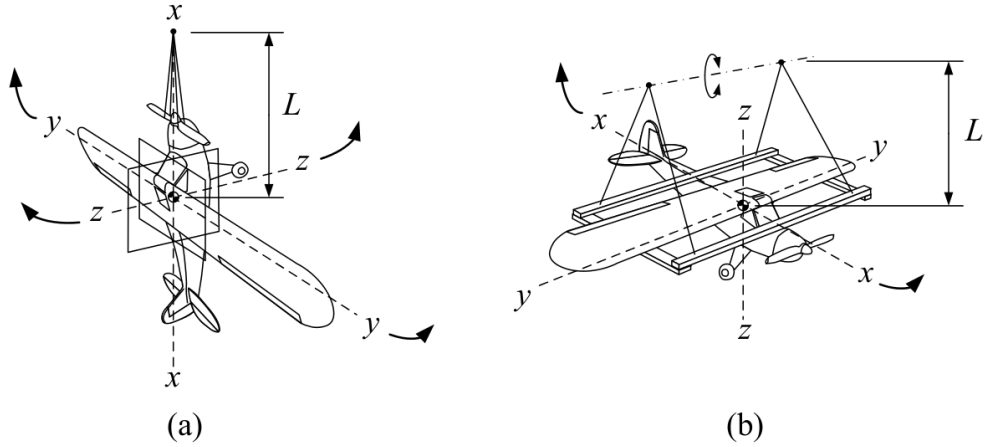


FIGURE 2.10: Various Compound Pendulum Configurations - [5]

- **Centre of Gravity Estimation**

The centre of gravity is estimated by having the aircraft on two weighting pans. The force readings on the pans provide the position of the centre of gravity of the aircraft relative to a pre-defined reference point.

- **Inertias Estimation**

As illustrated in Figure 2.10, the inertias could be obtained by fixing the UAV to a swinging gear. For each inertia, the aircraft is orientated such that its datum line stays parallel to the ground. Oscillations around each of the three axis of the aircraft are then excited and the inertias I_{xx} , I_{yy} , and I_{zz} are obtained form Equation 2.7. However, when evaluating lateral inertias, the Huygens transportation of inertias is used to obtain both the inertia and the CG position, as the measured period of oscillation would not be for the aircraft, but for the combination aircraft and gear. To account for this, the period of oscillation of the gear alone should firstly be measured and afterwards the inertias of the aircraft could be obtained with sufficient accuracy. For example, to obtain I_{yy} , Equations 2.8 holds:

$$I_{yy} = \frac{T_{total}^2 W_{total} L_{total}}{4\pi^2} - \left(\frac{W_{total}}{g} + m_a \right) L_{total}^2 - \frac{T_{gear}^2 W_{gear} L_{gear}}{4\pi^2} \quad (2.8)$$

where

T_{total} is the period of oscillation of the aircraft with the swing gear.

W_{total} is the weight of aircraft with the swing gear.

L_{total} The distance between the centre of gravity of the aircraft with the swing gear and its axis of oscillation.

T_{gear} is the period of oscillation of the swing gear alone.

W_{gear} is the weight of the swing gear alone.

L_{gear} The distance between the centre of gravity of the swing gear alone and its axis of oscillation.

m_a is the equivalent mass of the aircraft resulting from aerodynamic effects.

Regarding product of inertias, due to the aircraft symmetry the only one to be considered is I_{xz} . It is obtained by measuring the moment of inertia of the aircraft about an axis tilted by an angle θ from the longitudinal axis in the vertical plane. Equation 2.9 holds:

$$I_{xz} = \frac{I_{xx} \cos^2 \theta + I_{zz} \sin^2 \theta - I_\theta}{\sin 2\theta} \quad (2.9)$$

This experimental set up, despite its simple procedure presents a major limitation. It takes into account the aerodynamic effects on the aircraft mass, which for a light UAV are difficult to estimate. These become significant as the UAV is light and have a greater impact on the effective mass of the aircraft. Thus the results obtained from this method are not of a great accuracy.

2.5.1.2 Mass Properties Statistical Estimation

In 2009, Carlo L. Botasso et al. developed a procedure for the identification of the inertial properties of small size UAVs[6]. The proposed procedure consisted of subjecting the air vehicle to a perpendicular motion. Having obtained the time histories of attitudes and angular rates, the maximum likelihood method is used to estimate the inertia tensor components.

- **Experimental Set-up**

By subjecting a rigid body to perpendicular motion, its inertia tensor can be estimated. Figure 2.11 shows at left a small rotorcraft UAV: a supporting structure is made of a steel plate with a flared hole in the middle and of four steel rods; the supporting structure is suspended to a hemisphere, which is in

turn connected to a supporting frame. The hemisphere works as a spherical joint with small friction and allows for roll and pitch oscillations of up to 35 deg of amplitude, and for 360 deg yawing rotations.

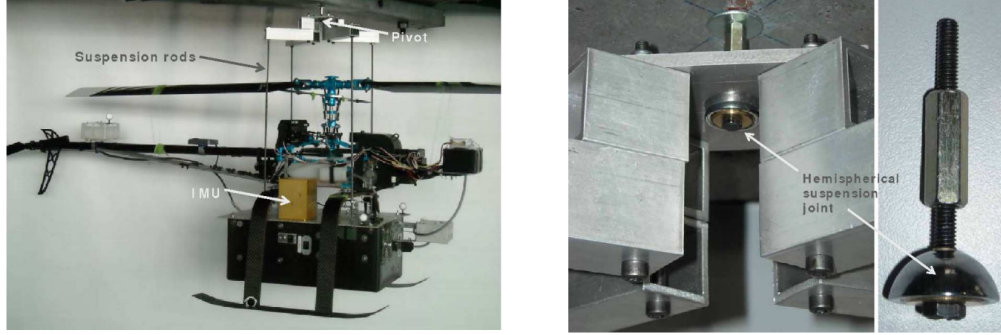


FIGURE 2.11: At left: small rotorcraft UAV with steel rods and IMU, suspended at a pivot point. At right: detail of the pivot.[6]

• Equations of Motion

The system has a known mass and centre of gravity and exhibits a simple rigid pendulum dynamics. It can be modelled by the Euler second law as:

$$J_O \dot{\omega} + \omega \times J_O \omega = m_O \quad (2.10)$$

where

ω is the body angular velocity.

m_O moment of all external forces about the pivot O.

J_O is the inertia tensor of the UAV.

$$J_O = \begin{bmatrix} I_{xx} & I_{xy} & I_{xz} \\ I_{xy} & I_{yy} & I_{yz} \\ I_{xz} & I_{yz} & I_{zz} \end{bmatrix} \quad (2.11)$$

• Parameters Estimation

The maximum likelihood estimation (MLE) method is then employed to estimate the various inertia of the UAV.

This method relies on statistical analysis and is limited by the MLE algorithm used. Additionally, the quality of the data may require filtering before any useful

usage. It is however claimed to provide more accurate estimation of the mass properties of relatively heavy UAVs with more inertia when compared to the pendulum method.

2.5.2 Mass Properties Estimation with XFLR5

XFLR5 provides the capability of estimating the centre of gravity (CG) and inertias of an airframe. It takes as inputs the complete geometrical definition of the airframe, including wings, vertical and horizontal tail-planes and the fuselage.

The software assumes:

- The fuselage mass is distributed along each section and at each section centroid is located a point mass.
- The lifting surface mass is distributed both in the chordwise and spanwise directions. The lifting surface is assumed to be constituted of a grid of point masses.

2.6 System Identification

As defined by Zadeh[20], system identification is the determination, on the basis of observed input and output, of a system within a specified class of systems to which the system under test is equivalent. It can be understood as the development of a mathematical model representing a physical system, based on imperfect observed data.

This definition implies that for a given physical system, multiple mathematical models representing its behaviour exist. In order to select which model, the parsimony principle is applied. As discussed by Morelli and Klein[21], it states that of all models in a specified class that exhibit the desired characteristics, the simplest one should be preferred. The system identification definition also outlines that the system identification is based on observation of the input and output measurements for the studied system. These observations are generally corrupted by measurement and process noise. Statistical theories and methods are thus introduced to take the noise into account when performing system identification.

The most important requirement for a mathematical model is its usefulness. The mathematical model should be usable either to predict a certain behaviour of the system under pre defined conditions or the values of the parameters used to build the model could provide the desired insight on the system behaviour. In both cases, the mathematical model should be simple enough to be useful and complex enough to capture the important dependencies the measurements illustrate.

2.6.1 System Identification for Aircraft Applications

There are three general problems in aircraft dynamics and control studies:

- Simulation: Given the input and the system, what is the output?
- Control: Given the system and the output, what is the input?
- System Identification: Given the input and the output, what is the system?

Although modern computational techniques and wind tunnel test could provide good insight into the aircraft dynamics, there are still several motivations for identifying aircraft models from test data:

- Expanding the flight envelope for new aircraft, which can include but is not limited to quantifying the stability and control impact of the aircraft modifications or special flight conditions.
- Developing flight simulators which require accurate representation of the aircraft dynamics in all flight regimes.
- Obtaining more comprehensive aircraft mathematical models which are used for control law design.
- Verifying aircraft specification compliance.

When applying system identification to aircraft, the aircraft dynamics equations are established and a set of experiments is designed to obtain the measurement of input and output data. The aircraft dynamics equations are directly derived from the Newton's second law of motion, and describe the translational and rotational motion of the aircraft around its centre of gravity. In the vector form, they are:

$$\begin{aligned} m\dot{\mathbf{V}} + \boldsymbol{\omega} \times m\mathbf{V} &= \mathbf{F}_G(\zeta) + \mathbf{F}_T + \mathbf{F}_A(\mathbf{V}, \boldsymbol{\omega}, \mathbf{u}, \boldsymbol{\theta}) \\ J_O\dot{\boldsymbol{\omega}} + \boldsymbol{\omega} \times J_O\boldsymbol{\omega} &= \mathbf{M}_T + \mathbf{M}_A(\mathbf{V}, \boldsymbol{\omega}, \mathbf{u}, \boldsymbol{\theta}) \end{aligned} \quad (2.12)$$

where

m is the mass of the aircraft.

ζ are the Euler angles indicating the attitude of the aircraft relative to fixed Earth axes.

\mathbf{V} and $\boldsymbol{\omega}$ are the translational and rotational velocity vectors.

\mathbf{u} is the inputs vector.

$\boldsymbol{\theta}$ is a vector of parameters specifying the aerodynamic characteristics of the aircraft. \mathbf{F}_G , \mathbf{F}_T , and \mathbf{F}_A are the gravitational, thrust and aerodynamic forces applied on the aircraft. \mathbf{M}_T , and \mathbf{M}_A are the thrust and aerodynamic moments applied on the aircraft. J_O is the inertia tensor.

The system identification applied to aircrafts could then be defined as the determination of a model structure for the aerodynamic forces and moments \mathbf{F}_A and \mathbf{M}_A and the estimation of the unknown aerodynamic parameters $\boldsymbol{\theta}$ contained in the model structure. In the case of a known model structure, the system identification process is simplified to the parameter estimation process. Usually, the aerodynamic forces and moments depend on linear variation of the aircraft states and control deflections leading to linear time-invariant aerodynamic model formulation.

The aircraft system identification can thus be several steps as illustrated by Figure 2.12:

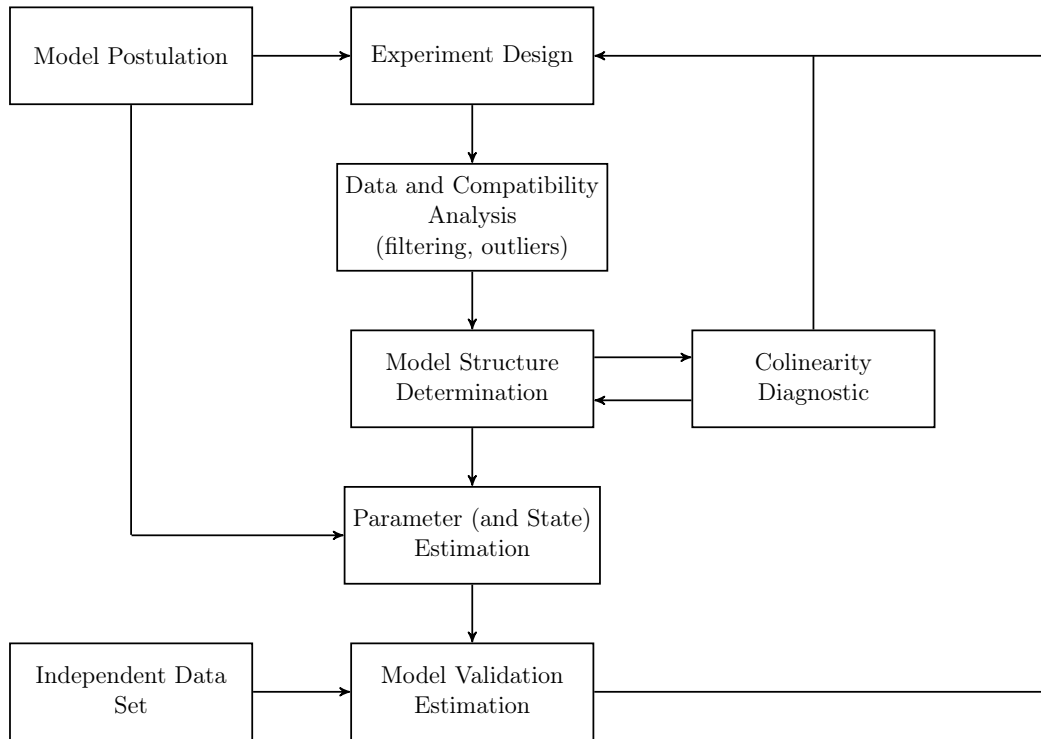


FIGURE 2.12: System Identification for Aircraft Applications Process.

- **Model Postulation:** The model postulation is based on a priori knowledge of the aircraft dynamics and aerodynamic characteristics. The model could express the aerodynamic forces and moments applied on the aircraft as linear, polynomial or spline functions in the states and control deflections, with time invariant parameters (aerodynamic and control derivatives) quantifying the contribution of each on the total aerodynamic force or moment. Some models could include unsteady aerodynamics but that will not be covered within the scope of the presented work.
- **Experiment Design:** The experiment design comprises the selection of the instrumentation, the specification of the aircraft configuration and flight conditions, and the manoeuvres to be performed during the test. The instrumentation is meant to record at constant sampling intervals the inputs and outputs required to identify the system. For an aircraft, these are for the inputs: the throttle position and the control surfaces deflections. The outputs are: the air relative velocity (airspeed, angle of attack and sideslip angle), the Euler attitude angles, the angular velocities, the translational

accelerations, and eventually the aircraft configuration. The available instrumentation for this project has been discussed in precedent sections of the literature review.

The experiment design also comprises the input design. The control surfaces and/or throttle inputs influence the aircraft response and hence the accuracy of the system identification. In order to obtain parameters estimates with a high accuracy, there are optimised inputs developed for system identification applied to aircrafts.

- **Data Compatibility Analysis:** The data compatibility analysis is applied to the measured aircraft response to inputs in order to verify data accuracy, as these measurements could contain systematic errors.
- **Model Structure Determination:** The model structure determination consists of determining the appropriate form of the mathematical model from a class of models, based on the measured data. Generally, it consists of choosing a specific polynomial expansion in the aircraft motion and control variables which will model a component of the aerodynamic forces and moments acting on the aircraft, from the class of all possible polynomials. This polynomial should also follow the parsimony principle. It should be simple enough to be useful and complex enough to adequately capture the physical measurements. A good model fits the data well, facilitates the estimation of unknown parameters with good precision and accuracy and could be used for prediction purposes.
- **Parameter (and State) Estimation:** Parameter Estimation is a principal part of system identification. After developing a mathematical model describing the aircraft dynamics, it is essential to estimate the various parameters it contains. There are various methods used for parameter estimation and those are described in subsequent sections of this literature review.
- **Collinearity Diagnosis:** Depending on the chosen estimation technique, a collinearity diagnosis may be required. If using linear regression methods, the model terms can be correlated to some extent. The collinearity diagnostic consists of detecting the presence of collinearity among the model terms and assessing the extend to which this collinearity adversely affects the estimated parameters.

- **Model Validation:** The mathematical model obtained should finally be validated, regardless of how it was found. This prediction capability of the model is checked on data that was not used in the identification process. The measured input for prediction data is given to the mathematical model to compute predicted response which are compared with measured values. The differences between the predicted values from the model and the measured data should not exhibit any pattern. This indicates that the model sufficiently capture all the deterministic components in the measured output.

The next paragraph discuss the various parameter estimation techniques at our disposal for this project.

2.6.2 Parameter Estimation Techniques

It is important to estimate the aerodynamic and control parameters of an aircraft, as these parameters are useful for verifying and validating pre-flight prediction based on computational tools, empirical calculations or static wind tunnel testing, or for improving flight control systems and designing flight simulators. This section presents the most commonly used techniques for parameter estimation:

- The Least Square Method: This technique minimises a cost function, based on the sum of squared differences between the measurement and the model to estimate the parameters.
- Maximum Likelihood Method: This technique estimates the parameters by maximising the probability of the measured data and the model coinciding.
- M-Estimators: This is a widely used robust estimation technique. It is based on the same principle as the Least Square Method but it takes into account the effect of the outliers by adding a positive defined function ρ to the squared differences before minimising the cost function.
- Frequency Domain Method: The frequency domain methods use the Fourier Integral to transform the time domain data to frequency domain and apply conventional techniques in the frequency domain.

- Real Time Parameter Estimation: It is sometimes required to estimate the parameters in real time in order to improve the flying/handling qualities of the aircraft in flight.

Here are presented more detailed descriptions of the Ordinary Least Square Method and the Maximum Likelihood Method.

2.6.2.1 Ordinary Least Square Method

A system can be represented as:

$$\begin{aligned} \mathbf{y} &= \mathbf{X}\boldsymbol{\theta} \\ \mathbf{z} &= \mathbf{X}\boldsymbol{\theta} + \boldsymbol{\nu} \end{aligned} \quad (2.13)$$

where

\mathbf{y} is the true output.

\mathbf{X} is the regressors matrix.

$\boldsymbol{\theta}$ is the parameters vector.

\mathbf{z} is the measured output (from the experiment).

$\boldsymbol{\nu}$ is the noise from the experiment.

To apply the ordinary least square method, a cost function should be defined as:

$$J(\boldsymbol{\theta}) = \frac{1}{2}(\mathbf{z} - \mathbf{X}\boldsymbol{\theta})^T(\mathbf{z} - \mathbf{X}\boldsymbol{\theta}) \quad (2.14)$$

Minimising the cost function defined in Equation 2.14 yields to:

$$\hat{\boldsymbol{\theta}} = (\mathbf{X}^T\mathbf{X})^{-1}\mathbf{X}^T\mathbf{z} \quad (2.15)$$

where

$\hat{\boldsymbol{\theta}}$ is the vector of parameter estimates.

It is necessary into any parameter estimation process to define the covariance matrix which helps assess the quality of the parameter estimates. It is defined as:

$$\text{cov}(\hat{\boldsymbol{\theta}}) = E[(\hat{\boldsymbol{\theta}} - \boldsymbol{\theta})(\hat{\boldsymbol{\theta}} - \boldsymbol{\theta})^T] \quad (2.16)$$

2.6.2.2 Maximum Likelihood Method

The maximum-likelihood estimation (MLE) is a method of estimating the parameters of a statistical model. When applied to a data set and given a statistical model, maximum-likelihood estimation provides estimates for the model's parameters.

- **Probability Density Function**

According to statistics, the data vector $y = (y_1, \dots, y_m)$ is a random sample from an unknown population. The goal of data analysis is to identify the population that is most likely to have generated the sample. In statistics, each population is identified by a corresponding probability distribution. Associated with each probability distribution is a unique value of the model's parameter. As the parameter changes in value, different probability distributions are generated. A model can then be defined as the family of probability distributions indexed by the model's parameters. Let $f(y|w)$ denote the probability density function (PDF) that specifies the probability of observing the data vector y given the parameter w :

$$f(y|w) = f(y_1|w)f(y_2|w)\dots f(y_m|w) \quad (2.17)$$

- **Likelihood Function**

Given a set of parameter values, the corresponding probability distribution function will show that some data are more probable than other data. Our interest lies in finding the one probability distribution function, among all the probability densities that the model prescribes, that is most likely to have produced the data given the observed data and a model of interest. We then define the likelihood function, $\mathbb{L}(w|y)$ such as:

$$\mathbb{L}(w|y) = f(y|w) \quad (2.18)$$

- Maximum Likelihood Estimation

The principle of maximum likelihood estimation states that the desired probability distribution is the one that makes the observed data most likely. Meaning we must seek the value of the parameter vector w that maximizes the likelihood function $L(w|y)$: The resulting parameter vector, which is sought by searching the multi-dimensional parameter space, is called the MLE estimate, and is denoted by $w_{MLE} = (w_{1,MLE}, w_{2,MLE}, \dots, w_{k,MLE})$. It should be noted that the likelihood estimate may not exist or be unique. We will assume that the MLE estimate exists and is unique subsequently.

As the likelihood and log-likelihood functions $\mathbb{L}(w|y)$ and $\ln \mathbb{L}(w|y)$ are monotonically related to each other, the same MLE estimate is obtained by maximizing either one. To obtain a maximum, we use the likelihood equations:

$$\begin{aligned} \frac{\partial \ln \mathbb{L}(w|y)}{\partial w_i} &= 0 \\ \frac{\partial^2 \ln \mathbb{L}(w|y)}{\partial w_i^2} &< 0 \end{aligned} \quad (2.19)$$

2.6.3 Maximum Likelihood Estimation for Aircraft Application

The Maximum Likelihood Estimation has been widely used among other techniques to estimate aircraft parameters as it produces realistic results and its estimates exhibit several desirable statistical properties.

The concept of the MLE applied to aircraft parameter estimation is summarised in Figure 2.13.

The output error approach is an iterative process where the test vehicle is simulated in parallel with the postulated model. The output error, also called residual or innovation is used to build the MLE cost function. This cost function is minimised by the optimisation algorithm which produces the desired estimates. The

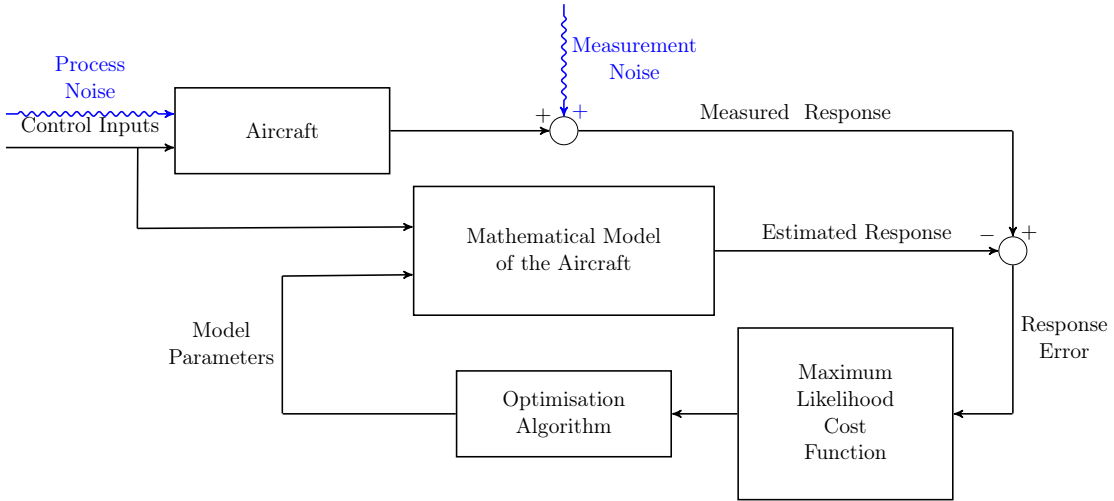


FIGURE 2.13: Maximum Likelihood Estimation for Aircraft Applications

estimates are given as inputs to the mathematical model of the aircraft. The mathematical model computes both an estimated output and a sensitivity. The process is repeated until a convergence criteria is reached.

The aircraft mathematical model is described as a linear time-invariant model. When considering process noise into the parameter estimation process, a Kalman Filter is included to the state estimator. As it is computationally easier to find minima than maxima, the optimisation algorithm is used to find the aircraft parameters minimising the Maximum Likelihood Estimation cost function which is defined as the negative logarithm of the previously defined likelihood function.

2.7 Kalman Filtering for Aircraft Applications

In case the aircraft is subjected to random external disturbances, the mathematical model defined for the system identification becomes stochastic. In this case, the various aircraft states should be estimated in addition to the model parameters. The Kalman Filter or Linear Quadratic Estimation is an algorithm that uses a series of measurements observed over time, containing noise and other inaccuracies, and produces estimates of unknown variables that tend to be more precise than those based on a single measurement alone. As the model studied in the work presented in this thesis is non-linear, it is necessary to use an Extended Kalman Filter, able to cope with non linearities in the measured data.

2.7.1 Extended Kalman Filter

The Extended Kalman Filter is the non linear version of the classic Kalman Filter. It presents as main advantages:

- It incorporates noise effects in the filtering estimation process.
- It has a relatively simple algorithmic approach and all falls into a single programming loop.
- It is a recursive method, meaning it needs only the previous and current experimental states to perform the estimation. No historical data is required.
- It allows to use different sensors in order to do the measurements.

2.7.2 Background Theory

As described by Wong et Al.[\[4\]](#) the extended Kalman filter theory is based on two steps:

- The prediction: Here, the algorithm uses previous measured data and its knowledge of the dynamic system to predict the current state.
- The update: Here, the algorithm uses the measurement of the current state to improve the quality of the state prediction.

2.8 Relevance of the Literature Review in Respect to the Work Presented in the Thesis

2.8.1 Previous Research at Cranfield University

The work presented in this thesis is a complement to previous work carried out at Cranfield University by previous MSc students Quentin Mauviel[\[9\]](#) and Henoc Guimeno[\[22\]](#) in 2012 and previous PhD student Peter Thomas[\[5\]](#) in 2010.

The present thesis pushes forward the previous work as it is planned to be conducted both in a wind tunnel and outdoor, unlike the flight testing performed by former students. It makes use of state of the art hardware available. The UAV industry has encountered an exponential growth in the past few years alongside with the flight controllers and various hardware necessary to make an unmanned vehicle fly. One of the major difficulties encountered by previous students was the measurement or estimation of both the angle of attack and sideslip angle of the UAV. Accurate measurements during flight test require an angle of attack boom, which inherently modifies the dynamics of the aircraft. Various estimation techniques have been developed but did not present a great level of accuracy. This created discrepancies between the flight dynamics model and the flight test data that could not be accounted for.

This thesis also aims to develop a comprehensible System Identification methodology suitable for similar fixed wing aircraft. This tool will ease the future development of fixed wing aircraft system identification models.

Additionally, for the current work, modifications are planned to be made to the aircraft geometry to allow further improvement in the hardware implementation.

2.8.2 Choices and Limitations

The 3DR Pixhawk is chosen as the main board for the data acquisition system. However due to stock availability in the UK, a clone has been purchased. AVL has been selected to obtain the aerodynamic and control derivatives of the UAV thanks to its straightforwardness and great accuracy. The mass properties are determined with the computational tool embedded in XFLR5. Regarding the UAV system identification, the Maximum Likelihood Method is chosen without an extended Kalman Filter algorithm. Justification for these choices are detailed as follows:

- The 3DR Pixhawk presents several advantages when compared to the Intel Edison. Despite its lower computation power and less flexibility, the 3DR Pixhawk is a specialised board for UAVs. It does not require external sensors and its size and weight are adapted for airborne applications. Additionally, the included sensors have good enough characteristics when compared to the ones considered for the Intel Edison. Last but not least, the compatibility

with the Ardupilot firmware makes the 3DR Pixhawk easier to program and to interface with other components than the Intel Edison, for instance the control of servos and the telemetry. It also provides an automated data logging through the Ardupilot software.

- The studied UAV operates at a relative low speed, thus low Reynolds number. This implies that the viscous effects are dominant over the inertial effects on the UAV. AVL uses a Vortex Lattice Method which is able to capture viscous drag despite a low level of accuracy. Additionally, the fuselage is not taken into account when developing the aerodynamic model within AVL. From those reasons, discrepancies may arise between the simulation model data and the wind tunnel test data. This will allow to investigate further the contribution of viscous effects on the dynamics of the UAV. Additionally, AVL allows to be called within a batch file run through MATLAB. Angle sweeps could then easily be performed and the various aerodynamic and control derivatives obtained for different attitude configurations. This is used to populate the flight dynamics model with look-up tables.
- The mass properties of the aircraft could be obtained by either a full CAD model or a full laser geometry definition. These two methods are time consuming and out of the scope of this thesis. Additionally, the studied UAV is made out of foam, thus its mass is relatively low. Its inertia effects are negligible when compared to its aerodynamics effects. Moreover, the experimental methods presented in this literature review require extensive experimental equipment. The mass properties estimation tool provided by XFLR5 is therefore a suitable solution for this study. The clear user interface of XFLR5 makes the definition of aerofoil sections easy when compared to other VLM software packages as AVL. However, uncertainties in the results are expected as XFLR5 does not take into account the internal cavity in the UAV fuselage (used for casing the hardware).
- Unlike the least-squares estimation which is primarily a descriptive tool, the Maximum Likelihood Estimation is a preferred method of parameter estimation in statistics and is an indispensable tool for many statistical modelling techniques, in particular in non-linear modelling with non-normal data.

Chapter 3

Aircraft & Instrumentation Description

3.1 General Specifications

The aircraft under analysis in this thesis is the Multiplex EasyStar II¹, which is a conventional motor glider made out of ELAPOR, as illustrated in Figure 3.1. This structural material is not only light but provides robustness to the aircraft and makes it less susceptible to crashes and impacts. The manufacturer characteristics are as follows:

- typical take off mass: 700g;
- fuselage length: 977mm;
- wing span: 1370mm;
- wing aspect ratio: 7.9;
- control surfaces: elevator, aileron, rudder;
- actuators: 4 servo motors;
- propulsion: an electric motor with retractable propeller;

the aircraft is fitted with the data acquisition system.

¹<http://www.multiplex-rc.de/>

FIGURE 3.1: Multiplex EasyStar II²

3.2 Airframe Geometry

The Body Axes Centre (BAC) of the aircraft has been chosen at the intersection of the fuselage centre line and the line perpendicular to it and going through the point of intersection of the fuselage and the wing leading edge. All aerodynamic coefficient are calculated with respect to the BAC and the equations of motion for both the system identification and the flight dynamics model are done at the BAC.

The position of the BAC relative to the nose of the aircraft is summarised in Table 3.1. All subsequent positions will be given relative to the BAC unless stated otherwise.

	$x(\text{mm})$	$y(\text{mm})$	$z(\text{mm})$
BAC	240	0	0

TABLE 3.1: Aircraft BAC Position relative to Nose Tip.

²<http://www.modellhobby.de/>.

3.2.1 Lifting Surfaces Geometry

After defining the general dimensions of the aircraft, it is necessary for the aerodynamic modelling of the aircraft to define the aerofoil section of the lifting surfaces. The aerofoil sections of the tail and fin have been determined using a string at mid-span and are supposed to be constant on the entire span of the lifting surfaces. The wing aerofoil has been evaluated at the wing root by measuring its slot in the fuselage which is used when building the aircraft. The fin and the tail have the same aerofoil section which is a symmetric aerofoil and represented in Figure 3.2. The wing has a low cambered aerofoil which is represented in figure 3.3.

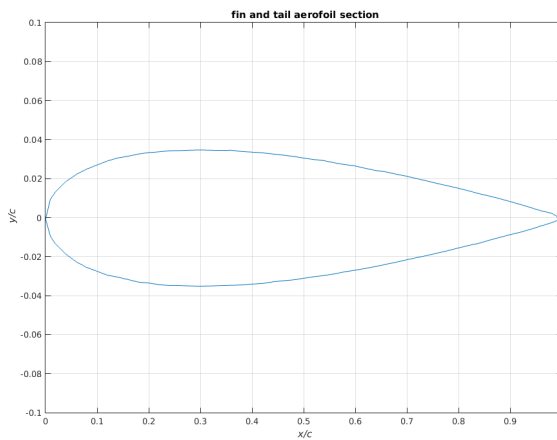


FIGURE 3.2: Tail and Fin aerofoil section.

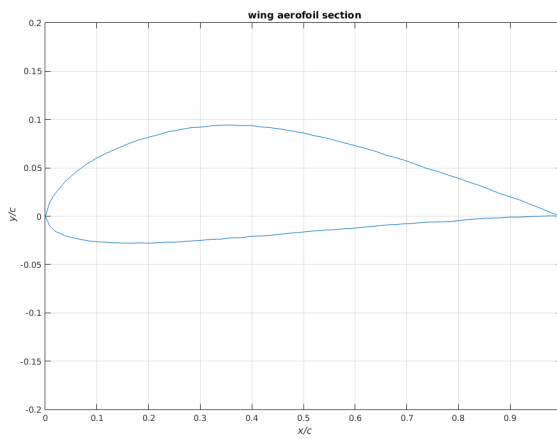


FIGURE 3.3: Wing Aerofoil Section.

The position of the lifting surfaces relative to the BAC, their area, span, root and mean aerodynamic chord are summarised in Table 3.2.

	x (mm)	y (mm)	z (mm)	Area (dm ²)	Span (mm)	Root chord (mm)	MAC (mm)
Wing	0	0	52	23.6	1370	200	179
Tail	635	0	15	4.27	480	10	-
Fin	510	0	20	1.69	170	13	-

TABLE 3.2: Lifting Surfaces Geometrical Characteristics.

3.2.2 Fuselage

The fuselage is not relevant when performing the aerodynamic modelling of the aircraft. The effect of the fuselage on the aerodynamics of the aircraft is negligible when compared to the lifting surfaces when using the Vortex Lattice Method.

3.2.3 Control Surfaces

The aircraft has three primary control surfaces:

- 2 paired ailerons;
- a rudder;
- an elevator.

The position and dimensions of the lifting surfaces is summarised in Table 3.3.

	x (mm)	y (mm)	z (mm)	Span (mm)	Location of hinge (mm)
Aileron	0	240	52	250	30
Rudder	635	0	20	155	40
Elevator	510	0	15	160	35

TABLE 3.3: Control Surfaces Geometrical Characteristics.

3.3 Instrumentation

The data acquisition system of the aircraft is summarised in Figure 3.4. It consists of:

- A 3DR Pixhawk autopilot, as discussed in the literature review;
- A GPS and Magnetometre, part of the Pixhawk kit;
- An RC Reveiver;
- A PPM Encoder, which is used to transform the Pulse-width modulation (PWM) signal from the radio controller into Pulse-position modulation (PPM) signal (the Pixhawk understands only PPM signals);
- An I²C ³ expansion board, which is used to have multiple I²C ports on the Pixhawk;
- An airspeed sensor, as discussed in the literature review;
- A power distribution board, which is used to distribute electric power to the Pixhawk and the brush-less motor of the aircraft;
- A telemetry module, as discussed in the literature review;
- a data logging device, as discussed in the literature review;
- a safety button which is programmed to trigger the data logging;
- a buzzer, which notifies the state of the Pixhawk (initialising, ready, armed, error, ect...);

3.3.1 3DR Pixhawk autopilot

The board used for this thesis is the open source 3DR Pixhawk. It is able to take as input the various signals from the radio controller, excite the control surfaces servos and the electric motor, and store the flight data. The loads on the airframe will create movements in all directions of the whole aircraft which are recorded by the IMU embedded in the 3DR Pixhawk. The autopilot is also compatible with various other sensors. Readings from both the IMU and the external sensors are saved in a data logging SD-card initially set up in the autopilot.

The 3DR Pixhawk is fully compatible with the Ardupilot firmwares. For this project, the "plane"⁴ Ardupilot firmware has been installed in the autopilot. A

³<http://www.i2c-bus.org/i2c-bus/>

⁴<http://plane.ardupilot.com/>

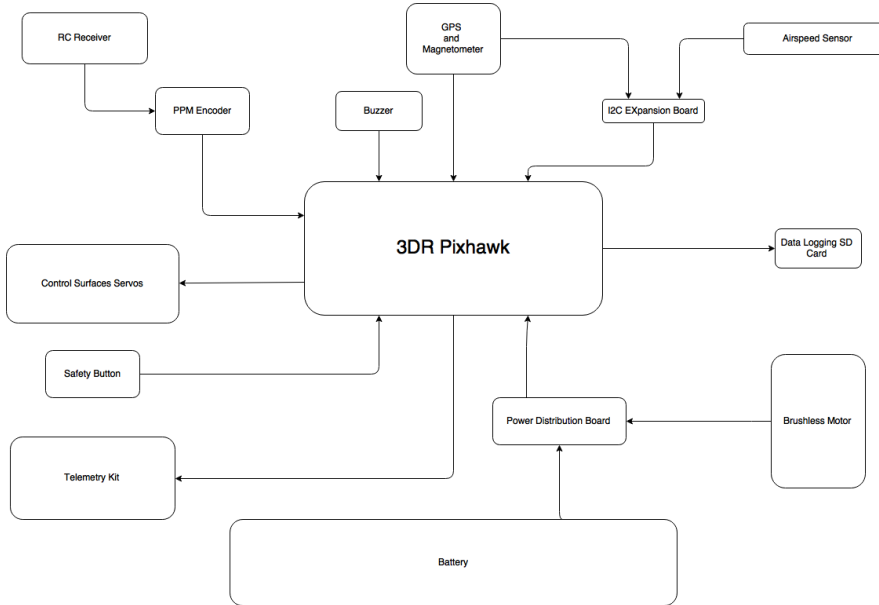


FIGURE 3.4: Instrumentation bloc diagram.

firmware is the skill-set code running on the hardware, which configures it for the kind of vehicle used. It configures the internal software of the 3DR Pixhawk to control a typical fixed wing airplane, with the possibility of choosing the type of control surfaces available.

The inputs from the Radio Receiver are PPM signals and the 3DR Pixhawk uses I²C connection to make reading from other sensors.

The internal IMU installed in the 3DR Pixhawk is made of:

- a Invensense MPU 6000⁵ 3-axis accelerometer/gyroscope. Its output are digital values of the angular rates and accelerations for all three axis.
- a ST Micro LSM303D⁶ 3-axis 14-bit accelerometer/magnetometer.
- a MEAS MS5611⁷ barometer, which records the pressure and thus the pressure altitude of the aircraft, with a resolution of 10cm.
- ST Micro L3GD20⁸ 3-axis 16-bit gyroscope.

⁵<http://store.invensense.com/ProductDetail/MPU6000-InvenSense-Inc/420595/>

⁶<http://eu.mouser.com/ProductDetail/STMicroelectronics/LSM303D/>

⁷<http://www.meas-spec.com/downloads/MS5611-01BA03.pdf>

⁸<http://www.st.com/web/en/resource/technical/document/datasheet/DM00036465.pdf>

3.3.2 RC Receiver

The RC receiver chosen for the project is a Spektrum DSM2⁹ Aircraft Module receiver. It is used to receive the controls from the pilots transmitter and to send them to the autopilot. It works with PWM signals that need to be translated into PPM signals for the autopilot. A PPM encoder is used for this matter.

The RC receiver can output 9 Channels but 4 are used for this project as follows:

- Channel 1: Aileron
- Channel 2: Elevator
- Channel 3: Throttle
- Channel 4: Rudder

The servo control from the RC Receiver to the servos is done by sending each servo a PWM (Pulse-Width Modulation) signal, a series of repeating pulses of variable width. The PWM signals have been experimentally measured with the control deflection as well as the throttle percentage. A linear fit has been applied to the measured data after removing the outliers (with $t_{n-2} = 2$) and the following linear relationships have been obtained (y is the control deflection in degrees or percentage for the throttle and x is the PWM signal from the RC receiver in nano-seconds):

- Elevator:

$$y = -0.047x + 72.55 \quad R^2 = 0.9839$$

- Rudder:

$$y = 0.057x - 83.40 \quad R^2 = 0.9852$$

- Aileron:

$$y = -0.066x + 97.86 \quad R^2 = 0.9920$$

- Throttle:

$$y = 0.102x - 103.02 \quad R^2 = 0.9989$$

These relationships are obtained from Figure 3.5.

⁹<https://www.spektrumrc.com/Products/Default.aspx?ProdID=SPMMSJR720>

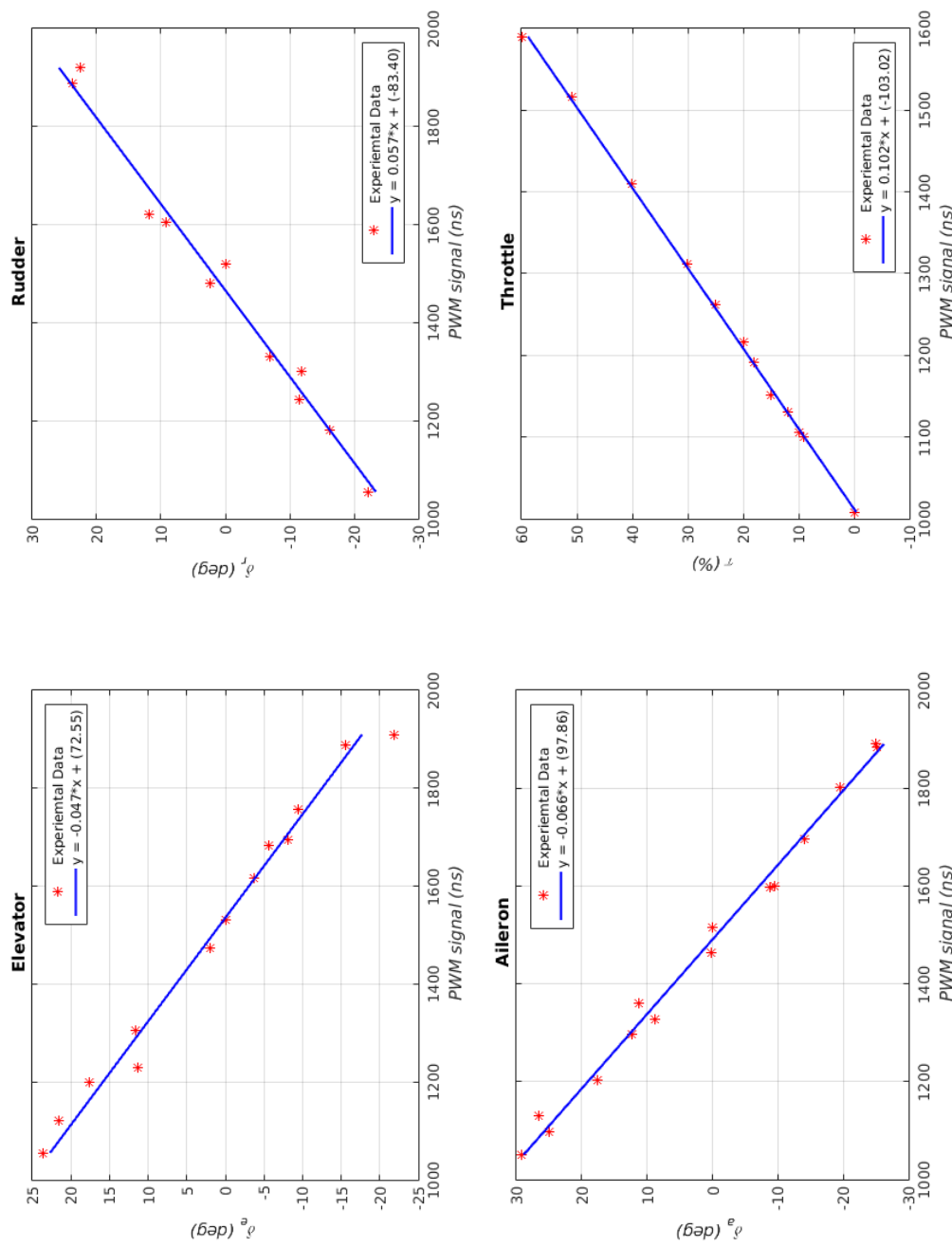


FIGURE 3.5: Control Deflections and Throttle PWM signals map.

3.3.3 Airspeed Sensor

An airspeed sensor is used to measure the airspeed of the aircraft. Although the testing is planned to be carried out in a wind tunnel where the wind characteristics are well known, it has been anticipated that the project may involve outdoor flight testing or future projects might.

The chosen airspeed sensor is the Measurement Specialties 4525DO¹⁰. It is a Pitot Static tube with a resolution of roughly 0.84Pa. The air velocity is calculated following the equation:

$$V = \left[\frac{2(P_{Total} - P_{Static})}{\rho_{air}} \right]^{\frac{1}{2}} \quad (3.1)$$

3.3.4 Telemetry Module

A telemetry module is used to connect the aircraft to the ground station and monitor the aircraft states during the test. The module chosen for this project is the 3DR Radio Set¹¹ working at 433MHz. It sends data from the aircraft at a low frequency (depending on the distance between the ground station and the aircraft) to the ground station via a MAVLink Micro Air Vehicle Communication Protocol¹².

3.3.5 Data Logging

The flight data is logged in a micro-SD card and downloaded via the ground station software. The logging frequency depends on the parameter. Table 3.4 gives the data logging frequency for the parameters of interest in the work presented in this thesis.

As the system identification depends on the sampling frequency, a linear interpolation has been performed on the data which is recorded at a lower frequency to match with the desired 50Hz frequency.

¹⁰<http://www.meas-spec.com/downloads/MS4525DO.pdf>

¹¹<https://store.3drobotics.com/products/3dr-radio-set>

¹²<http://qgroundcontrol.org/mavlink/start>

	Frequency Hz
Time	50
Euler Angles (ϕ, θ, ψ)	50
Translational accelerations (a_x, a_y, a_z)	50
Control deflections and Throttle ($\delta_e, \delta_a, \delta_r, \tau$)	10
Airspeed (V_0)	10

TABLE 3.4: Data Logging Frequencies.

3.3.6 Ground Station Software

The software used as the ground station is Mission Planner¹³, which is a full-featured ground station application for the ArduPilot autopilots. It is initially used to calibrate all the sensors of the 3DR Pixhawk and set the various parameters of all sensors and flight modes.

During the test, it is used to monitor the states of the aircraft and perform initial analysis of the data airborne. After the test, Mission Planner is used to download the data from the the data logging micro-SD card to the computer as a ".mat" file ready to use in MATLAB.

3.4 Mass Properties

The mass properties of the airframe have been estimated using XFLR5. The airframe mass properties were estimated and afterwards the instrumentation mass properties were taken into account with a MATLAB script.

3.4.1 Airframe Mass Properties

Using XFLR5, the estimated mass properties of the airframe are as detailed in Table 3.5.

¹³<http://planner.ardupilot.com/>

	<i>Mass</i> (g)	<i>x_{CG}</i> (mm)	<i>y_{CG}</i> (mm)	<i>z_{CG}</i> (mm)	<i>I_{xx}</i> (g.m ²)	<i>I_{yy}</i> (g.m ²)	<i>I_{zz}</i> (g.m ²)	<i>I_{xz}</i> (g.m ²)
Fuselage	119	—	—	—	—	—	—	—
Wing	148	—	—	—	—	—	—	—
Tail	17	—	—	—	—	—	—	—
Fin	7	—	—	—	—	—	—	—
Airframe	291	-156	0	-37.3	17.5	19.5	35.2	2.04

TABLE 3.5: Airframe Mass Properties Relative to BAC.

3.4.2 Instrumentation Mass Properties

The instrumentation mass properties are taken into account in order to estimate the mass properties of the whole aircraft. The aircraft motor, servos and the electronic speed controller are taken into account too. Only the instrumentation items with a mass greater than 10 grams are accounted for. each element is assumed to be a point mass, considering their relative small size when compared to the aircraft. The mass and position of each instrumentation items is given in Table 3.6.

	<i>Mass</i> (g)	<i>x</i> (mm)	<i>y</i> (mm)	<i>z</i> (mm)
Battery	181	190	0	-11.5
Speed Controller	41	-150	0	0
Motor	76	-190	0	-95
Servo Rudder	10	-78	-45	0
Servo Elevator	10	-78	45	0
Servo Aileron 1	10	-98	-330	-52
Servo Aileron 2	10	-98	330	-52
Telemetry Kit	22	0	0	0
RC Receiver	16	50	0	30
Pixhawk	41	50	0	0

TABLE 3.6: Instrumentation Mass and Position Relative to BAC.

The aircraft mass properties are then computed using a MATLAB script and are given in Table 3.7.

	$Mass$ (g)	x_{CG} (mm)	y_{CG} (mm)	z_{CG} (mm)	I_{xx} ($g.m^2$)	I_{yy} ($g.m^2$)	I_{zz} ($g.m^2$)	I_{xz} ($g.m^2$)
Aircraft	708	-45	0	-20	20.5	31.1	46.8	3

TABLE 3.7: Aircraft Mass Properties Relative to BAC.

It appears that the propulsion set has a large impact on the aircraft mass properties. The CG position is 25% of the MAC aft the BAC which is in the limits recommended by the aircraft manufacturer (maximum 43% of the MAC aft the BAC). The aircraft should thus be statically stable in this configuration.

Chapter 4

6 Degrees of Freedom Model Development & Description

This chapter presents the development of a 6 DoF Simulation Model of the EasyStar II aircraft in MATLAB/Simulink. It starts by presenting the development of the Equations of Motions and the presents the other aspects of the 6 DoF modelling with an emphasis on the aerodynamic sub-model. A linearised model is subsequently presented and the effects of airspeed and centre of gravity position on the modal characteristics of the linearised model are discussed.

4.1 Equations of Motion Sub-Model

A sub-model solving the equations of motion of a rigid aircraft using its mass properties and the total forces and moments acting on it have been developed. Prior to that an understanding of the Axes Systems and the aircraft orientation is a prerequisite.

4.1.1 Axes and Orientation

4.1.1.1 Earth Axes System

The Earth Axes System, shown in Figure 4.1 enables to describe the aircraft motion and trajectories relative to Earth. The Earth axes ($x_0; y_0; z_0$) is defined

with (O_x) pointing North, (O_y) pointing East and (O_z) downwards. The datum of the Earth axes system is attached to the aircraft such that the (O_{xy}) plane is parallel to the earth surface and the centre coincides with the body axes centre. This axes system assumes a flat Earth and should solely be used for short aircraft motions.

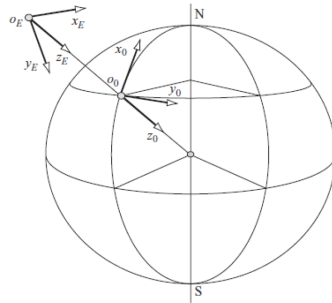


FIGURE 4.1: Earth Axes System[7].

4.1.1.2 Body Axes System

The Body Axes System, shown in Figure 4.2, is attached to the aircraft and is used to described its local motion. The Body Axes System is centered at the Body Axes Center (BAC) and (O_x) pointing towards the aircraft nose datum, (O_y) pointing towards the right wing and (O_z) completes the direct trihedral.

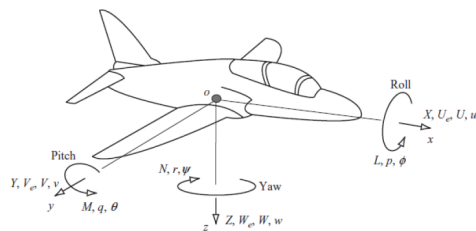


FIGURE 4.2: Body Axes System[7].

4.1.1.3 Euler Angles

The Euler angles give the relative orientation of the body axes when compared to the Earth axes. They are defined as roll angle (ϕ); pitch angle (θ) and yaw angle (ψ) and shown on Figure 4.3.

The Euler angles are given by Equation 4.1.

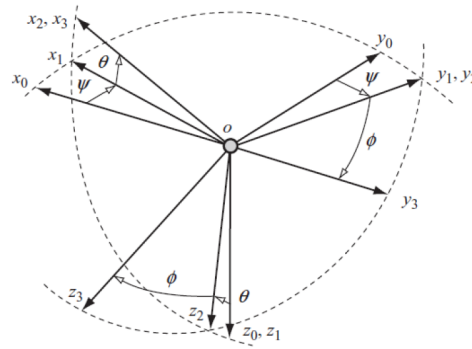


FIGURE 4.3: Euler Angles[7].

$$\begin{bmatrix} ox_3 \\ oy_3 \\ oz_3 \end{bmatrix} = DCM \begin{bmatrix} ox_0 \\ oy_0 \\ oz_0 \end{bmatrix} \quad (4.1)$$

Where the matrix DCM is the Direction Cosine Matrix and is defined as:

$$DCM = \begin{bmatrix} \cos \theta \cos \psi & \cos \theta \sin \psi & -\sin \theta \\ \sin \phi \sin \theta \cos \psi - \cos \phi \sin \psi & \sin \phi \sin \theta \sin \psi + \cos \phi \cos \psi & \sin \phi \cos \theta \\ \cos \phi \sin \theta \cos \psi + \sin \phi \sin \psi & \cos \phi \sin \theta \sin \psi + \sin \phi \cos \psi & \cos \phi \cos \theta \end{bmatrix} \quad (4.2)$$

4.1.1.4 Stability Axes and Wind Axes

The aerodynamic characteristics of the aircraft are usually given in Stability and Wind Axes systems. The stability axes are defined via the angle of attack of the fuselage (α) by a rotation from x_b to x_{stab} , as shown on Figure 4.4. The wind axes are defined via the sideslip angle (β) by a rotation from x_{stab} to x_{wind} . Relation between stability axes and body axes is given as follows:

$$\begin{bmatrix} X \\ Y \\ Z \end{bmatrix}_s = \begin{bmatrix} \cos \alpha & 0 & \sin \alpha \\ 0 & 1 & 0 \\ -\sin \alpha & 0 & \cos \alpha \end{bmatrix} \begin{bmatrix} X \\ Y \\ Z \end{bmatrix}_b \quad (4.3)$$

Relation between Wind and Body axes is:

$$\begin{bmatrix} X \\ Y \\ Z \end{bmatrix}_w = \begin{bmatrix} \cos \alpha \cos \beta & \sin \beta & \sin \alpha \cos \beta \\ -\cos \alpha \sin \beta & \cos \beta & -\sin \alpha \sin \beta \\ -\sin \alpha & 0 & \cos \alpha \end{bmatrix} \begin{bmatrix} X \\ Y \\ Z \end{bmatrix}_b \quad (4.4)$$

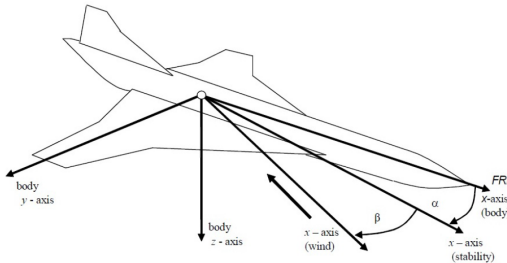


FIGURE 4.4: Stability and Wind Axes Systems[8]

4.1.2 6 DoF Equations of Motion of a Rigid Aircraft

A sub-model solving the equations of motion of a rigid aircraft using its mass properties and the total forces and moments acting on the aircraft have been developed. It consists of:

- A block evaluating the translational and rotational dynamics;
- A block evaluating the rotational kinematics;
- A block evaluating the navigation equations;
- A block computing the Direction Cosine Matrices;
- A block evaluating the Gravitational Forces and Moments.

And overview of the Sub-Model is shown in Figure 4.5.

4.1.2.1 Translational and Rotational Dynamics

In air vehicle simulation, it is necessary to compute the vehicle accelerations in the Body Axes Reference knowing the moments and forces acting on the airframe.

The following assumptions were made when computing those accelerations:

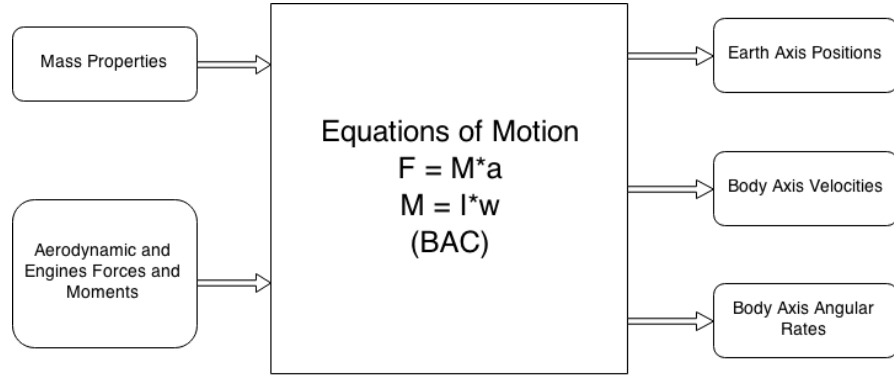


FIGURE 4.5: Equations of Motion Sub-System.

- The airframe is a rigid body. This means that the structure maintains a fixed relative position in space at all time;
- The Body Axes Centre and the centre of gravity of the aircraft are not coincident.
- The curvature of Earth is neglected;
- The aircraft mass is assumed to be constant.

As the inertias of the aircraft are evaluated about the BAC, the equations of translational and rotational dynamics in the matrix form is:

$$\begin{bmatrix} m & 0 & 0 & 0 & md_x & -md_y \\ 0 & m & 0 & -md_z & 0 & md_x \\ 0 & 0 & m & md_y & -md_x & 0 \\ 0 & -md_z & md_y & [I_{xx}]_b & 0 & -[I_{xz}]_b \\ md_z & 0 & -md_x & 0 & [I_{yy}]_b & 0 \\ -md_y & md_x & 0 & -[I_{xz}]_b & 0 & [I_{zz}]_b \end{bmatrix} \begin{bmatrix} \dot{U} \\ \dot{V} \\ \dot{W} \\ \dot{P} \\ \dot{Q} \\ \dot{R} \end{bmatrix} =$$

$$\begin{bmatrix} X + mRV - mQW + md_x(Q^2 + R^2) - md_yPQ - md_zPR \\ Y - mRU + mPW - mdxPQ + md_y(P^2 + R^2) - md_zQR \\ Z + mQU - mPV - md_xPR + md_yQR + md_z(P^2 + Q^2) \\ L - QR([I_{zz}]_b - [I_{yy}]_b) - PQ[I_{xz}]_b - (PV - QU)md_y + (RU - PW)md_z \\ M - PR([I_{xx}]_b - [I_{zz}]_b) - (P^2 - R^2)[U_{xz}]_b - (QU - PV)md_x - (QW - RV)md_z \\ N - PQ([I_{yy}]_b - [I_{xx}]_b) - QR[U_{xz}]_b - (RU - PW)md_x - (QW - RV)md_y \end{bmatrix}$$

4.1.2.2 Rotational Kinematics

This block computes the Euler angles of the aircraft, relative to the Earth Axes Reference. It takes as input the rotational rates previously evaluated. The equation governing this block in the matrix form is:

$$\begin{bmatrix} \dot{\phi} \\ \dot{\theta} \\ \dot{\psi} \end{bmatrix} = \begin{bmatrix} 1 & \sin \phi \tan \theta & \cos \phi \tan \theta \\ 0 & \cos \phi & -\sin \phi \\ 0 & \sin \phi \sec \theta & \cos \phi \sec \theta \end{bmatrix} \begin{bmatrix} P \\ Q \\ R \end{bmatrix} \quad (4.5)$$

4.1.2.3 Navigation Equations

The simulation model should be able to output the position of the aircraft relative to earth. This performed by firstly obtaining the velocities in the Earth Axes reference knowing the velocities in the Body Axes reference and performing an integration afterwards:

$$\begin{bmatrix} V_N \\ V_E \\ V_D \end{bmatrix} = DCM^{-1} \begin{bmatrix} U \\ V \\ W \end{bmatrix} \quad (4.6)$$

$$\begin{bmatrix} P_N \\ P_E \\ h \end{bmatrix} = \int \begin{bmatrix} V_N \\ V_E \\ V_D \end{bmatrix} dt \quad (4.7)$$

4.1.2.4 Gravitational Equations

The gravitational force in the Earth axes reference is given by:

$$F_{grav_E} = \begin{bmatrix} 0 \\ 0 \\ mg \end{bmatrix} \quad (4.8)$$

Using the direction cosine matrix, the gravitational force in the body axes reference is computed as,

$$F_{grav_b} = DCM \begin{bmatrix} 0 \\ 0 \\ mg \end{bmatrix} = mg \begin{bmatrix} -\sin \theta \\ \sin \phi \cos \theta \\ \cos \phi \cos \theta \end{bmatrix} \quad (4.9)$$

The moments due to gravitational force are also evaluated. The cross product methodology is used and:

$$M_{grav_b} = \begin{bmatrix} x_{CG} \\ y_{CG} \\ z_{CG} \end{bmatrix} \times mg \begin{bmatrix} -\sin \theta \\ \sin \phi \cos \theta \\ \cos \phi \cos \theta \end{bmatrix} \quad (4.10)$$

4.2 6 DoF Model Development

Here is presented the methodology used to build a 6 DoF model of the aircraft within he MATLAB/Simulink environment. The various assumptions and simplifications taken during the model development are subsequently listed and a mock test of is afterwards carried out.

4.2.1 Methodology

The 6 DoF Model of the Aircraft has been developed in Simulink. Figure 4.6 shows an overview of the data flow. The various subsystems used are described in the following subsections. The blocks evaluating the gravitational forces and equations of motions have been described in previous sections and will not be covered here.

4.2.1.1 Aerodynamic Forces and Moments

The total aerodynamics loads acting on the aircraft are estimated within this block. It takes as input the air data of the aircraft and the various control surfaces deflections, as shown on Figure 4.7.

The aerodynamic coefficients are obtained from both an XFLR5 model and a AVL model. The coefficients are obtained assuming small angles of incidence

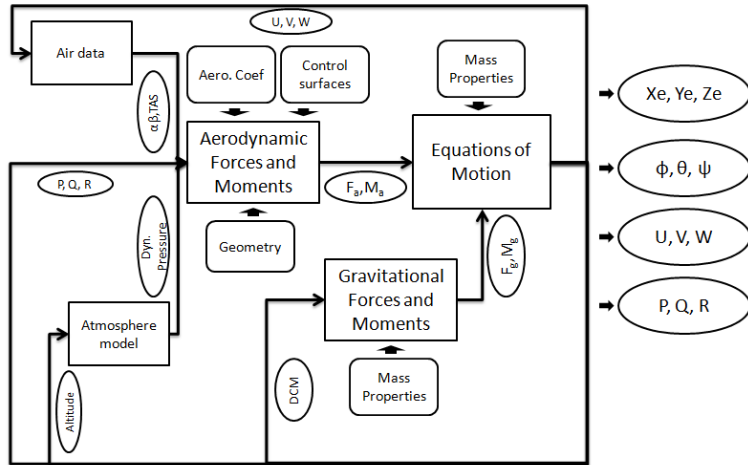


FIGURE 4.6: 6 DoF Model Data Flow Chart[9].

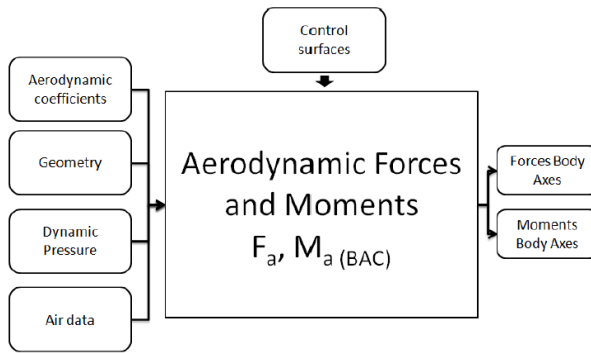


FIGURE 4.7: Aerodynamic and Engines Loads Subsystem[9].

and sideslip, and are defined in the stability axes, with the moment coefficients referenced to the BAC (Body Axes Centre).

The coefficients evaluated within this block are as defined in Table 4.1.

Force/ Moment	Coefficient	Definition
Lift	C_L	$\frac{L}{\bar{q}S_w}$
Drag	C_D	$\frac{D}{\bar{q}S_w}$
Side Force	C_Y	$\frac{Y}{\bar{q}S_w}$
Roll	C_l	$\frac{\mathcal{L}}{\bar{q}S_w b}$
Pitch	C_m	$\frac{M}{\bar{q}S_w \bar{c}}$
Yaw	C_n	$\frac{N}{\bar{q}S_w b}$

TABLE 4.1: Aerodynamic Coefficients Definition.

With \bar{q} is the dynamic pressure, S_w the wing reference area, b the wing span and \bar{c} the mean aerodynamic chord of the aircraft.

The coefficients are computed making use of a linear approximation:

- Longitudinal Forces and Moments:

The lift and pitching moment coefficients are functions of the angle of attack α , the Mach number M , the elevator angle δ_e , the pitch rate q and various other parameters:

$$C_L = f(\alpha, M, \delta_e, q, \dots) \quad (4.11a)$$

$$C_m = f(\alpha, M, \delta_e, q, \dots) \quad (4.11b)$$

Assuming small angle manoeuvres, a linear approximation can be used and the lift and pitching moment coefficients can be written as linear combinations of the previously defined parameters¹.

$$C_L = C_{L_0} + C_{L_\alpha} \alpha + C_{L_{\delta_e}} \delta_e + C_{L_q} \frac{\bar{c}}{2V} q \quad (4.12a)$$

$$C_m = C_{m_0} + C_{m_\alpha} \alpha + C_{m_{\delta_e}} \delta_e + C_{m_q} \frac{\bar{c}}{2V} q \quad (4.12b)$$

- Lateral/Directional Forces and Moments:

The side force, rolling and yawing moment coefficients are functions of the sideslip angle β , the aileron angle δ_a , the rudder angle δ_r , the roll rate p , the yaw rate r and various other parameters:

$$C_Y = f(\beta, \delta_a, \delta_r, p, r, \dots) \quad (4.13a)$$

$$C_l = f(\beta, \delta_a, \delta_r, p, r, \dots) \quad (4.13b)$$

$$C_n = f(\beta, \delta_a, \delta_r, p, r, \dots) \quad (4.13c)$$

¹The coefficients relative to pitch rate q are multiplied by $\frac{\bar{c}}{2V}$ in order to obtain a dimensionless coefficient, V being the TAS (True Airspeed).

For the same reasons as before, the side force, the rolling and yawing moments are written as linear combinations of the previously defined parameters.

$$C_Y = C_{Y_\beta} \beta + C_{Y_{\delta_a}} \delta_a + C_{Y_{\delta_r}} \delta_r + (C_{Y_p} p + C_{Y_r} r) \frac{b}{2V} \quad (4.14a)$$

$$C_l = C_{l_\beta} \beta + C_{l_{\delta_a}} \delta_a + C_{l_{\delta_r}} \delta_r + (C_{l_p} p + C_{l_r} r) \frac{b}{2V} \quad (4.14b)$$

$$C_n = C_{n_\beta} \beta + C_{n_{\delta_a}} \delta_a + C_{n_{\delta_r}} \delta_r + (C_{n_p} p + C_{n_r} r) \frac{b}{2V} \quad (4.14c)$$

- Drag force:

The drag coefficient is calculated as a function of the angle of attack α , the Mach number M , the elevator angle δ_e and the pitch rate q . Despite assuming small angle manoeuvres, a linear approximation can not be used as the drag is greatly affected by viscous effects. The drag is thus modelled with a quadratic relation with the lift coefficient and a sum of the increments in drag due to lifting surfaces deflections.

$$C_D = C_{D_0} + \frac{1}{\pi e AR} (C_L - C_{L_0})^2 + C_{D_{\delta_e}} + C_{D_{\delta_a}} + C_{D_{\delta_r}} \quad (4.15)$$

Where C_{D_0} is the zero lift drag coefficient, e , the Oswald efficiency coefficient, AR the wing aspect ratio, C_{L_0} the minimum drag lift, and $C_{D_{\delta_e}}$, $C_{D_{\delta_a}}$, $C_{D_{\delta_r}}$ the drag increments due to control deflections.

4.2.1.2 Air Data

This subsystems evaluates the angle of attack, sideslip angle and true airspeed of the aircraft as shown on Figure 4.8.

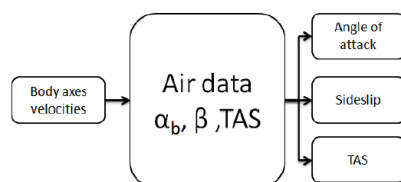


FIGURE 4.8: Air Data Subsystem[9].

4.2.1.3 Atmosphere

This subsystem represents the atmosphere in which the simulation is done, as shown on Figure 4.9. It is made of a block provided by Cranfield University evaluating the Pressure, Temperature, Density and Speed of sound for a off-ISA atmosphere. This block has been augmented to output the True Air Speed (TAS), dynamic pressure and Mach Number.

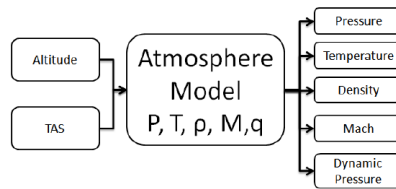


FIGURE 4.9: Atmosphere Subsystem[9].

4.2.1.4 Gravitational Forces and Moments

The theory behind this block has been detailed in previous sections. It evaluates the gravitational forces and moments acting on the aircraft with as input the mass properties and the Direction Cosine Matrix, as shown on Figure 4.10

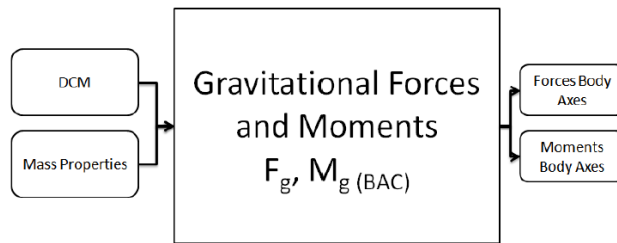


FIGURE 4.10: Gravitational Forces and Moments Subsystem[9].

4.2.1.5 Mass Properties

The mass properties are constant throughout the simulations. Thus, the mass properties block is a constant block from the MATLAB workspace.

4.2.2 Model Assumptions and Simplifications

Due to the high complexity of air vehicle simulations as well as time and computational restrictions, a number of assumption and simplifications have been taken during the 6 DoF model development:

4.2.2.1 Aerodynamic Block Assumptions and Simplifications

- The operating true airspeed of the aircraft is assumed to be between 5.1m/s and 17m/s.
- The VLM is accurate only considering small angle manoeuvres, so the body angle of attack is taken from -5 to 8 degrees, the sideslip angle from -10 to 10 degrees and the control deflections from -25 to 25 degrees.
- The aerodynamic forces and moments coefficients are calculated with linear approximations except for the Drag coefficient which uses a second order polynomial relation with the lift coefficient.
- The motor is not modelled.

4.2.2.2 Other Assumptions and Simplifications

- The Equations of motion equations developed in the previous chapter assume a symmetric aircraft. However, depending on the loading case, the aircraft centre of gravity may not be aligned with the geometric axis of symmetry of the aircraft.
- No ground effect is modelled and the aircraft starts it flight from an initial position at a given altitude and airspeed.
- Atmospheric turbulences are not modelled.
- The airframe is rigid.

4.2.3 Model Testing

The 6 DoF model is implemented and tested to verify that it runs without any error. All rotational rates and Euler angles are set to zero and the flight conditions are defined in Table 4.2 (The control deflections are fixed to constants throughout the simulation).

	δ_e (°)	δ_a (°)	δ_r (°)	H_p (m)	EAS (m/s)
Initial Values	-2	1	0	91.44	10

TABLE 4.2: Model Testing Initial Flight Conditions.

As the model is not trimmed, the aircraft is expected to exhibit the following flight characteristics:

- The value of elevator will create a negative pitching moment which will make the aircraft to enter a decent in the first place, gain airspeed, and stabilise itself at an altitude level for a few seconds. It will subsequently loose airspeed due to the lack of thrust and enter a new decent. This process will repeat cyclically until the aircraft touches the ground;
- The non trimmed aileron will create a bank angle inducing a sideslip angle;
- The sideslip angle will introduce a yawing moment. This yaw-roll coupling will make the aircraft enter in a spiral;
- Eventually due to the high bank angle, the aircraft will not be able to generate enough lift to stabilise itself at an altitude level and will keep descending with an increasing decent rate.

Figures 4.11 and 4.12 show the flight trajectory of the aircraft relative to Earth.

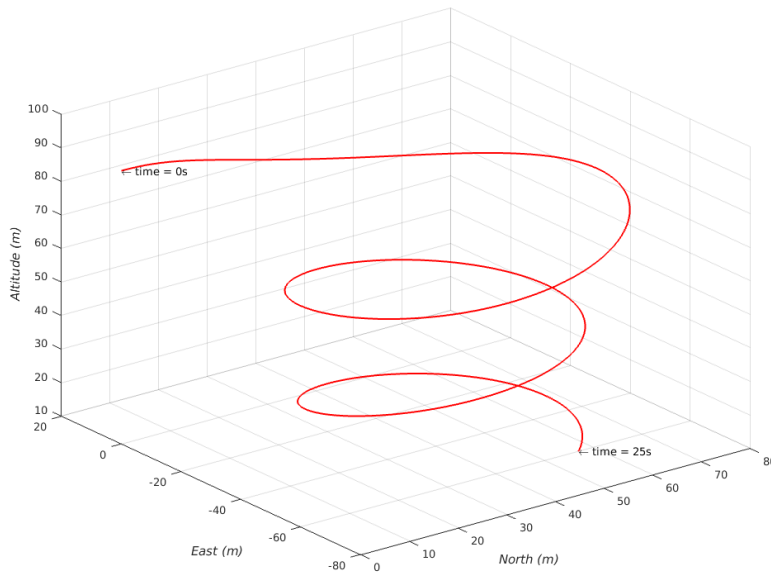


FIGURE 4.11: Test Model Flight Trajectory.

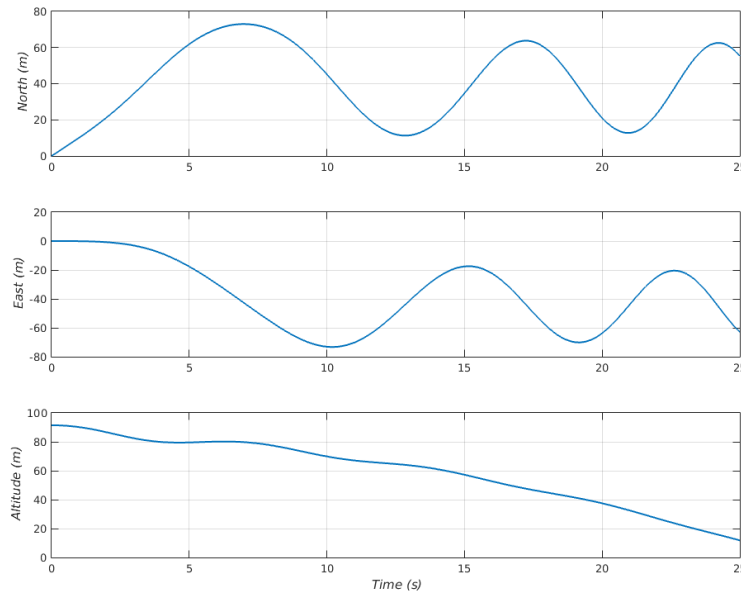


FIGURE 4.12: Earth Axes Reference Test Position.

4.3 Model Trimming

The main dynamic modes of the aircraft are simulated and validated in subsequent chapters. This requires an initial steady and straight flight configuration before applying the perturbation that will excite each dynamic mode. Therefore, the

aircraft is trimmed in a steady straight flight, whose the characteristics are defined as follows:

- The True Airspeed is fixed to constant;
- As the thrust is not modelled, the altitude is free to decrease;
- The rotational rates ($[p, q, r]$) are fixed to zero;
- The aircraft is constrained to head North.

As the rotational rates are fixed to zero, the dynamics of the aircraft are non existent. The equations of motion could then be simplified to the effects of aerodynamics and gravitational forces solely. This translates into the following equations:

$$\begin{aligned} X_{aero}(\delta_e, \alpha, \delta_a, \delta_r) + X_{grav_b}(\theta) &= 0 \\ Y_{aero}(\beta, \delta_a, \delta_r) &= 0 \\ Z_{aero}(\delta_e, \alpha, \delta_a, \delta_r) + Z_{grav_b}(\theta) &= 0 \\ L_{aero}(\alpha, \delta_a, \delta_r) &= 0 \\ M_{aero}(\alpha, \delta_e) + M_{grav_b}(\theta) &= 0 \\ N_{aero}(\alpha, \delta_a, \delta_r) &= 0 \end{aligned} \tag{4.16}$$

Considering the equations governing the air data acquisition,

$$\begin{aligned} U &= V_0 \cos \alpha \cos \beta \\ V &= V_0 \sin \beta \\ W &= V_0 \sin \alpha \cos \beta \\ \theta &= \alpha + \gamma \end{aligned} \tag{4.17}$$

This leads to a system of 11 ($\alpha, \beta, \gamma, \theta, \delta_e, \delta_a, \delta_r, U, V, W$) non linear equations. These equations have been solved using the MATLAB trim function.

Here is presented the trimming results using the MATLAB trim function at an airspeed of 10 m/s. Results are summarised in Table 4.3. This trimming procedure has been repeated at various airspeeds when doing the discussion on the dynamic modes characteristics and the model validation.

Verification of those values have been carried out for 200 seconds and the results are shown in Figures 4.13, 4.14 and 4.15.

	δ_e (°)	δ_a (°)	δ_r (°)
Trim Values	-1.01	-0.01	0.03

TABLE 4.3: MATLAB trim Function Trimming Results.

The MATLAB trim function leads to flight angles and Euler angles which are summarised in Table 4.4.

	α (°)	β (°)	ϕ (°)	θ (°)	ψ (°)
Trim Values	-1.842	0	0.004	-0.100	1.000

TABLE 4.4: MATLAB trim Function States Results.

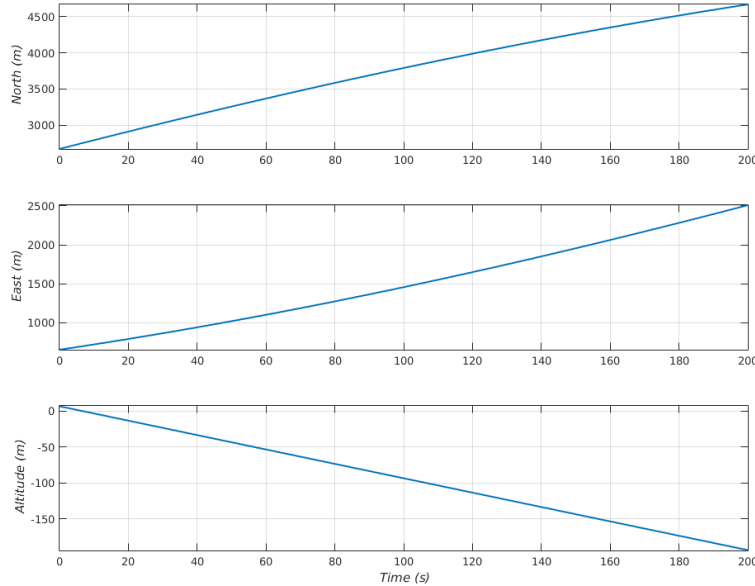


FIGURE 4.13: Earth Axes Reference Trimmed Position.

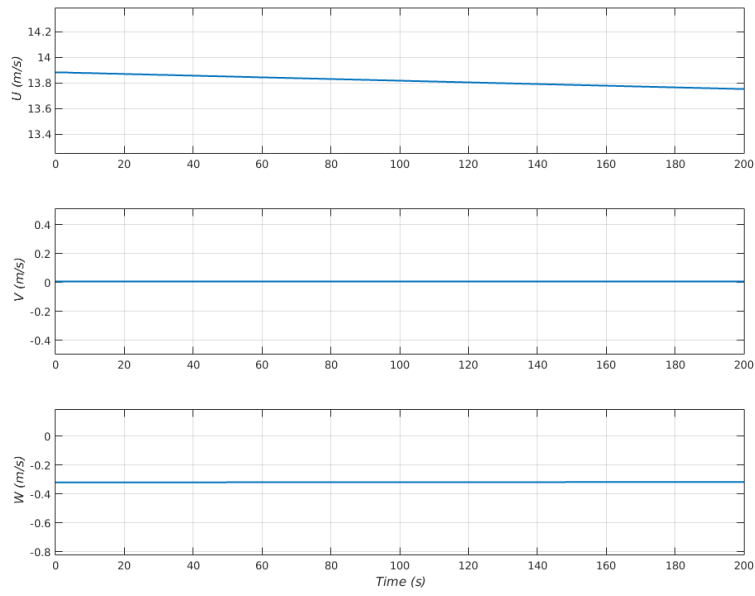


FIGURE 4.14: Trimmed Model Body Axes Reference Velocities.

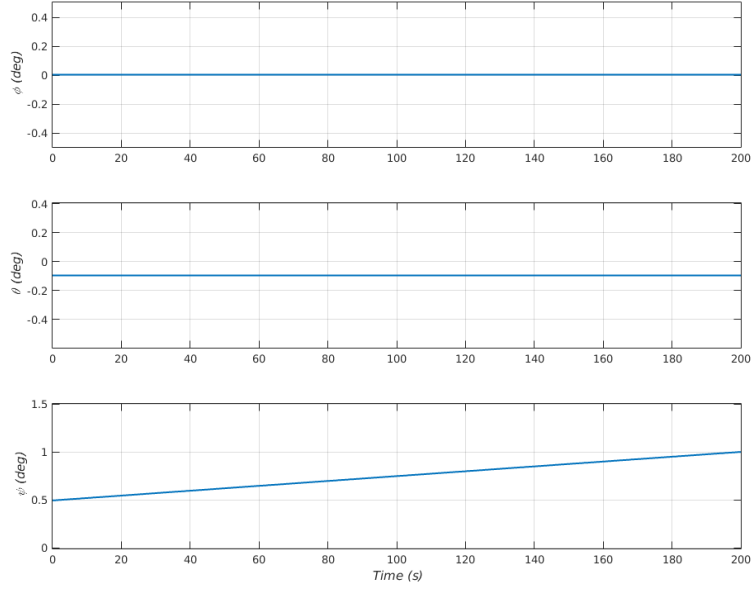


FIGURE 4.15: Trimmed Model Euler Angles.

4.4 Model Linearisation

The model presents non linearities as non linear functions have been used during its development. As input disturbances from trim values are generally of small amplitude, a linear model would be a good approximation to the full simulation

model. In addition, a linear model would allow to simulate aircraft response with less computational time. Furthermore, it would allow an analytical analysis leading to dynamic modes characteristics (eigenvalues, damping ratio, frequency, time constant) without the use of graphical methods.

4.4.1 Linearisation and Decoupling Methodology

The linear model is defined in the state space representation. The state space representation is a mathematical model of a dynamic system as a set of input, output and state variables related by first-order differential equations. This formulation could then be used to produce a set of transfer function linking each of the system outputs to each of the inputs.

$$\begin{aligned}\dot{\mathbf{x}}(t) &= A\mathbf{x}(t) + B\mathbf{u}(t) \\ \mathbf{y}(t) &= C\mathbf{x}(t) + D\mathbf{u}(t)\end{aligned}\tag{4.18}$$

where,

$$\dot{\mathbf{x}} = \begin{bmatrix} \dot{u} \\ \dot{v} \\ \dot{w} \\ \dot{p} \\ \dot{q} \\ \dot{r} \\ \dot{\phi} \\ \dot{\theta} \\ \dot{\psi} \end{bmatrix} \quad \mathbf{y} = \begin{bmatrix} u \\ v \\ w \\ p \\ q \\ r \\ \phi \\ \theta \\ \psi \end{bmatrix} \quad \mathbf{u} = \begin{bmatrix} \delta_e \\ \delta_a \\ \delta_r \end{bmatrix} \tag{4.19}$$

The coupled matrices A, B, C and D are defined in Equation 4.20. The matrix elements marked in red are those related to the longitudinal motion, those in green are related to the lateral and directional motion.

$$A = \begin{bmatrix} x_u & 0 & x_w & 0 & x_q & 0 & 0 & x_\theta & 0 \\ 0 & y_v & 0 & y_p & 0 & y_r & y_\phi & 0 & y_\psi \\ z_u & 0 & z_w & 0 & z_q & 0 & 0 & z_\theta & 0 \\ 0 & l_v & 0 & l_p & 0 & l_r & l_\phi & 0 & l_\psi \\ m_u & 0 & m_w & 0 & m_q & 0 & 0 & m_\theta & 0 \\ 0 & n_v & 0 & n_p & 0 & n_r & n_\phi & 0 & n_\psi \\ 0 & 0 & 0 & 1 & 0 & 0 & 0 & 0 & 0 \\ 0 & 0 & 0 & 0 & 1 & 0 & 0 & 0 & 0 \\ 0 & 0 & 0 & 0 & 0 & 1 & 0 & 0 & 0 \end{bmatrix}$$

$$B = \begin{bmatrix} x_{\delta_e} & 0 & 0 \\ 0 & y_{\delta_a} & y_{\delta_r} \\ z_{\delta_e} & 0 & 0 \\ 0 & l_{\delta_a} & l_{\delta_r} \\ m_{\delta_e} & 0 & 0 \\ 0 & n_{\delta_a} & n_{\delta_r} \\ 0 & 0 & 0 \\ 0 & 0 & 0 \\ 0 & 0 & 0 \end{bmatrix} \quad (4.20)$$

$$C = \begin{bmatrix} 1 & 0 & 0 & 0 & 0 & 0 & 0 & 0 & 0 \\ 0 & 1 & 0 & 0 & 0 & 0 & 0 & 0 & 0 \\ 0 & 0 & 1 & 0 & 0 & 0 & 0 & 0 & 0 \\ 0 & 0 & 0 & 1 & 0 & 0 & 0 & 0 & 0 \\ 0 & 0 & 0 & 0 & 1 & 0 & 0 & 0 & 0 \\ 0 & 0 & 0 & 0 & 0 & 0 & 1 & 0 & 0 \\ 0 & 0 & 0 & 0 & 0 & 0 & 0 & 1 & 0 \\ 0 & 0 & 0 & 0 & 0 & 0 & 0 & 0 & 1 \\ 0 & 0 & 0 & 0 & 0 & 0 & 0 & 0 & 0 \end{bmatrix}$$

The matrix D is a matrix of zeros with 9 lines and 3 columns.

The elements of matrices A and B are the concise aerodynamic derivatives of the aircraft. As the elements of the matrices neither related to longitudinal motion

nor to lateral motion are of negligible size when compared to the others, the state space representation of the linear model could be decoupled. The matrices A, B, C and D for each case are:

- Longitudinal Dynamics:

$$A = \begin{bmatrix} x_u & x_w & x_q & x_\theta \\ z_u & z_w & z_q & z_\theta \\ m_u & m_w & m_q & m_\theta \\ 0 & 0 & 1 & 0 \end{bmatrix} \quad B = \begin{bmatrix} x_{\delta_e} \\ z_{\delta_e} \\ m_{\delta_e} \\ 0 \end{bmatrix} \quad C = I^{4 \times 4} \quad D = 0^{4 \times 1} \quad (4.21)$$

- Lateral/Directional Dynamics:

$$A = \begin{bmatrix} y_v & y_p & y_r & y_\phi & y_\psi \\ l_v & l_p & l_r & l_\phi & l_\psi \\ n_v & n_p & n_r & n_\phi & n_\psi \\ 0 & 1 & 0 & 0 & 0 \\ 0 & 0 & 1 & 0 & 0 \end{bmatrix} \quad B = \begin{bmatrix} y_{\delta_a} & y_{\delta_r} \\ l_{\delta_a} & l_{\delta_r} \\ n_{\delta_a} & n_{\delta_r} \\ 0 & 0 \\ 0 & 0 \end{bmatrix} \quad C = I^{5 \times 5} \quad D = 0^{5 \times 2} \quad (4.22)$$

4.4.2 Linear Model Modal Analysis

The analysis of the eigenvalues values of the model is an easy way of assessing the dynamic modes of the aircraft. This analysis has been done for equivalent airspeeds (EAS) from 6m/s to 16m/s and the results for the Short Period Pitching Oscillations, Phugoid, Dutch Roll and Roll mode are presented in the subsequent sub-sections. The SPPO has been analysed at different CG positions as well.

4.4.2.1 Short Period Pitching Oscillations (SPPO)

The SPPO is a damped oscillation in pitch with a frequency of approximately 16 to 20 rad/s for light fixed wing hobby aircrafts. The principal variables are pitch attitude θ and pitch rate q with airspeed V_e remaining largely constant. Solving

Equation 4.18 in the longitudinal sense as described in 4.21 in order to obtain the eigenvalues of the system gives:

$$s^2 - (m_q + z_w)s + (m_q z_w - m_w V_e) = s^2 + 2\zeta_s \omega_s s + \omega_s^2 = 0 \quad (4.23a)$$

thus,

$$2\zeta_s \omega_s \approx -(m_q + z_w) \quad (4.23b)$$

$$\omega_s \approx \sqrt{m_q z_w - m_w V_e} \quad (4.23c)$$

It should be noted that for similar airplanes, the parameters m_q , z_w and m_w are generally real negative[23]. Thus by increasing the airspeed, the SPPO frequency should increase and the damping ratio behaviour is less predictable. The effect of the airspeed on the linear model SPPO characteristics is summarised in Table 4.5².

EAS (m/s)	6	8	10	12	14	16
Frequency (rad/s)	8.44	11.2	14	16.7	19.5	22.3
Damping Ratio	0.638	0.636	0.635	0.635	0.634	0.634

TABLE 4.5: SPPO Airspeed Effects of the Linearised Model

As expected, the frequency of the SPPO of the linearised model increases with the airspeed while the damping ratio remains constant throughout the flight envelope.

The effect on modal characteristics of the SPPO of the centre of gravity position has been studied too and the results are presented in Table 4.6³.

CG (% MAC)	11.70	17.19	24.35	25.46
Frequency (rad/s)	14.0	13.7	13.1	13.0
Damping Ratio	0.635	0.658	0.722	0.732

TABLE 4.6: SPPO CG Position Effects of the Linearised Model

Bringing the centre of gravity further behind the BAC slightly reduces the natural frequency of the SPPO, and there is a high increase in the damping coefficient of

²These values are at constant CG position, CG = 11.70% MAC.

³These values are at constant equivalent airspeed, EAS = 10m/s.

the aircraft. However, this might destabilise the aircraft if the CG goes behind the centre of pressure of the wings.

4.4.2.2 Phugoid

The Phugoid is a low frequency oscillation in speed. The principal variables are pitch attitude θ , airspeed V_e and altitude h . It is generally very lightly damped. Cook[7] shows that:

$$w_p \approx \sqrt{\frac{\rho_a g S_w C_L}{m}} \approx \frac{g\sqrt{2}}{V_0} \quad (4.24a)$$

$$\zeta_p \approx \frac{1}{\sqrt{2}} \left(\frac{C_D}{C_L} \right) \quad (4.24b)$$

Thus the Phugoid natural frequency is inversely proportional to the initial airspeed V_0 and the damping coefficient is a function of the lift and drag coefficients. Increasing the airspeed increases both the lift and drag coefficients and makes the effect of the airspeed on the damping ratio less predictable. The effect of the airspeed on the linear model Phugoid characteristics is summarised in Table 4.7.

EAS (m/s)	6	8	10	12	14	16
Frequency (rad/s)	0.806	0.812	0.817	0.815	0.814	0.815
Damping Ratio	-0.0736	-0.0160	-0.0017	0.0286	0.0491	0.0602

TABLE 4.7: Phugoid Airspeed Effects of the Linearised Model.

The linear model Phugoid is unstable at airspeeds less than 12m/s (negative damping ratio) and its natural frequency is not equal to the one theoretically predicted by Equations 4.24. The unstable Phugoid is due to the CG position in the model⁴ and the theoretical estimates are assuming a stable Phugoid.

4.4.2.3 Dutch Roll

The Dutch Roll is a classical damped oscillation in yaw, which couples into roll. The Dutch Roll is the lateral/directional equivalent of the SPPO and the principal

⁴Other CG positions have been tested with and give a stable Phugoid.

variables are yaw attitude ψ , roll attitude ϕ , and yaw rate r and roll rate p with airspeed V_e remaining largely constant. Solving Equation 4.18 in the lateral sense as described in 4.22 in order to obtain the eigenvalues of the system gives:

$$s^2 - (n_r + y_v)s + (n_r y_v - n_v y_r) = s^2 + 2\zeta_s \omega_d s + \omega_d^2 = 0 \quad (4.25a)$$

thus,

$$2\zeta_d \omega_d \approx -(n_r + y_v) \quad (4.25b)$$

$$\omega_d \approx \sqrt{n_r y_v - n_v y_r} \quad (4.25c)$$

The effect of the airspeed on the individual parameters n_r , y_v , n_v and y_r is not straightforward, but by introducing the concept of dimensional aerodynamic stability derivatives, Cook[7] proved that the Dutch Roll natural frequency squared is directly proportional to the airspeed ($\omega_d^2 \propto V_0$). Thus by increasing the airspeed, the Dutch Roll frequency should increase and the damping ratio behaviour is less predictable. The effect of the airspeed on the linear model Dutch Roll characteristics is summarised in Table 4.8.

EAS (m/s)	6	8	10	12	14	16
Frequency (rad/s)	4.33	5.44	6.61	7.80	8.99	10.20
Damping Ratio	0.109	0.136	0.151	0.160	0.166	0.169

TABLE 4.8: Dutch Roll Airspeed Effects of the Linearised Model.

As expected, the frequency of the Dutch Roll of the linearised model increases with the airspeed through the flight envelope while the damping ratio highly increases until airspeeds of around 12m/s before settling to a relatively constant value.

4.4.2.4 Roll Mode

The Roll mode is a non oscillatory lateral mode which is decoupled from the Dutch Roll. It is generally represented by a exponential lag in rolling motion with time constant T_r . It is proved that the time constant of the Roll mode can be written as[7]:

$$T_r \approx -\frac{1}{l_p} \quad (4.26)$$

The effect of the airspeed on the linear model Roll mode characteristics is summarised in Table 4.9.

EAS (m/s)	6	8	10	12	14	16
Time Constant (s)	0.0534	0.0403	0.0323	0.0270	0.0231	0.0203

TABLE 4.9: Roll Mode Airspeed Effects of the Linearised Model.

The time constant of the Roll mode of the linearised model slightly decreases with the airspeed through the flight envelope. Increasing the airspeed means increasing the lift generated by the wings, thus greater wing loading. It then requires less time to create a rolling moment on the aircraft, meaning a lower roll mode time constant.

Chapter 5

System Identification Methodology

This chapter presents the system identification procedure developed for the Easystar II, which is applicable to any conventional fixed aircraft with an elevator, a rudder, ailerons and a throttle stick. It follows the system identification process presented in the literature review (Figure 2.12). All state space representation development and reduced order models are derived from Michael V. Cook's equations in the second edition of his book: *Flight Dynamics Principles*[7].

5.1 Model Postulation and Structure Determination

The model postulation is based on the knowledge of the aircraft dynamics. A linear coupled dynamic model of the aircraft in the longitudinal and lateral directions is considered. The linear model is defined in the state space representation:

$$\begin{aligned}\dot{\mathbf{x}}(t) &= A\mathbf{x}(t) + B\mathbf{u}(t) \\ \mathbf{y}(t) &= C\mathbf{x}(t) + D\mathbf{u}(t)\end{aligned}\tag{5.1a}$$

where,

$$\dot{\mathbf{x}} = \begin{bmatrix} \dot{u} \\ \dot{v} \\ \dot{w} \\ \dot{p} \\ \dot{q} \\ \dot{r} \\ \dot{\phi} \\ \dot{\theta} \\ \dot{\psi} \end{bmatrix} \quad \mathbf{y} = \begin{bmatrix} u \\ v \\ w \\ p \\ q \\ r \\ \phi \\ \theta \\ \psi \end{bmatrix} \quad \mathbf{u} = \begin{bmatrix} \delta_e \\ \delta_a \\ \delta_r \\ \tau \end{bmatrix} \quad (5.1b)$$

The aircraft instrumentation logs the states, outputs and inputs, except for the forward, lateral and vertical speeds. These speeds are defined as:

$$u = v_e \cos(\alpha) \cos(\beta) \quad (5.2a)$$

$$v = v_e \sin(\beta) \quad (5.2b)$$

$$w = v_e \sin(\alpha) \cos(\beta) \quad (5.2c)$$

where v_e is the disturbance in airspeed, α and β respectively the disturbance in angle of attack and sideslip angle from a trimmed position. The aircraft instruments does not log α and β but following the methodology presented by O. Castillo[24] for small angle perturbations:

$$\alpha = \theta - \tan^{-1} \left(\frac{V_D}{\sqrt{V_N^2 + V_E^2}} \right) \quad (5.3a)$$

$$\beta = \psi - \tan^{-1} \left(\frac{V_E}{V_N} \right) \quad (5.3b)$$

where V_N , V_E and V_D are the aircraft velocity components pointing Northwards, Eastwards, downward respectively. In our case, it is assumed that the aircraft

during the test is heading North with no down speed. Thus,

$$\alpha = \theta \quad (5.4a)$$

$$\beta = \psi \quad (5.4b)$$

and

$$u = v_e \cos(\theta) \cos(\psi) \quad (5.4c)$$

$$v = v_e \sin(\psi) \quad (5.4d)$$

$$w = v_e \sin(\theta) \cos(\psi) \quad (5.4e)$$

In order to simplify the system identification problem, the state space representation of the aircraft dynamics is decoupled in longitudinal and lateral/directional dynamics respectively.

5.1.1 Longitudinal Dynamics

The longitudinal dynamics state space representation equations of the aircraft are:

$$\begin{aligned} \dot{\mathbf{x}}(t) &= A\mathbf{x}(t) + B\mathbf{u}(t) \\ \mathbf{y}(t) &= C\mathbf{x}(t) + D\mathbf{u}(t) \end{aligned} \quad (5.5a)$$

where,

$$\dot{\mathbf{x}} = \begin{bmatrix} \dot{u} \\ \dot{w} \\ \dot{q} \\ \dot{\theta} \end{bmatrix} \quad \mathbf{y} = \begin{bmatrix} u \\ w \\ q \\ \theta \end{bmatrix} \quad \mathbf{u} = \begin{bmatrix} \delta_e \\ \tau \end{bmatrix} \quad (5.5b)$$

and,

$$A = \begin{bmatrix} x_u & x_w & x_q & x_\theta \\ z_u & z_w & z_q & z_\theta \\ m_u & m_w & m_q & m_\theta \\ 0 & 0 & 1 & 0 \end{bmatrix} \quad B = \begin{bmatrix} x_{\delta_e} & x_\tau \\ z_{\delta_e} & z_\tau \\ m_{\delta_e} & m_\tau \\ 0 & 0 \end{bmatrix} \quad C = I^{4 \times 4} \quad D = 0^{4 \times 2} \quad (5.5c)$$

The aim of the system identification in the case of the longitudinal dynamics is then to estimate the parameters elements of the matrices A and B , with a sufficient confidence interval. As there are many parameters to estimates at once, in order to simplify further the problem, a reduced order model is considered for the Short Period Pitching Oscillations.

5.1.1.1 Short Period Pitching Oscillations (SPPO)

The Short Period Pitching Oscillations, as shown in Figure 5.1, are highly damped oscillations at a high frequency of the aircraft in the longitudinal sense. High changes in angle of attack and pitch rate are characteristics of this dynamic mode. An elevator impulse is required to excite the SPPO.

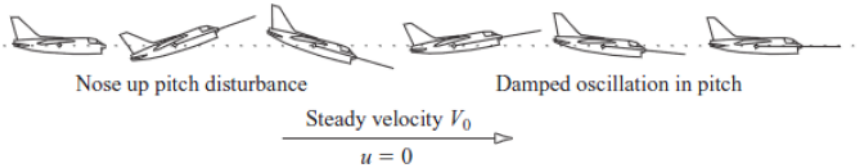


FIGURE 5.1: SPPO Illustration[7].

The reduced order state space representation of the SPPO dynamics is thus:

$$\begin{bmatrix} \dot{w} \\ \dot{q} \end{bmatrix} = \begin{bmatrix} z_w & z_q \\ m_w & m_q \end{bmatrix} \begin{bmatrix} w \\ q \end{bmatrix} + \begin{bmatrix} z_{\delta_e} & z_\tau \\ m_{\delta_e} & m_\tau \end{bmatrix} \begin{bmatrix} \delta_e \\ \tau \end{bmatrix} \quad (5.6)$$

This reduced order model allows to estimate some of the parameters with the correct input, as the aircraft response is expected. In addition, some of the parameters in Equation 5.5c are known to have constant values for all aircraft (acceleration of gravity for example). Having obtained the parameters from the SPPO reduced

order model and the constant parameters, a suitable parameter estimation process can be applied to a data set with a well designed input to the overall longitudinal dynamics model and the other parameters can be estimated. The models used for estimating each of the parameters for the longitudinal dynamics are summarised in Table 5.1.

Parameters	Model	Value
x_u	Global Longitudinal	-
x_w	Global Longitudinal	-
x_q	Global Longitudinal	-
x_θ	Constant	$-g$
z_u	Global Longitudinal	-
z_w	SPPO	-
z_q	SPPO	-
z_θ	Global Longitudinal	-
m_u	Global Longitudinal	-
m_w	SPPO	-
m_q	SPPO	-
m_θ	Constant	0
x_{δ_e}	Global Longitudinal	-
x_τ	Global Longitudinal	-
z_{δ_e}	SPPO	-
z_τ	SPPO	-
m_{δ_e}	SPPO	-
m_τ	SPPO	-

TABLE 5.1: Longitudinal Parameters.

5.1.2 Lateral/Directional Dynamics

The lateral/directional dynamics state space representation equations of the aircraft are:

$$\begin{aligned}\dot{\mathbf{x}}(t) &= A\mathbf{x}(t) + B\mathbf{u}(t) \\ \mathbf{y}(t) &= C\mathbf{x}(t) + D\mathbf{u}(t)\end{aligned}\tag{5.7a}$$

where,

$$\dot{\mathbf{x}} = \begin{bmatrix} \dot{v} \\ \dot{p} \\ \dot{r} \\ \dot{\phi} \\ \dot{\psi} \end{bmatrix} \quad \mathbf{y} = \begin{bmatrix} v \\ p \\ r \\ \phi \\ \psi \end{bmatrix} \quad \mathbf{u} = \begin{bmatrix} \delta_a \\ \delta_r \end{bmatrix} \quad (5.7b)$$

and,

$$A = \begin{bmatrix} y_v & y_p & y_r & y_\phi & y_\psi \\ l_v & l_p & l_r & l_\phi & l_\psi \\ n_v & n_p & n_r & n_\phi & n_\psi \\ 0 & 1 & 0 & 0 & 0 \\ 0 & 0 & 1 & 0 & 0 \end{bmatrix} \quad B = \begin{bmatrix} y_{\delta_a} & y_{\delta_r} \\ l_{\delta_a} & l_{\delta_r} \\ n_{\delta_a} & n_{\delta_r} \\ 0 & 0 \\ 0 & 0 \end{bmatrix} \quad C = I^{5 \times 5} \quad D = 0^{5 \times 2} \quad (5.7c)$$

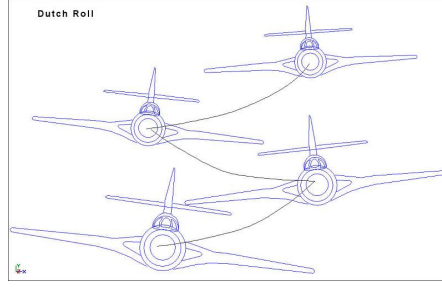
As for the longitudinal dynamics, the system identification in the case of the lateral/directional dynamics aims to estimate the parameters elements of the matrices A and B , with a sufficient confidence interval. As there are many parameters to estimates at once, in order to simplify further the problem, reduced order models are considered for the Dutch Roll and the Roll Mode.

5.1.2.1 Dutch Roll

The Dutch Roll, as shown in Figure 5.2, is a highly damped coupled oscillatory mode in yaw and roll of the aircraft. A rudder perturbation introduces a motion in yaw. The aerodynamic loads acting on the vertical fin are mostly responsible for the damping and stiffness of the Dutch Roll. However, oscillations in yaw will introduce oscillations in roll as well. This is due to both the dihedral characteristics of the aircraft and the fact that the relative airspeed will increase over one wing and decrease over the other. In order to excite the Dutch Roll, a series rudder doublet input is produced at a frequency close to the Dutch Roll natural frequency.

The reduced order state space representation of the Dutch Roll dynamics is thus:

¹<http://rcuniverse.com>.

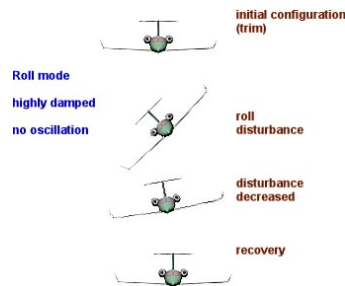
FIGURE 5.2: Dutch Roll Illustration¹.

$$\begin{bmatrix} \dot{v} \\ \dot{r} \end{bmatrix} = \begin{bmatrix} y_v & y_r \\ n_v & n_r \end{bmatrix} \begin{bmatrix} v \\ r \end{bmatrix} + \begin{bmatrix} y_{\delta_a} & y_{\delta_r} \\ n_{\delta_a} & n_{\delta_r} \end{bmatrix} \begin{bmatrix} \delta_a \\ \delta_r \end{bmatrix} \quad (5.8)$$

This Dutch Roll reduced order model allows to estimate the parameters in Equation 5.8.

5.1.2.2 Roll Mode

The roll mode, as shown in Figure 5.3, is a non oscillatory lateral response of the aircraft. From a straight steady flight, an aileron input creates a rolling moment as one wing produces more lift than the other. The roll rate increases exponentially until it reaches a relatively constant value. The roll mode is excited by a small ailerons step.

FIGURE 5.3: Roll Mode illustration².

The reduced order state space representation of the roll mode dynamics is thus:

$$\begin{bmatrix} \dot{p} \\ \dot{\phi} \end{bmatrix} = \begin{bmatrix} l_p & l_\phi \\ 1 & 0 \end{bmatrix} \begin{bmatrix} p \\ \phi \end{bmatrix} + \begin{bmatrix} l_{\delta_a} & l_{\delta_r} \\ 0 & 0 \end{bmatrix} \begin{bmatrix} \delta_a \\ \delta_r \end{bmatrix} \quad (5.9)$$

²From <http://people.rit.edu>

The roll mode reduced order model allows to estimate the parameters in Equation 5.9. Just as the longitudinal model, some of the parameters in Equation 5.7c are known to have constant values. Having obtained the parameters from the Dutch Roll and roll mode reduced order models and the constant parameters, a suitable parameter estimation process can be applied to a data set with a well designed input to the overall lateral/directional dynamics model and the other parameters can be estimated. The models used for estimating each of the parameters for the lateral/directional dynamics are summarised in Table 5.2.

Parameters	Model	Value
y_v	Dutch Roll	-
y_p	Global Lateral	-
y_r	Dutch Roll	-
y_ϕ	Constant	g
y_ψ	Constant	0
l_v	Global Lateral	-
l_p	Roll Mode	-
l_r	Global Lateral	-
l_ϕ	Constant	0
l_ψ	Constant	0
n_v	Dutch Roll	-
n_p	Global Lateral	-
n_r	Dutch Roll	-
n_ϕ	Constant	0
n_ψ	Constant	0
y_{δ_a}	Dutch Roll	-
y_{δ_r}	Dutch Roll	-
l_{δ_a}	Roll Mode	-
l_{δ_r}	Roll Mode	-
n_{δ_a}	Dutch Roll	-
n_{δ_r}	Dutch Roll	-

TABLE 5.2: Lateral/Directional Parameters.

5.2 Experiment Design

5.2.1 Experimental Set-up

The tests are planned to be carried out in the 8×4 atmospheric boundary layer wind tunnel of Cranfield University wind tunnel facilities. The wind tunnel is a

low speed open return tunnel, with a flow speed range of 5m/s to 17m/s.

The aircraft is held by four 70cm long strings in order to avoid it touching the wind tunnel walls.

A first series of flight test is carried out outdoor as the aircraft is ready before the arrangements for the the wind tunnel. Afterwards, a series of dynamic wind tunnel tests is planned to be done in the 8×4 wind tunnel. The test procedure is the same for both the flight testing and the wind tunnel test and is subsequently described.

5.2.2 Test Procedure

5.2.2.1 Pre-Flight Check

Before performing any testing, the aircraft, the ground station software and the telemetry are checked. It consists of the following steps:

- Full charge of the battery;
- Check of the propulsion and the control surfaces deflections.
- Check of the telemetry and ground software;
- Check of the data logging by saving and processing mock data;
- Wiping the memory of the data logging SD-card.

In case any anomaly is detected, the fault is either corrected or the test postponed.

A RC-plane test pilot was required for all pre-test and actual flight/wind tunnel test. His role is to take off, fly the aircraft, trim it to the required airspeed and altitude, perform the correct inputs to the control surfaces and safely return the aircraft to the ground station. He also provides assistance in setting up of the aircraft and the pre-flight check, with his previous experience with RC-planes.

The tasks for the flight/wind tunnel test are defined during the pre-flight test and the inputs required for the test are explained to the test pilot. The team is then divided as:

- Test Engineer 1³: Selects which piece of instrumentation is to be fitted in the aircraft; Communicates the required inputs to the test pilot and takes note of the flight conditions;
- Test Engineer 2⁴: Monitors the ground station software; Records the testing time, the flight conditions, and the test inputs;
- Test Pilot⁵: Flies the aircraft.

5.2.2.2 Flight/Wind Tunnel Test

The procedure for the test is:

- The aircraft is connected to the ground station software and the motor armed;
- The test pilot takes control of the aircraft takes off;
- The test engineer 1 communicates the airspeed and altitude for the test pilot and the test pilot trims the aircraft accordingly;
- The test engineer 2 checks the aircraft trimming at the correct flight conditions on the ground station software.
- The test engineer 1 tells the test pilot what input to perform and when he is ready, the test engineer 2 records the time;
- The test pilot performs the manoeuvre under the supervision of the test engineer 2 who checks the ground station software;
- Once the test is completed, the test engineer 2 records the time;
- The procedure is repeated for all the scheduled inputs;
- After the last test, the test pilot lands the aircraft.

In the case of the wind tunnel test, the test engineer 1 is responsible for setting the wind tunnel speed.

This procedure is illustrated in Figure 5.4.

³Boris Tane, MSc Aerospace Dynamics 2014/2015, Cranfield University

⁴Adnan Asif, MSc Aerospace Dynamics 2014/2015, Cranfield University

⁵Ioannis Katsoulis, Pre-MSc course 2014/2015, Cranfield University

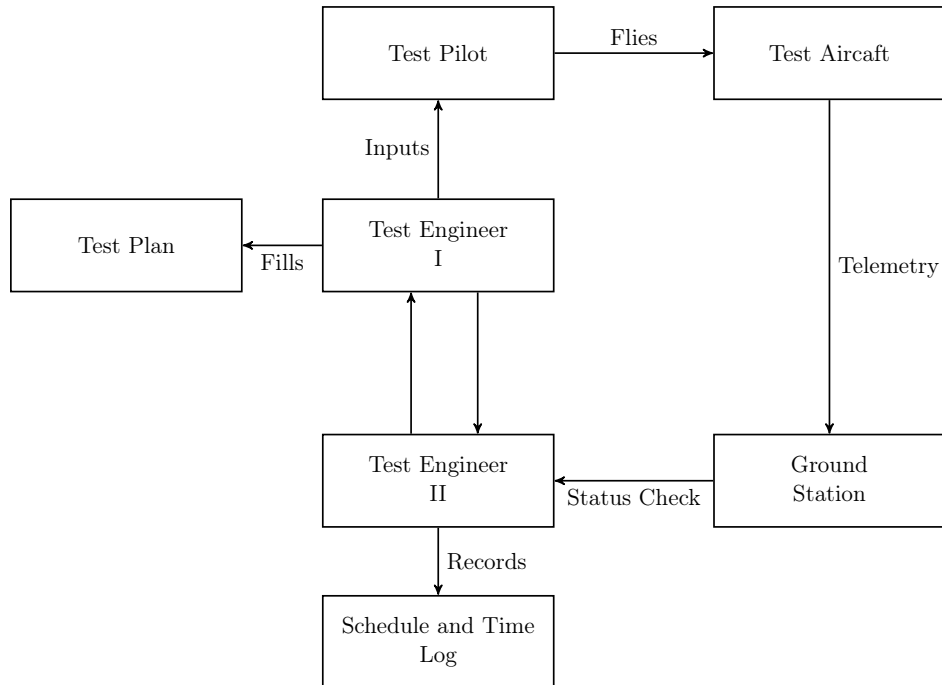


FIGURE 5.4: Flight/Wind Tunnel Test Process.

5.2.3 Flight Test

A first series of flight test sorties are organised. The flight tests are carried out at the amateur RC planes field in Newport Pagnell. In the longitudinal sense, the flight tests consist of Short Period Pitching Oscillations (SPPO) tests and Phugoid tests for the validation and a custom input in order to excite the aircraft in a mode allowing to estimate the remaining parameters. In the lateral/directional sense, the flight tests are Dutch Roll tests and Roll mode tests for the validation and a custom inputs in aileron in order to estimate the remaining parameters. However, the aircraft is flown initially without any instrumentation in order to check the pilot's handling and insure safety during the actual testing.

5.2.3.1 Longitudinal Dynamic Stability

The data required for the longitudinal dynamic stability analysis is the various longitudinal states of the aircraft as well as the elevator input. The tests are done at three different airspeeds, as summarised in Table 5.3.

The SPPO is also tested at different CG positions.

	Input Type		
	SPPO	Phugoid	3-2-1-1 δ_e
Airspeed V_e (m/s)			
6			
10			
16			

TABLE 5.3: Longitudinal Dynamic Stability Analysis Flight Test Matrix.

5.2.3.2 Lateral/Directional Dynamic Stability

The data required for the lateral/directional dynamic stability analysis is the various lateral/directional states of the aircraft as well as the aileron and rudder inputs. The tests are done at three different airspeeds, as summarised in Table 5.4.

	Input Type		
	Dutch Roll	Roll Mode	3-2-1-1 δ_a
Airspeed V_e (m/s)			
6			
10			
16			

TABLE 5.4: Lateral/Directional Dynamic Stability Analysis Flight Test Matrix.

5.2.3.3 Timescale

The dynamic stability analysis testing is planned to last a day. The details of the test scheduling are in Table 5.5.

Test	Duration (minutes)	Number	Total Duration (minutes)
Longitudinal	20	3	60
Lateral/Directional	15	4	60
			120

TABLE 5.5: Dynamic Stability Analysis Flight Test Time-scale.

Due to the lengths of the tests, the flight testing requires three sorties.

5.2.4 Dynamic Wind Tunnel Test

In the longitudinal sense, the wind tunnel tests consist of a Short Period Pitching Oscillations (SPPO) test for the validation and a custom input in order to excite the aircraft in a mode allowing to estimate the remaining parameters. In the lateral/directional sense, the wind tunnel tests are a Dutch Roll and a Roll mode test for the validation and two custom inputs (in aileron and rudder deflection respectively) in order to estimate the remaining parameters.

5.2.4.1 Longitudinal Dynamic Stability

The data required for the longitudinal dynamic stability analysis is the same as for the flight test. The tests are done at three different airspeeds, as summarised in Table 5.6.

	Input Type	
	SPPO	3-2-1-1 δ_e
Airspeed V_e (m/s)		
6		
10		
16		

TABLE 5.6: Longitudinal Dynamic Stability Analysis Test Matrix.

5.2.4.2 Lateral/Directional Dynamic Stability

The data required for the lateral/directional dynamic stability analysis is the same as for the flight test. The tests are done at three different airspeeds, as summarised in Table 5.7.

	Input Type		
	Dutch Roll	Roll Mode	3-2-1-1 δ_a
Airspeed V_e (m/s)			
6			
10			
16			

TABLE 5.7: Lateral/Directional Dynamic Stability Analysis Test Matrix.

5.2.4.3 Timescale

The dynamic stability analysis testing is planned to last a day. The details of the test scheduling are in Table 5.8.

Test	Duration (minutes)	Number	Total Duration (minutes)
Longitudinal	20	2	40
Lateral/Directional	15	4	60
			100

TABLE 5.8: Dynamic Stability Analysis Testing Time-scale.

A first set of testing are carried out between 9:00 and 1:00, taking into account the battery charging time. From 2:00 to 4:30, a second set of test are carried out to insure consistency in the data.

5.2.5 Input Design

5.2.5.1 Longitudinal Dynamics

Inputs are required to excite the different longitudinal dynamic modes for the parameter estimation and validation of the 6 DoF flight dynamics model. The amplitude and frequency of the excitations are based on previous knowledge of the dynamic characteristics of the aircraft. These come from both the previous work conducted on the EasyStar II and the linearised flight dynamics model presented in previous chapters.

Regarding the custom input for the parameter estimation, the methodology presented by Klein and Morelli[21] is used. For simplicity and the inability to automate the inputs, a single-input design approach has been used. The different known modes of the aircraft allow to estimate some parameters and get an understanding of the aircraft dynamics. Thus neither a frequency sweep nor multi-sine input would be suitable for the custom input. The multi-step approach has been chosen. From the these types of inputs, the 3-2-1-1 input has been selected. It consists of a step of width 3 at positive amplitude, followed by a step of 2 widths at negative amplitude and 2 steps of width 1 at positive and negative amplitudes receptively. The unit width is selected to be half the period of the expected dominant mode of the aircraft. Thus the unit duration of the 3-2-1-1 is dependent on the flight conditions. In case during the testing the 3-2-1-1 is found to destabilise the aircraft and/or drive it off flight conditions due to its long step of width 3, the 2-1-1 is used instead. For the 2-1-1, the unit width is selected to be equal to $0.7/(2f_n)$, where f_n is the natural frequency of the aircraft dominant mode in the tested direction.

The inputs are thus:

- SPPO: Short elevator impulse, duration $\approx 0.5\text{s}$;
- Phugoid: Elevator step, duration $\approx 2\text{s}$;

- Custom input: Elevator 3-2-1-1, unit duration depending on airspeed.

Those ideal inputs are illustrated in Figure 5.5.

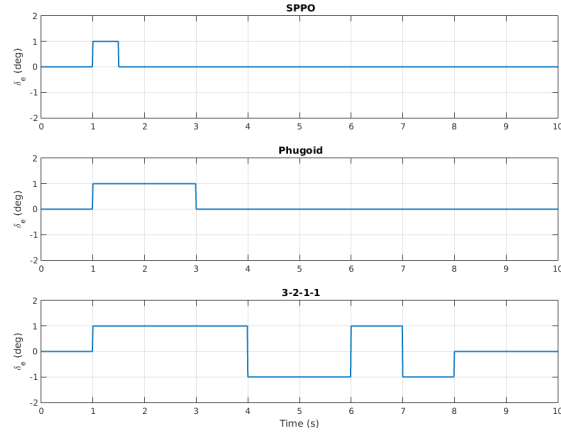


FIGURE 5.5: Dynamic Stability Analysis Inputs Representation.

5.2.5.2 Lateral/Directional Dynamics

Inputs are required to excite the different lateral/directional dynamic modes for the parameter estimation and validation of the 6 DoF flight dynamics model. Just as the longitudinal dynamics inputs, the amplitude and frequency of the excitations are based on previous knowledge of the dynamic characteristics of the aircraft.

The inputs are thus:

- Dutch Roll: Series of rudder steps, frequency ≈ 2 rad/s;
- Roll Mode: Short aileron impulse, duration ≈ 1 s;;
- Custom input: Aileron 3-2-1-1, unit duration depending on airspeed.

Those ideal inputs are illustrated in Figure 5.6.

All the inputs presented in this section are balanced perturbations about the trim condition, such as the flight condition remains essentially unchanged, and the aircraft parameters are considered constant throughout the entire manoeuvre. The inputs are defined starting from the trim value which is assumed to be zero here, but would not necessarily be zero during the testing.

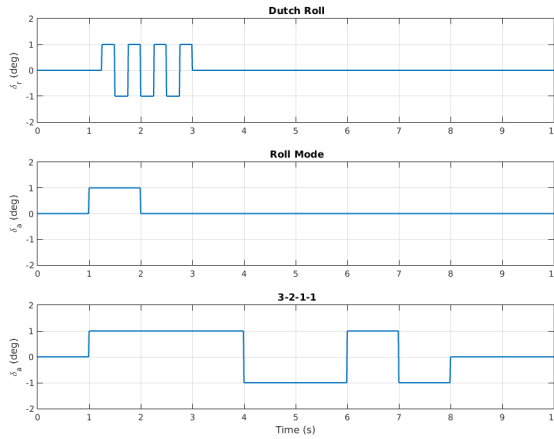


FIGURE 5.6: Lateral/Directional Dynamic Stability Analysis Inputs Representation.

5.3 Data Analysis Methodology

In order to remove process noise from test data, a low pass filter is implemented. The noise is generally of higher frequency than the pilot's inputs. A second order Butterworth low pass filter has been selected for this matter, for various reasons:

- It is a digital filter with no phase shift in the processed signal;
- It is an Infinite Impulse Response (IIR) filter which has a good computational efficiency when compared to Finite Impulse Response (FIR) filters;
- The second order is able to remove the noise better than the first order filter while keeping the computing time low;
- The filter is easily implement within the MATLAB environment.

5.3.1 Butterworth Filter Principle

The Butterworth filter is designed to have a flat frequency response in the pass-band, with a second order filter decrease of -12 dB per octave.

The gain $G(\omega)$ of a second order Butterworth low pass filter is given in terms of the transfer function $H(s)$ as:

$$G^2(\omega) = |H(j\omega)| = \frac{G_0^2}{1 + \left(\frac{\omega}{\omega_c}\right)^4} \quad (5.10)$$

where ω_c is the cutoff frequency of the filter and G_0 the gain at zero frequency.

For stability purposes, the transfer function $H(s)$ is chosen such as it can be written as[25]:

$$H(s) = \frac{G_0}{\prod_{i=1}^n (s - s_k)/\omega_c} \quad (5.11)$$

The denominator of $H(s)$ is a Butterworth polynomial in s .

5.3.2 Butterworth Filter Implementation

In order to use the Butterworth filter for our analysis, the cutoff frequency is fixed to be a certain fraction of the entire frequency spectrum of the test data. Several values have been tried and a cutoff frequency defined as 0.05 of the maximum frequency in the spectrum of the test data appears to significantly filter the data, removing the process noise while keeping fairly unchanged the dynamics of the aircraft as well as the pilots inputs.

5.4 Maximum Likelihood Estimation Methodology

This section presents the development of the Maximum Likelihood Estimation for a stochastic dynamic system described by differential equations with process noise. The problem is afterwards simplified for a deterministic non-linear system and an optimisation algorithm based on the output-error approach is presented.

5.4.1 Aircraft Model

A wide range of aircraft system identification problems could be characterised by a discrete-time measurement made on a continuous-time dynamic system. We will consider a linear model of the aircraft in the longitudinal and lateral directions.

A stochastic forcing term is added to the linear dynamic equations to account for inadequacy in the linear model as shown in Equation 5.12.

$$\mathbf{x}_{k+1} = \Phi \mathbf{x}_k + \Gamma \mathbf{u}_k + \mathbf{w}_k \quad (5.12a)$$

$$\mathbf{z}_k = C \mathbf{x}_k + D \mathbf{u}_k + \boldsymbol{\nu}_k \quad (5.12b)$$

where

\mathbf{x} is the state vector.

\mathbf{u} is the control input.

\mathbf{z} is the measurement vector.

\mathbf{w} is the process noise.

$\boldsymbol{\nu}$ is the measurement noise.

Φ , Γ , C and D are the discrete-time system matrices.

The process and measurement noise \mathbf{w}_k and $\boldsymbol{\nu}_k$ are assumed to be independent sequences of zero-mean Gaussian noise of covariances \mathcal{Q} and \mathcal{Q} .

The state space representation is a mathematical model of a dynamic system as a set of input, output and state variables related by first-order differential equations. The continuous state space equations are then:

$$\dot{\mathbf{x}}(t) = A\mathbf{x}(t) + B\mathbf{u}(t) + B_w\mathbf{w}(t) \quad (5.13a)$$

$$\mathbf{y}(t) = C\mathbf{x}(t) + D\mathbf{u}(t) \quad (5.13b)$$

$$\mathbf{z}(i) = \mathbf{y}(i) + \boldsymbol{\nu}(i) \quad i = 1, 2, \dots, N \quad (5.13c)$$

The mean value and covariance of the initial states are defined by,

$$E[\mathbf{x}(0)] = \bar{\mathbf{x}}_0 \quad E\{[\mathbf{x}(0) - \bar{\mathbf{x}}_0][\mathbf{x}(0) - \bar{\mathbf{x}}_0]^T\} = \mathcal{P}_0 \quad (5.14)$$

The white Gaussian noise $\mathbf{w}(t)$ and $\boldsymbol{\nu}(i)$ have their mean values and covariance defined as:

$$E[\mathbf{w}(t)] = 0 \quad E[\mathbf{w}(t_i)\mathbf{w}^T(t_j)] = \mathcal{Q}(t_i)\delta(t_i - t_j) \quad (5.15a)$$

$$E[\boldsymbol{\nu}(i)] = 0 \quad E[\boldsymbol{\nu}(i)\boldsymbol{\nu}^T(j)] = \mathcal{R}(i)\delta_{ij} \quad (5.15b)$$

The unknown but constant set of parameters $\boldsymbol{\theta}$ is in general contained in:

- The elements of the linear system matrices A, B, C, D ;
- The elements of the process noise matrix B_w and the noise covariance matrices \mathcal{Q} and \mathcal{R} ;
- The initial state vector mean value $\bar{\mathbf{x}}_0$ and covariance \mathcal{P}_0 .

Thus,

$$\boldsymbol{\theta} = f(A, B, C, D, B_w, \mathcal{Q}, \mathcal{R}, \bar{\mathbf{x}}_0, \mathcal{P}_0) \quad (5.16)$$

5.4.2 Maximum Likelihood Cost Function

As defined in the literature review, the probability density function that specifies the probability of observing a data vector $y = (y_1, \dots, y_m)$ given the parameter w , $f(y|w)$ is:

$$f(y|w) = f(y_1|w)f(y_2|w)\dots f(y_m|w) \quad (5.17)$$

The likelihood function $\mathbb{L}(w|y)$ is the probability distribution function of obtaining the data vector with the unkown parameter given:

$$\mathbb{L}(w|y) = f(y|w) \quad (5.18)$$

It helps in finding the one probability distribution function, among all the probability densities that the model prescribes, that is most likely to have produced the data given the observed data and a model of interest. Let's evaluate the likelihood function of the aircraft model previously defined for a sequence of measurements $Z_N = [\mathbf{z}(1), \mathbf{z}(2), \dots, \mathbf{z}(N)]^T$ denoted $\mathbb{L}[Z_N; \boldsymbol{\theta}]$:

$$\mathbb{L}[Z_N; \boldsymbol{\theta}] = \mathbb{L}[\mathbf{z}(1), \mathbf{z}(2), \dots, \mathbf{z}(N); \boldsymbol{\theta}] \quad (5.19)$$

Recalling the Bayes' theorem,

$$P(A|B) = \frac{P(B|A)P(A)}{P(B)} \quad (5.20)$$

where,

A and B are events

$P(A)$ and $P(B)$ are the probabilities of A and B without regard to each other.

$P(A|B)$, a conditional probability, is the probability of A given that B is true.

$P(B|A)$, is the probability of B given that A is true.

Equation 5.19 yields by successive application of the Bayes' theorem to:

$$\begin{aligned} \mathbb{L}[Z_N; \boldsymbol{\theta}] &= \mathbb{L}[\mathbf{z}(1), \mathbf{z}(2), \dots, \mathbf{z}(N); \boldsymbol{\theta}] \\ &= \mathbb{L}[\mathbf{z}(N)|Z_{N-1}; \boldsymbol{\theta}] \mathbb{L}[Z_{N-1}; \boldsymbol{\theta}] \\ &= \mathbb{L}[\mathbf{z}(N)|Z_{N-1}; \boldsymbol{\theta}] \mathbb{L}[\mathbf{z}(N-1)|Z_{N-2}; \boldsymbol{\theta}] \mathbb{L}[Z_{N-2}; \boldsymbol{\theta}] \\ &= \vdots \\ &= \prod_{i=1}^N \mathbb{L}[\mathbf{z}(i)|Z_{i-1}; \boldsymbol{\theta}] \end{aligned} \quad (5.21)$$

For computational purposes, it is advantageous to minimise the negative logarithm likelihood function, rather than to maximise the likelihood function. The maximum likelihood parameters estimator can then be expressed as:

$$\begin{aligned}
\hat{\boldsymbol{\theta}} &= \max_{\boldsymbol{\theta}} \mathbb{L}[Z_N; \boldsymbol{\theta}] \\
&= \max_{\boldsymbol{\theta}} \prod_{i=1}^N \mathbb{L}[\mathbf{z}(i)|Z_{i-1}; \boldsymbol{\theta}] \\
&= \min_{\boldsymbol{\theta}} \sum_{i=1}^N -\ln\{\mathbb{L}[\mathbf{z}(i)|Z_{i-1}; \boldsymbol{\theta}]\}
\end{aligned} \tag{5.22}$$

Recalling that the measurement and process noise $\mathbf{w}(t)$ and $\boldsymbol{\nu}(i)$ are assumed to be Gaussian white noise, the output $\mathbf{z}(i)$ also has the same properties, thus:

$$\mathbb{L}[\mathbf{z}(i)|Z_{i-1}; \boldsymbol{\theta}] = \mathbb{L}[\mathbf{z}(i); \boldsymbol{\theta}] \tag{5.23}$$

Additionally, just as $\mathbf{w}(t)$ and $\boldsymbol{\nu}(i)$, $\mathbf{z}(i)$ is uniquely defined by its main value and covariance matrix:

$$E[\mathbf{z}(i); \boldsymbol{\theta}] \equiv \hat{\mathbf{y}}(i|i-1) \tag{5.24a}$$

$$\begin{aligned}
Cov[\mathbf{z}(i); \boldsymbol{\theta}] &\equiv E\{[\mathbf{z}(i) - \hat{\mathbf{y}}(i|i-1)][\mathbf{z}(i) - \hat{\mathbf{y}}(i|i-1)]^T\} \\
&= E[\boldsymbol{\nu}(i)\boldsymbol{\nu}^T(i)] \\
&\equiv \mathcal{B}(i)
\end{aligned} \tag{5.24b}$$

with,

$$\boldsymbol{\nu}(i) = \mathbf{z}(i) - \hat{\mathbf{y}}(i|i-1) \tag{5.24c}$$

$\hat{\mathbf{y}}(i|i-1)$ is the predicted output estimate at time t_i , knowing the output at time t_{i-1} ; $\boldsymbol{\nu}(i)$ is the vector of innovations and $\mathcal{B}(i)$ their covariance matrix.

The information or probability density distribution of the innovations $\boldsymbol{\nu}(i)$ approaches a Gaussian distribution; for sufficiently high sampling rates, the likelihood function for one measurement is $\mathbb{L}[\mathbf{z}(i); \boldsymbol{\theta}]$ can then be written as:

$$\mathbb{L}[\mathbf{z}(i); \boldsymbol{\theta}] = (2\pi)^{-n_0/2} \det[\mathcal{B}(i)]^{-1/2} \exp\left[-\frac{1}{2}\boldsymbol{\nu}(i)\mathcal{B}^{-1}(i)\boldsymbol{\nu}(i)\right] \tag{5.25}$$

n_0 is the number of output variables and N the number of data points.

The negative logarithmic likelihood function for all measurements is thus,

$$-\ln[\mathbb{L}(Z_N; \boldsymbol{\theta})] = \frac{1}{2} \sum_{i=1}^N [\mathbf{v}(i)^T \mathcal{B}^{-1}(i) \mathbf{v}(i) + \ln\{\det[\mathcal{B}(i)]\}] + \frac{Nn_0}{2} \ln(2\pi) \quad (5.26)$$

The constant term in 5.26 has no effect on the optimisation process and can be dropped out of the equation. Thus the maximum likelihood cost function is:

$$J(\boldsymbol{\theta}) \equiv -\ln[\mathbb{L}(Z_N; \boldsymbol{\theta})] = \frac{1}{2} \sum_{i=1}^N [\mathbf{v}(i)^T \mathcal{B}^{-1}(i) \mathbf{v}(i) + \ln\{\det[\mathcal{B}(i)]\}] \quad (5.27)$$

The problem of determining the maximum likelihood cost function is therefore simplified to finding the mean value and the covariance matrix of the innovations $\mathbf{v}(i)$.

5.4.3 Optimisation Algorithm: Output Error Approach

The MLE lies on selecting the values of the estimates that make the data most plausible. The optimisation algorithm will thus find the value of the parameters vector $\boldsymbol{\theta}$ which minimises the maximum likelihood cost function $J(\boldsymbol{\theta})$. This cost function is, as shown in the previous section, based on the mean value and the covariance matrix of the innovations $\mathbf{v}(i)$. The complexity of finding this mean value and covariance matrix of the innovations $\mathbf{v}(i)$ comes from the process noise. A Kalman Filter is included to the state estimator when the process noise is considered. However in the case of the problem this thesis deals with, the process noise $\mathbf{w}(i)$ could be neglected when compared with the measurement noise $\mathbf{v}(i)$.

With this simplification, the aircraft is a deterministic linear dynamic system (with no stochastic component). In this case, the the dynamic system is simplified and

the continuous state space equations become:

$$\dot{\mathbf{x}}(t) = A\mathbf{x}(t) + B\mathbf{u}(t) \quad \mathbf{x}(0) = \mathbf{x}_0 \quad (5.28a)$$

$$\mathbf{y}(t) = C\mathbf{x}(t) + D\mathbf{u}(t) \quad (5.28b)$$

$$\mathbf{z}(i) = \mathbf{y}(i) + \boldsymbol{\nu}(i) \quad i = 1, 2, \dots, N \quad (5.28c)$$

The measurement noise $\boldsymbol{\nu}(i)$ is a zero-mean Gaussian noise with constant diagonal covariance matrix such as:

$$E[\boldsymbol{\nu}(i)] = 0 \quad E[\boldsymbol{\nu}(i)\boldsymbol{\nu}^T(j)] = \mathcal{R}\delta_{ij} \quad (5.28d)$$

In this case, the innovations become the output errors or residuals and the maximum likelihood cost function becomes:

$$J(\boldsymbol{\theta}) = \frac{1}{2} \sum_{i=1}^N [\mathbf{v}(i)^T \mathcal{R}^{-1}(i) \mathbf{v}(i)] + \frac{N}{2} \ln[\det(\mathcal{R})] \quad (5.29)$$

The output error optimisation algorithm is illustrated in Figure 5.7.

For such a system, the unknown parameters $\boldsymbol{\theta}$ are elements of the matrices A , B , C , D , \mathcal{R} , and the initial conditions vector \mathbf{x}_0 .

$$\boldsymbol{\theta} = f(A, B, C, D, \mathcal{R}, \mathbf{x}_0) \quad (5.30)$$

The optimisation process starts by finding the covariance matrix \mathcal{R} :

$$\left. \frac{\partial J(\boldsymbol{\theta})}{\partial \mathcal{R}} \right|_{\hat{\mathcal{R}}} = 0 \Rightarrow \hat{\mathcal{R}} = \frac{1}{N} \sum_{i=1}^N [\mathbf{v}(i)\mathbf{v}^T(i)] \quad (5.31a)$$

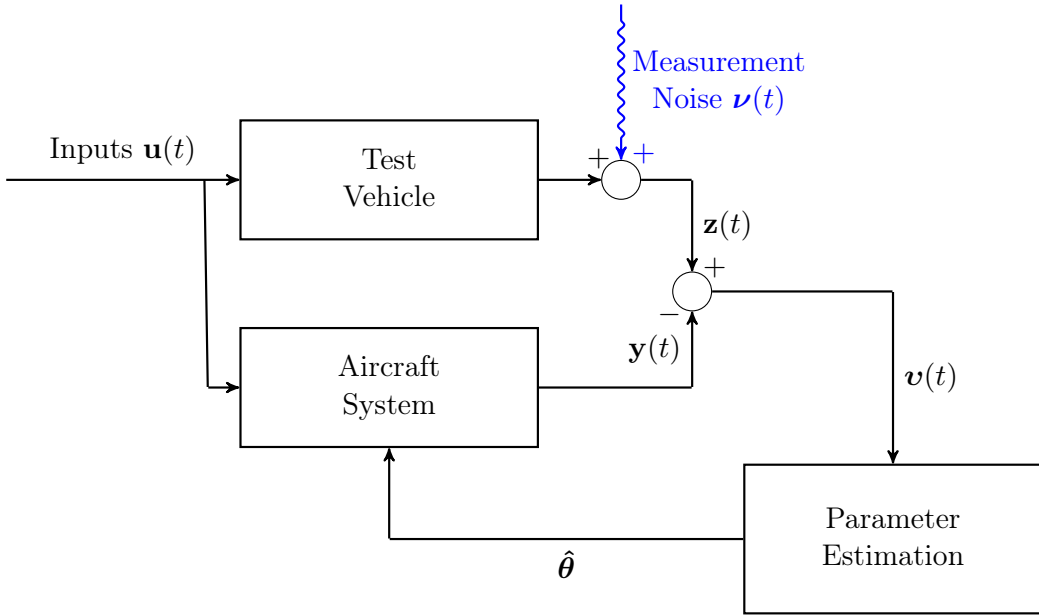


FIGURE 5.7: Output Error Optimisation Algorithm

Recalling Equation 5.29, the far right term is a constant and is not of interest for the optimisation algorithm. By replacing the innovations covariance matrix by the value obtained in Equation 5.31, the log-likelihood cost function becomes:

$$J(\boldsymbol{\theta}) = \frac{1}{2} \sum_{i=1}^N \mathbf{v}(i) \hat{\mathcal{R}}^{-1} \mathbf{v}^T(i) \quad (5.32a)$$

$$= \frac{1}{2} \sum_{i=1}^N [\mathbf{z}(i) - \mathbf{y}(i)] \hat{\mathcal{R}}^{-1} [\mathbf{z}(i) - \mathbf{y}(i)]^T \quad (5.32b)$$

Optimising this cost function is done using a simple Newton-Raphson method. The gradient of the cost function is obtained as:

$$\frac{\partial J(\boldsymbol{\theta})}{\partial \boldsymbol{\theta}} = \sum_{i=1}^N \frac{\partial \mathbf{v}^T(i)}{\partial \boldsymbol{\theta}} \hat{\mathcal{R}}^{-1} \mathbf{v}(i) \quad (5.33a)$$

$$= - \sum_{i=1}^N \frac{\partial \mathbf{y}^T(i)}{\partial \boldsymbol{\theta}} \hat{\mathcal{R}}^{-1} \mathbf{v}(i) \quad (5.33b)$$

which is in a vector with elements:

$$\frac{\partial J(\boldsymbol{\theta})}{\partial \boldsymbol{\theta}_j} = - \sum_{i=1}^N \frac{\partial \mathbf{y}^T(i)}{\partial \boldsymbol{\theta}_j} \hat{\mathcal{R}}^{-1} \mathbf{v}(i) \quad j = 1, 2, \dots, n_p \quad (5.33c)$$

with n_p the number of parameters.

The elements of the second-order gradient matrix or Hessian matrix are defined as:

$$\frac{\partial^2 J(\boldsymbol{\theta})}{\partial \boldsymbol{\theta}_j \partial \boldsymbol{\theta}_k} = \sum_{i=1}^N \frac{\partial \mathbf{y}^T(i)}{\partial \boldsymbol{\theta}_j} \hat{\mathcal{R}}^{-1} \frac{\partial \mathbf{y}(i)}{\partial \boldsymbol{\theta}_k} - \sum_{i=1}^N \frac{\partial^2 \mathbf{y}(i)}{\partial \boldsymbol{\theta}_j \partial \boldsymbol{\theta}_k} \hat{\mathcal{R}}^{-1} \mathbf{v}(i) \quad (5.34)$$

with $j, k = 1, 2, \dots, n_p$.

The second order partial derivative term in Equation 5.34 is multiplied by the residual $\mathbf{v}(i)$, as the parameters vector gets close to the solution, the whole term tends to zero. It is then safe to neglect this second order partial derivative term in the optimisation algorithm.

Using the right approximation for the Hessian matrix and applying the modified Newton-Raphson method, the estimate for the parameter vector change is:

$$\Delta \hat{\boldsymbol{\theta}} = \left[\sum_{i=1}^N \frac{\partial \mathbf{y}^T(i)}{\partial \boldsymbol{\theta}} \hat{\mathcal{R}}^{-1} \frac{\partial \mathbf{y}(i)}{\partial \boldsymbol{\theta}} \right]_{\boldsymbol{\theta}=\boldsymbol{\theta}_0}^{-1} \left[\sum_{i=1}^N \frac{\partial \mathbf{y}^T(i)}{\partial \boldsymbol{\theta}} \hat{\mathcal{R}}^{-1} \mathbf{v}(i) \right]_{\boldsymbol{\theta}=\boldsymbol{\theta}_0} \quad (5.35)$$

The parameter vector change defined in Equation 5.35 is computed and the parameters in the aircraft mathematical model are updated. This process is repeated until an algorithm convergence criteria is satisfied.

5.4.4 Quality of the Estimates

Let's denote n_o the number of outputs and n_p the number of parameters. The elements of the $n_o \times n_p$ matrix $\partial \mathbf{y} / \partial \boldsymbol{\theta}$ are called the output sensitivities. These elements quantify the effect on the estimated outputs of any change in the parameters. As the estimated covariance matrix of the innovations $\hat{\mathcal{R}}$ is typically diagonal, for a good matrix inversion in Equation 5.35, the output sensitivities must be linearly independent and non-zero. In this case, minimising the output

error leads to a well conditioned problem and accurate values of the parameter estimates $\boldsymbol{\theta}$.

The numerical approach to evaluating the output sensitivities is based on an approximation of the definition of numerical partial derivatives:

$$\frac{\partial \mathbf{y}}{\partial \boldsymbol{\theta}} = \frac{\mathbf{y}(\boldsymbol{\theta}_0 + \delta\boldsymbol{\theta}_j) - \mathbf{y}(\boldsymbol{\theta}_0)}{|\delta\boldsymbol{\theta}_j|} \quad j = 1, 2, \dots, n_p \quad (5.36a)$$

or

$$\frac{\partial \mathbf{y}}{\partial \boldsymbol{\theta}} = \frac{\mathbf{y}(\boldsymbol{\theta}_0 + \delta\boldsymbol{\theta}_j) - \mathbf{y}(\boldsymbol{\theta}_0 - \delta\boldsymbol{\theta}_j)}{2|\delta\boldsymbol{\theta}_j|} \quad j = 1, 2, \dots, n_p \quad (5.36b)$$

where $\delta\boldsymbol{\theta}_j$ is a vector with all zero elements but for the j th element, which contains the perturbation for parameter $\boldsymbol{\theta}_j$, and $|\delta\boldsymbol{\theta}_j|$ is its magnitude.

For all non linear deterministic systems, the derivative of the state vector and the output vector can be expressed as functions of the states, the inputs and the system parameters:

$$\dot{\mathbf{x}}(t) = f(\mathbf{x}, \mathbf{u}, \boldsymbol{\theta}) \quad \mathbf{x}(0) = \mathbf{x}_0 \quad (5.37a)$$

$$\mathbf{y} = h(\mathbf{x}, \mathbf{u}, \boldsymbol{\theta}) \quad (5.37b)$$

The output sensitivities can now be computed by differentiating Equations 5.37 with respect $\boldsymbol{\theta}_j$ to as:

$$\frac{d}{dt} \left(\frac{\partial \mathbf{x}}{\partial \boldsymbol{\theta}_j} \right) = \frac{\partial f}{\partial \mathbf{x}} \frac{\partial \mathbf{x}}{\partial \boldsymbol{\theta}_j} + \frac{\partial f}{\partial \boldsymbol{\theta}_j} \quad \frac{\partial \mathbf{x}(0)}{\partial \boldsymbol{\theta}_j} = 0 \quad j = 1, 2, \dots, n_p \quad (5.38a)$$

$$\frac{\partial \mathbf{y}}{\partial \boldsymbol{\theta}_j} = \frac{\partial h}{\partial \mathbf{x}} \frac{\partial \mathbf{x}}{\partial \boldsymbol{\theta}_j} + \frac{\partial h}{\partial \boldsymbol{\theta}_j} \quad j = 1, 2, \dots, n_p \quad (5.38b)$$

Let's now introduce the Fisher information matrix for our system denoted M , which is a way of measuring the amount of information that the observable variables Z_N from Equation 5.19 carry about the unknown parameters $\boldsymbol{\theta}$ upon which the probability of Z_N depends:

$$M \equiv -E \left[\frac{\partial^2 \ln \mathbb{L}(Z_N; \boldsymbol{\theta})}{\partial \boldsymbol{\theta} \partial \boldsymbol{\theta}^T} \right] = \sum_{i=1}^N \frac{\partial \mathbf{y}^T(i)}{\partial \boldsymbol{\theta}} \hat{\mathcal{R}}^{-1} \frac{\partial \mathbf{y}(i)}{\partial \boldsymbol{\theta}} \quad (5.39)$$

The Fisher information matrix is thus equivalent to the inverse of the first term on the right hand side of the parameter vector change derived in Equation 5.35 when $\boldsymbol{\theta} = \boldsymbol{\theta}_0$. Recalling that:

$$\Delta \hat{\boldsymbol{\theta}} = \boldsymbol{\theta}_0 - \hat{\boldsymbol{\theta}} \Rightarrow \hat{\boldsymbol{\theta}} = \boldsymbol{\theta}_0 - \Delta \hat{\boldsymbol{\theta}} \quad (5.40)$$

The maximum likelihood parameter estimate can then be written as:

$$\hat{\boldsymbol{\theta}} = \boldsymbol{\theta}_0 - M_{\boldsymbol{\theta}=\boldsymbol{\theta}_0}^{-1} \left[\frac{\partial J(\boldsymbol{\theta})}{\partial \boldsymbol{\theta}} \right]_{\boldsymbol{\theta}=\boldsymbol{\theta}_0} \quad (5.41)$$

The formulation in Equation 5.41 allows to define the minimum of the estimated parameter covariance matrix for an unbiased estimator, the Cramér-Rao bound, which is equal to the inverse of the Fisher information matrix. This means that the estimated parameter covariance matrix is greater or equal to the inverse of the Fisher information matrix:

$$Cov(\hat{\boldsymbol{\theta}}) \geq M_{\boldsymbol{\theta}=\boldsymbol{\theta}_0}^{-1} \quad (5.42)$$

5.4.5 Summary

The maximum likelihood estimation method for the output-error approach using the modified Newton-Raphson optimisation algorithm presented can be summarised as:

$$\begin{aligned}
\text{Parameter Estimates:} \quad & \hat{\boldsymbol{\theta}} = \boldsymbol{\theta}_0 + \Delta\hat{\boldsymbol{\theta}} \\
\text{Parameter Vector Change:} \quad & \Delta\hat{\boldsymbol{\theta}} = -M_{\boldsymbol{\theta}=\boldsymbol{\theta}_0}^{-1} g_{\boldsymbol{\theta}=\boldsymbol{\theta}_0} \\
\text{Cramér-Rao Inequality:} \quad & Cov(\hat{\boldsymbol{\theta}}) \geq M_{\boldsymbol{\theta}=\hat{\boldsymbol{\theta}}}^{-1} \\
\text{Fisher Information Matrix:} \quad & M_{\boldsymbol{\theta}=\boldsymbol{\theta}_0} = \sum_{i=1}^N \left[S^T(i) \hat{\mathcal{R}}^{-1} S(i) \right]_{\boldsymbol{\theta}=\boldsymbol{\theta}_0} \\
\text{Parameter Estimates Jacobian Matrix:} \quad & g_{\boldsymbol{\theta}=\boldsymbol{\theta}_0} = \sum_{i=1}^N \left[S^T(i) \hat{\mathcal{R}}^{-1} \mathbf{v}(i) \right]_{\boldsymbol{\theta}=\boldsymbol{\theta}_0} \\
\text{Output Sensitivity Matrix:} \quad & [s_{jk}(i)] = \left[\frac{\partial \mathbf{y}_j(i, \boldsymbol{\theta})}{\partial \theta_k} \right] \\
\text{Innovations:} \quad & \mathbf{v}(i) = \mathbf{z}(i) - \hat{\mathbf{y}}(i, \boldsymbol{\theta})
\end{aligned} \tag{5.43}$$

5.5 Model Validation

All tests are done at least twice in order to ensure repeatability in the data set. Having obtained the parameter estimates using one of the data sets, the other one is used for model validation. It consists in using the state space representation of the identified model with the inputs of the independent data set in order to simulate an output.

The validation is thus done both qualitatively and quantitatively:

- The qualitative validation consist of only comparing visually the graphs of the response of both the model and the test validation data.
- The quantitative validation is done in two steps.
 1. By comparing the modal characteristics (frequency, damping ratio and time constant) of the model and the validation test data.
 2. By doing a statistical analysis of the innovations.

5.5.1 Modal Characteristics Validation

The modal characteristics validation is a simple comparison of the model and the validation test modal characteristics. A model is considered validated if its modal characteristics are less than 35% different from the flight test data.

5.5.2 Statistical Validation

The statistical validation consist of plotting an histogram of the distribution of the innovations. If a Gaussian distribution as defined by its probability density function in Equation 5.44 could be fit to the histogram, the model is an acceptable representation of the aircraft dynamics and the innovations are due to random external variables.

$$f(x|\mu, \sigma) = \frac{1}{\sigma\sqrt{2\pi}} \exp^{-\frac{(x-\mu)^2}{2\sigma^2}} \quad (5.44)$$

where, x is the variable, μ its arithmetic mean and σ its standard deviation.

When evaluating the arithmetic mean value and standard deviation of the innovations as defined in Equations 5.45, the model could be validated if the mean value is close to zero and the standard deviation small enough when compared to the amplitude of the validation test data.

$$\mu(\mathbf{v}) = \frac{1}{N} \sum_{i=1}^N \mathbf{v}(i) \quad (5.45a)$$

$$\sigma(\mathbf{v}) = \sqrt{\frac{1}{N} \sum_{i=1}^N (\mathbf{v}(i) - \mu(\mathbf{v}))^2} \quad (5.45b)$$

Chapter 6

Flight Test and Parameters Estimation

This chapter presents the collected flight test data and the results of the parameters estimation. Firstly, the flight test schedule alongside the difficulties encountered when testing the aircraft are presented. A summary of the valid tests and conditions is highlighted¹. Subsequently, the results of the parameters estimation are presented and the effects of airspeed and centre of gravity position on the modal characteristics of the estimated model are presented and discussed.

6.1 Flight Test

There has been four flight test sorties and an extended amount of data has been collected. However, for various reasons, not all of the data could be usable for either the validation of the 6 Degrees of Freedom model or the system identification implementation. The difficulties encountered when or before conducting the flight test, generally resulting in rejecting the data, are:

- Hardware implementation anomalies: Not only getting the instrumentation up and running took more time than initially expected, but the aircraft has been crashed twice. This was due to a loss of connection between the RC transmitter and the aircraft. It has been found that the RC receiver was not

¹It should be noted that no wind tunnel test has been carried out due to maintenance on the tunnel.

fully operational and experienced random drops in range. A replacement one has been used. Each of the crashes resulted in damages on the aircraft, as illustrated in Figure 6.1². More time has been spent repairing the aircraft and ordering new parts (Pitot tubes and batteries).

- Weather conditions: Rain and high speed wind predictions delayed some test sorties.
- Trimming conditions: Despite the help of an experimented RC plane pilot, the collected data was not always adequately trimmed. This is the reason of rejection of most of the data.
- Inaccuracy in measurements: Some of the tests have been rejected due to inaccuracy in the measurements, especially the airspeed readings. Although the aircraft was adequately trimmed, during some tests the aircraft encountered gusts that changed the airspeed and made the data unusable for parameter estimation.



FIGURE 6.1: Damaged Aircraft after Crash on 09th July 2015.

In order to achieve different centre of gravity positions for the longitudinal dynamics tests, a ballast of mass 70g was placed at different positions in the nose of the

²The engine was detached from the aircraft, the Pitot tube lost, the battery overheated, and the nose and canopy damaged too.

aircraft. Due to it's small size, the mass properties where computed assuming it is a point mass. The four centre of gravity position tested are as detailed in Table 6.1.

	cg_0	cg_1	cg_2	cg_3
CG Position (% of MAC)	11.70	17.19	24.35	25.46

TABLE 6.1: Tested Centre of Gravity Positions.

The different flight conditions of each test sortie are presented in Table 6.2³.

	Date	Time	Wind Speed (mph)	Temp (°C)	Atmospheric Pressure (hPa)
Sortie 1	09/07/15	14:00	7	16	1022
Sortie 2	22/07/15	12:00	11	18	1013
Sortie 3	26/07/15	06:30	2	12	1002
Sortie 4	26/07/15	08:30	3	11	1002

TABLE 6.2: Flight Test Conditions.

³The wind speed, temperature and pressure are from weather forecasts.

Table 6.3 gives a summary of the total number of tests, and the percentage of valid test for each type of test conducted per sortie.

	Number of Tests	SPPO	Phugoid	3-2-1-1 δ_e	Dutch Roll	Roll Mode	3-2-1-1 δ_a
Sortie 1	Total	1	-	-	-	-	-
	Valid	0	-	-	-	-	-
	Valid %	0%	-	-	-	-	-
Sortie 2	Total	2	-	-	4	1	3
	Valid	0	-	-	1	1	3
	Valid %	0%	-	-	20%	100%	100%
Sortie 3	Total	3	-	-	-	-	-
	Valid	1	-	-	-	-	-
	Valid %	33%	-	-	-	-	-
Sortie 4	Total	12	7	9	7	2	-
	Valid	4	2	3	3	2	-
	Valid %	33%	28%	33%	43%	100%	-
Total	Total	18	7	9	11	3	3
	Valid	5	2	3	4	3	3
	Valid %	28%	28%	33%	36%	100%	100%

TABLE 6.3: Flight Tests.

Table 6.4 presents the details on each of the valid tests.

This flight test data is used not only for identifying the aircraft following the methodology presented in previous chapters, but also to validate the 6DoF model developed in previous chapters. As some of the tests of the same type (SPPO, Dutch Roll, ect...) are done at the same centre of gravity and at roughly the same airspeed, not all of the data is used for parameters estimation, but for the validation of the identified system instead.

6.2 Parameters Estimation

Here are presented the results of the MLE estimation method on the flight test data obtained. The Output-Error MLE algorithm from SIDPAC[26] has been used. The initial values provided to the MLE algorithm are obtained from the

	CG Position	EAS (m/s)	H_p (m)
SPPO	cg_2	5	17
	cg_0	4	14
	cg_1	5	26
	cg_1	4	16
	cg_1	4	22
Phugoid	cg_0	5	45
	cg_0	6	40
3-2-1-1 δ_e	cg_0	5	25
	cg_1	4	14
	cg_0	6	38
Dutch Roll	cg_3	14	22
	cg_0	5	35
	cg_0	5	35
	cg_0	4	41
Roll Mode	cg_3	18	21
	cg_0	4	25
	cg_0	4	17
3-2-1-1 δ_a	cg_3	15	18
	cg_3	18	20
	cg_3	16	15

TABLE 6.4: Valid Flight Tests.

previously developed linearised 6DoF model. Graphical methods⁴ are used accordingly to estimate the modal characteristics of the flight test data. Those modal characteristics are subsequently compared to the ones obtained from both the linearised 6DoF model and the identified model.

6.2.1 Short Period Pitching Oscillations (SPPO)

As the valid SPPO tests were carried at different CG positions and at roughly the same airspeed, the parameter estimation discussion will focus only on the effect of the CG position on the SPPO characteristics. Recalling the state space representation equation of the SPPO mode as in Equation 6.1, Table 6.5 presents the parameter estimates of the mode at all tested CG positions, the standard error, the percentage error and the 95% confidence interval on each estimate.

⁴Logarithmic Decrement method, Maximum slope method and Time constant method.

$$\begin{bmatrix} \dot{w} \\ \dot{q} \end{bmatrix} = \begin{bmatrix} z_w & z_q \\ m_w & m_q \end{bmatrix} \begin{bmatrix} w \\ q \end{bmatrix} + \begin{bmatrix} z_{\delta_e} & z_{\tau} \\ m_{\delta_e} & m_{\tau} \end{bmatrix} \begin{bmatrix} \delta_e \\ \tau \end{bmatrix} \quad (6.1)$$

Figure 6.2 shows the response in pitch rate for the SPPO test with the centre of gravity at position cg_0 , for both the flight test data and the identified model⁵. It is noticeable that the maximum amplitude of the innovation is 6.25% of the maximum amplitude of the measured q -response. Also, both the measured q -response and the identified model q -response have comparable frequencies and damping ratios. At this particular CG position, the identified model is a very suitable representation of the real aircraft.

Parameter	Estimate	Std Error	% Error	95% Confidence Interval
cg_0	z_w	-30.58	7.733	[-46.042 , -15.110]
	z_q	-146.6	36.11	[-218.824 , -74.376]
	z_{δ_e}	-13.81	3.556	[-20.927 , -6.702]
	z_{τ}	-5×10^{-3}	2×10^{-3}	[-0.009 , -0.002]
	m_w	2.884	0.708	[1.468 , 4.299]
	m_q	5.063	3.154	[-1.244 , 11.370]
	m_{δ_e}	0.506	0.309	[-0.114 , 1.126]
	m_{τ}	8×10^{-6}	1×10^{-4}	[0.000 , 0.000]
cg_1	z_w	-9.819	1.516	[-12.851 , -6.787]
	z_q	-24.36	3.116	[-30.592 , -18.129]
	z_{δ_e}	-1.151	0.173	[-1.497 , -0.805]
	z_{τ}	-3×10^{-4}	1×10^{-4}	[-0.001 , 0.000]
	m_w	5.371	0.715	[3.941 , 6.802]
	m_q	3.373	1.194	[-0.226 , 0.028]
	m_{δ_e}	-0.099	0.063	[-0.226 , 0.028]
	m_{τ}	2×10^{-4}	8×10^{-5}	[0.000 , 0.000]
cg_2	z_w	-7.789	0.652	[-9.094 , -6.483]
	z_q	1.932	2.065	[-2.198 , 6.061]
	z_{δ_e}	-0.125	0.143	[-0.410 , 0.160]
	z_{τ}	-4×10^{-4}	2×10^{-4}	[-0.001 , 0.000]
	m_w	-0.327	0.111	[-0.549 , -0.104]
	m_q	-6.776	0.351	[-7.479 , -6.073]
	m_{δ_e}	-0.626	0.024	[-0.674 , -0.577]
	m_{τ}	-7×10^{-4}	3×10^{-5}	[-0.001 , -0.001]

TABLE 6.5: SPPO Parameter Estimates.

⁵Similar figure for the other CG positions are in Appendices.

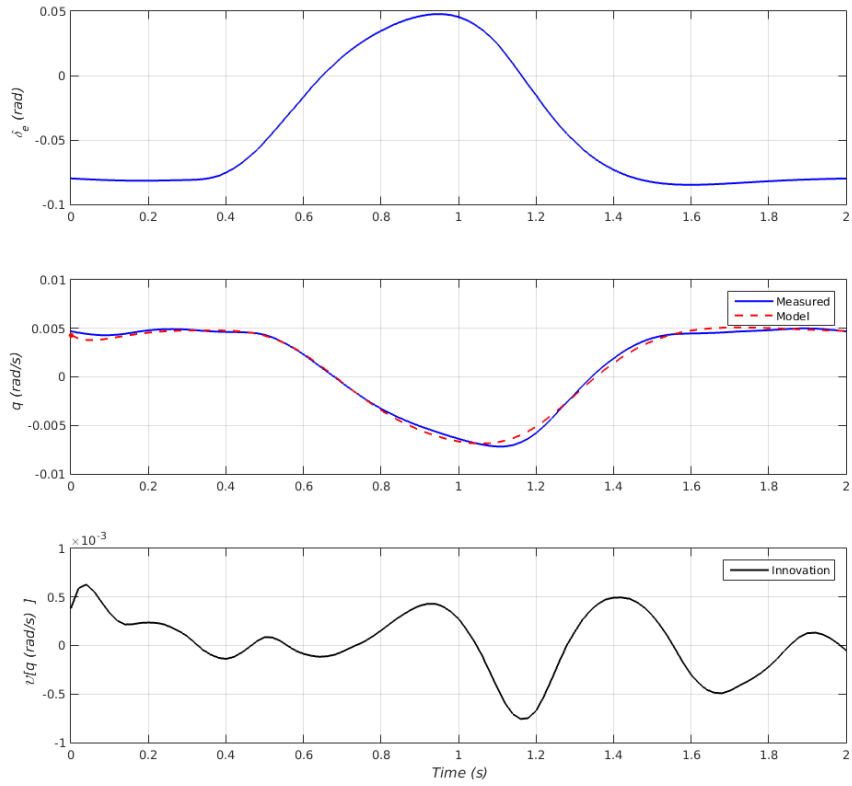


FIGURE 6.2: SPPO Flight Test data and Identified Model q -response.

A trend is observable in the parameters of the SPPO reduced model state space representation equation, the percentage errors are acceptable, and the 95% confidence intervals are not too wide for most parameters. It should also be noted that the parameters with the most significant percentage error are of very low values, especially the vertical force and pitching moment due to thrust (z_τ and m_τ) which could have been fixed to zero when performing the MLE estimation.

The frequency and damping of the system have a greater physical meaning when compared to parameter estimates. Table 6.6 presents a comparison of the identified model, the linearised 6DoF model and the flight test data for all three CG positions. Obtaining the frequency and damping ratio of the flight test data with graphical methods usually requires the time history to have at least one overshoot after the control surface input. For this reason, some of the valid test were not used for assessing the effect of the CG position on the aircraft SPPO with regards to the flight test data.

Figure 6.3 illustrates the data presented in Table 6.6.

	CG Position	Test Data	6 DoF Linearised Model	Identified Model
Frequency (rad/s)	cg_0	-	7.07	16.4
	cg_1	10.3	6.95	9.89
	cg_2	7.82	6.62	7.31
Damping Ratio	cg_0	-	0.640	0.779
	cg_1	0.913	0.658	0.326
	cg_2	0.998	0.727	0.996

TABLE 6.6: Effect of CG position on SPPO Characteristics - All models.

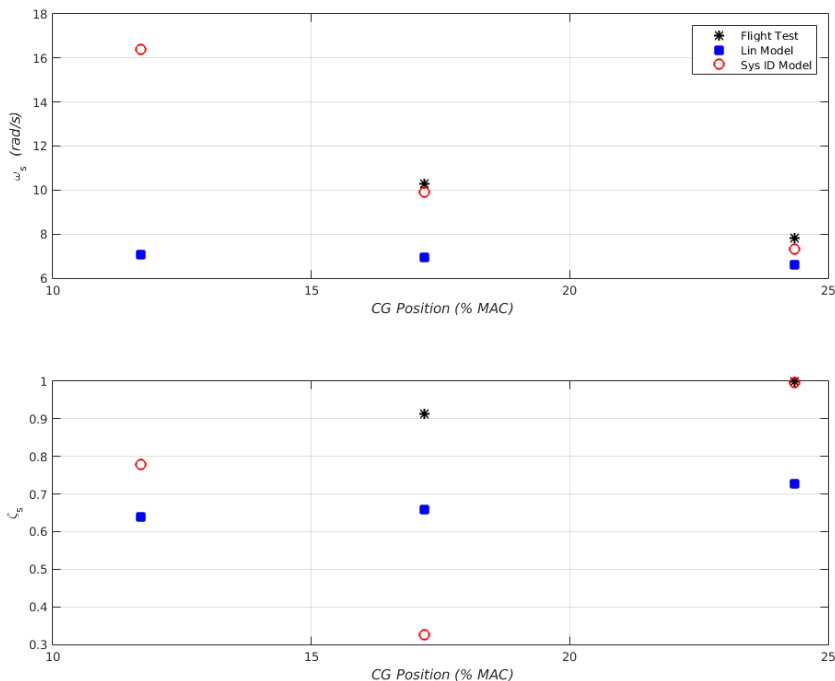


FIGURE 6.3: Effect of CG position on SPPO Characteristics - All models.

From Figure 6.3 arise several observations:

- The identified model characteristics are better fits to the flight test characteristics than the 6DoF linearised model.

The identified model is obtained making use of the flight test data and represents better the real aircraft than the linearised model. Assumptions and limitations in the 6DoF model development presented in previous chapters can be accounted for these discrepancies, especially:

1. The simulation has been carried out at an equivalent airspeed of 5 m/s when the operational flight envelope of the 6DoF model is from 5.1 m/s to 17m/s;
2. The mass properties calculation in the 6DoF model are not always an accurate representation of the mass properties during the test. The CG is not fixed as the various instrumentation parts are moved in and out of the aircraft in between tests and there is no quick way of checking they are at the adequate position;
3. The inaccuracy from the VLM model.

Nevertheless, these discrepancies are of relative small amplitude, with a maximum difference being between the frequencies at cg_1 , of 32% and the minimum difference between the damping ratios at cg_2 being of 6%.

- At cg_1 , the identified model damping ratio is not a good representation of the flight test data, with a damping ratio of 0.326 when compared to 0.913 from the flight test data (64% difference). This can be explained by the fact that the input was not perfectly as requested by the testing plan and created residual under-damped oscillations in the identified model. The aircraft response was not only a SPPO but a combination of other modes and the reduced order model assumed for the parameter estimation is not valid.
- Both the identified model and the flight test data follow the same trend in variations in SPPO frequency and damping ratio as the linearised model, reasons given in the chapter on the development of the 6DoF model.

Thus, the linearised 6DoF model could be improved by expanding its flight envelope. Also, fixed positions in the aircraft nose for the instrumentation would insure consistency in the mass properties calculations. The identified model is a very good fit to the SPPO flight test data.

6.2.2 Full Longitudinal Model (3-2-1-1 δ_e)

For the same reason as the SPPO, the discussion on the full longitudinal parameter estimation focuses on the effect of CG position on the longitudinal characteristics. Recalling the state space representation equation of the full longitudinal model,

as in Equation 6.2, Table 6.7 presents the parameter estimates of the model, the standard errors, the percentage error and the 95% confidence interval at all tested CG positions. It should be noted that in order to estimate the parameters, the results from the SPPO estimates have been used and set as constants in Equation 6.2. Thus, only the parameters x_u , x_w , x_q , x_{δ_e} , x_{τ} , z_u , z_{θ} , and m_u are estimated. Although the valid tests are not proper 3-2-1-1 inputs in elevator, they are a series of elevator deflection. As the model to be identified is a full longitudinal model, it is assumed that the identified parameters will accurately represent the aircraft dynamics.

$$\begin{bmatrix} \dot{u} \\ \dot{w} \\ \dot{q} \\ \dot{\theta} \end{bmatrix} = \begin{bmatrix} x_u & x_w & x_q & x_{\theta} \\ z_u & z_w & z_q & z_{\theta} \\ m_u & m_w & m_q & m_{\theta} \\ 0 & 0 & 1 & 0 \end{bmatrix} \begin{bmatrix} u \\ w \\ q \\ \theta \end{bmatrix} + \begin{bmatrix} x_{\delta_e} & x_{\tau} \\ z_{\delta_e} & z_{\tau} \\ m_{\delta_e} & m_{\tau} \\ 0 & 0 \end{bmatrix} \begin{bmatrix} \delta_e \\ \tau \end{bmatrix} \quad (6.2)$$

Figure 6.4 shows the response in pitch rate and pitch attitude to the elevator input at cg_0 . It is noticeable that the identified model is a poor representation of the flight test data. This can be explained by the fact that for the full longitudinal model, although the number of parameters to estimate have been reduced making use of previous knowledge on the system, there are too many states to fit simultaneously to end up with adequate results. Also, random changes in in-flight airspeed (due to atmospheric turbulence) led to perturbations in vertical and forward speed not following the pilot's input⁶.

⁶The airspeed would for example experience a sudden increase during the test.

Parameter	Estimate	Std Error	% Error	95% Confidence
				Interval
cg_0	x_u	5.150	1.205	23.4 [2.740 , 7.561]
	x_w	-30.49	17.26	56.6 [-65.003 , 4.032]
	x_q	-290.6	80.05	27.5 [-405.709 , -130.524]
	x_{δ_e}	-33.09	8.231	24.9 [-49.5498 , -16.625]
	x_τ	-0.020	3×10^{-3}	17.4 [-0.027 , -0.013]
	z_u	2.301	0.149	6.5 [2.003 , 2.599]
	z_θ	6.585	1.360	20.6 [3.865 , 9.304]
	m_u	-0.021	7×10^{-3}	37.2 [-0.037 , -0.005]
cg_1	x_u	-5.008	0.500	11.1 [-6.123 , -3.892]
	x_w	-189.9	22.16	11.7 [-237.261 , -145.635]
	x_q	-509.8	60.53	11.9 [-630.834 , -388.729]
	x_{δ_e}	-40.58	4.371	10.8 [-49.327 , -31.843]
	x_τ	-0.025	3×10^{-3}	11.5 [-0.0310 , -0.020]
	z_u	-0.166	0.029	17.9 [-0.225 , -0.107]
	z_θ	0.825	0.150	18.3 [0.524 , 1.127]
	m_u	0.190	0.015	8.1 [0.159 , 0.221]

TABLE 6.7: Full Longitudinal Parameter Estimates.

As the parameters for the SPPO had been fixed for the full longitudinal parameter estimation, its frequency and damping ratio remained unchanged. The full longitudinal model being a fourth order model the two other eigenvalues are for the Phugoid. These have been compared with the results from the 6DoF linearised model. The flight test data has not been used for this analysis as the graphical techniques implemented are not able to extract the Phugoid characteristics from the flight test time histories. Table 6.8 summarises the results⁷.

	CG Position	6 DoF Linearised Model	Identified Model
Frequency (rad/s)	cg_0	0.802	0.425
	cg_1	0.851	-
Damping Ratio	cg_0	-0.066	0.473
	cg_1	-0.058	-

TABLE 6.8: Effect of CG position on Phugoid Characteristics - All models.

⁷ "-" means the A matrix appeared to have a complex pair of eigenvalues (SPPO) and two distinct real negative eigenvalues (no Phugoid).

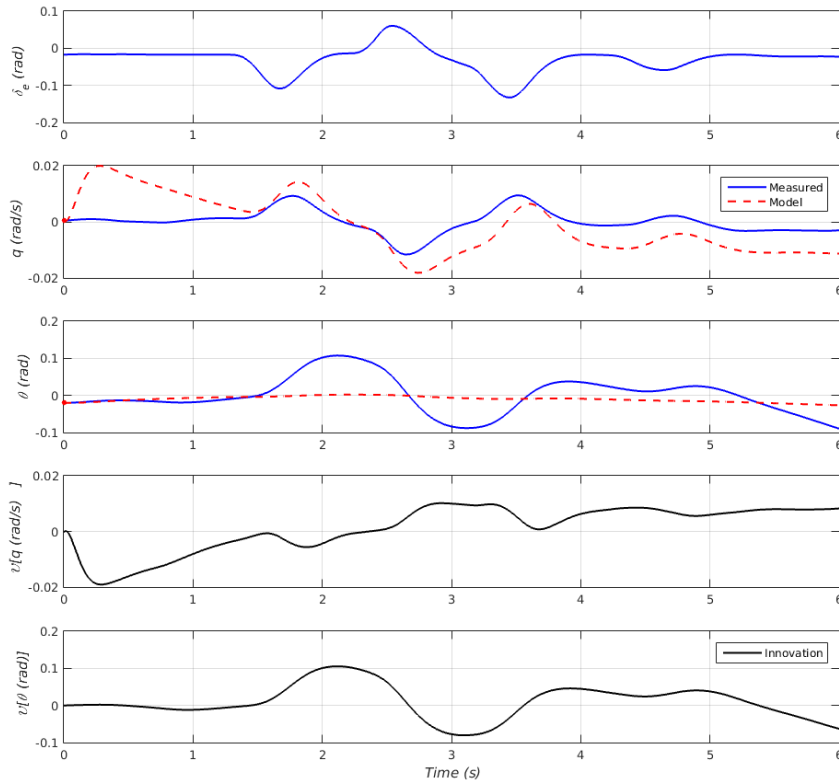


FIGURE 6.4: Full Longitudinal Flight Test data and Identified Model Response.

There is a 47% difference in frequency and a 114% difference in damping ratio between the 6DoF model and the identified model regarding the Phugoid characteristics. Thus, the instrumentation and the parameters estimation methodology presented in this thesis is not adequate when performing full longitudinal model parameter estimation.

The reasons of this poor quality parameter estimates could be:

- There are too many states to fit simultaneously;
- The a-priori values for the SPPO parameters are wrong;
- The pilot's input was not an adequate replica of the testing plan inputs;
- The airspeed readings were not as accurate as required.

6.2.3 Dutch Roll

As the valid Dutch Roll tests were carried at different airspeeds, the parameter estimation discussion will focus only on the effect of the airspeed on the Dutch Roll characteristics. Recalling the state space representation equation of the Dutch Roll as in Equation 6.3, Table 6.9 presents the parameter estimates of the mode at all tested airspeeds, the standard error, the percentage error and the 95% confidence interval on each estimate.

$$\begin{bmatrix} \dot{v} \\ \dot{r} \end{bmatrix} = \begin{bmatrix} y_v & y_r \\ n_v & n_r \end{bmatrix} \begin{bmatrix} v \\ r \end{bmatrix} + \begin{bmatrix} y_{\delta_a} & y_{\delta_r} \\ n_{\delta_a} & n_{\delta_r} \end{bmatrix} \begin{bmatrix} \delta_a \\ \delta_r \end{bmatrix} \quad (6.3)$$

Figure 6.5 shows the response in yaw rate for the Dutch Roll test at 5m/s airspeed, for both the flight test data and the identified model⁸. It is noticeable that the maximum amplitude of the innovation is 8.43% of the maximum amplitude of the measured r-response. Also, both the measured r-response and the identified model r-response have comparable frequencies and damping ratios. At this particular airspeed, the identified model is a very suitable representation of the real aircraft.

A trend is observable in the parameters of the Dutch Roll reduced model state space representation equation, the percentage errors are acceptable, and the 95% confidence intervals are not too wide for most parameters. It should also be noted that the parameters with the most significant percentage error are of very low values, especially the lateral force due to rudder deflection (y_{δ_r}).

For the same reasons as with the SPPO, the Dutch Roll frequency and damping are evaluated. Table 6.10 presents a comparison of the identified model, the linearised 6DoF model and the flight test data for all three airspeeds.

Figure 6.6 illustrates the data presented in Table 6.10.

⁸Similar figure for the other airspeed are in Appendices.

Parameter	Estimate	Std Error	% Error	95% Confidence Interval
4 m/s	y_v	8.909	3.558	[1.794 , 16.025]
	y_r	-22.36	7.113	[-36.588 , -8.137]
	y_{δ_a}	6.491	1×10^{-11}	[6.491, 6.491]
	y_{δ_r}	-0.398	0.093	[-0.585 , -0.211]
	n_v	6.727	1.501	[3.724 , 9.729]
	n_r	-11.67	3.593	[-18.859 , -4.489]
	n_{δ_a}	-150.4	0.000	[-150.381 , -150.381]
	n_{δ_r}	-0.290	0.021	[-0.332 , -0.249]
5 m/s	y_v	1.318	0.760	[-0.202 , 2.838]
	y_r	-9.366	1.291	[-11.947 , -6.785]
	y_{δ_a}	1.759	1×10^{-13}	[1.759, 1.759]
	y_{δ_r}	1×10^{-5}	0.046	[-0.093 , 0.093]
	n_v	4.074	0.150	[3.245 , 4.904]
	n_r	-4.774	0.789	[-6.352 , -3.197]
	n_{δ_a}	-21.35	0.000	[-21.350 , -21.350]
	n_{δ_r}	-0.241	0.014	[-0.269 , -0.212]
14 m/s	y_v	-1×10^{-5}	1.079	[-2.158 , -2.158]
	y_r	-28.64	6.786	[-42.213 , -15.068]
	y_{δ_a}	149.3	2×10^{-12}	[149.335, 149.335]
	y_{δ_r}	-0.091	0.090	[-0.273 , 0.090]
	n_v	1.548	0.367	[0.814 , 2.282]
	n_r	-2×10^{-5}	1.059	[-2.118 , 2.118]
	n_{δ_a}	-2309	0.000	[-2309 , -2309]
	n_{δ_r}	-0.143	0.017	[-0.178 , -0.109]

TABLE 6.9: Dutch Roll Parameter Estimates.

	EAS (m/s)	Test Data	6 DoF Linearised Model	Identified Model
Frequency (rad/s)	4	6.23	7.92	6.81
	5	6.89	3.81	5.65
	14	10.62	9.25	6.66
Damping Ratio	4	0.097	0.057	0.203
	5	0.139	0.085	0.306
	14	0.381	0.163	3×10^{-6}

TABLE 6.10: Effect of Airspeed on Dutch Roll Characteristics - All models.

From Figure 6.6 arise several observations:

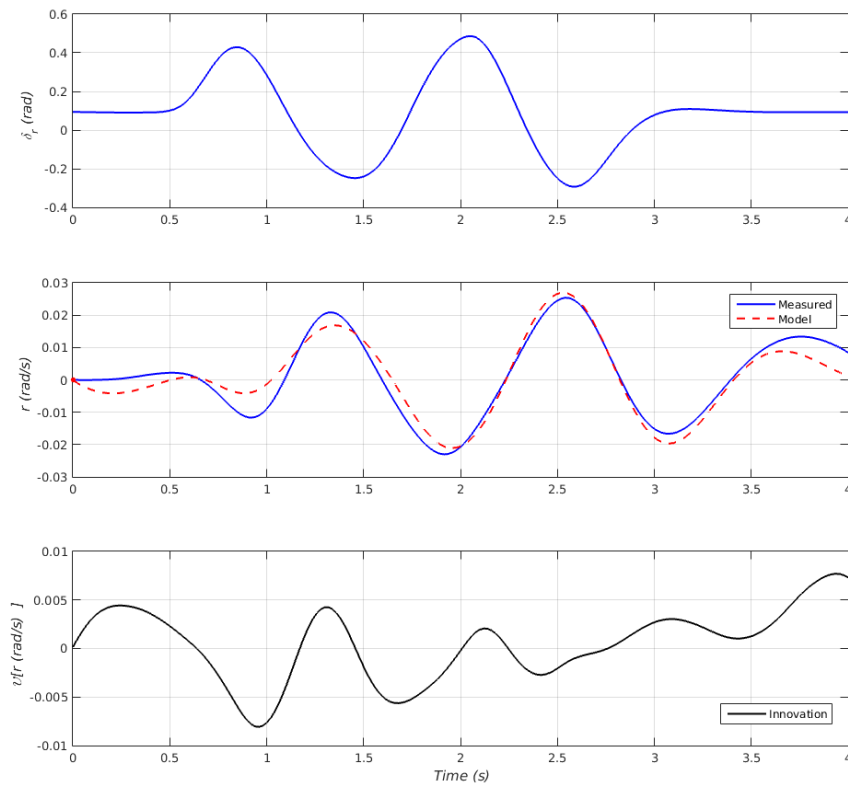


FIGURE 6.5: Dutch Roll Flight Test data and Identified Model r-response.

- The identified model characteristics are better fits to the flight test characteristics than the 6DoF linearised model at low airspeeds.

Assumptions and limitations in the 6DoF model development presented in previous chapters can be accounted for these discrepancies, especially:

1. The simulation has been carried out at an equivalent airspeed lower than 5.1 m/s, which are out of the flight envelope of the model;
2. The 6DoF model has been built making use of VLM models. Those models do not take into account the fuselage of the aircraft, thus the drag estimates are not fully representing the reality. This creates differences in the side force estimation, that leads to discrepancies in the Dutch Roll characteristics.

Nevertheless, these discrepancies are of relative small amplitude, with a maximum difference being between the frequencies at EAS = 5m/s, of 44% and the minimum difference between the damping ratios at EAS = 5m/s being of 38%.

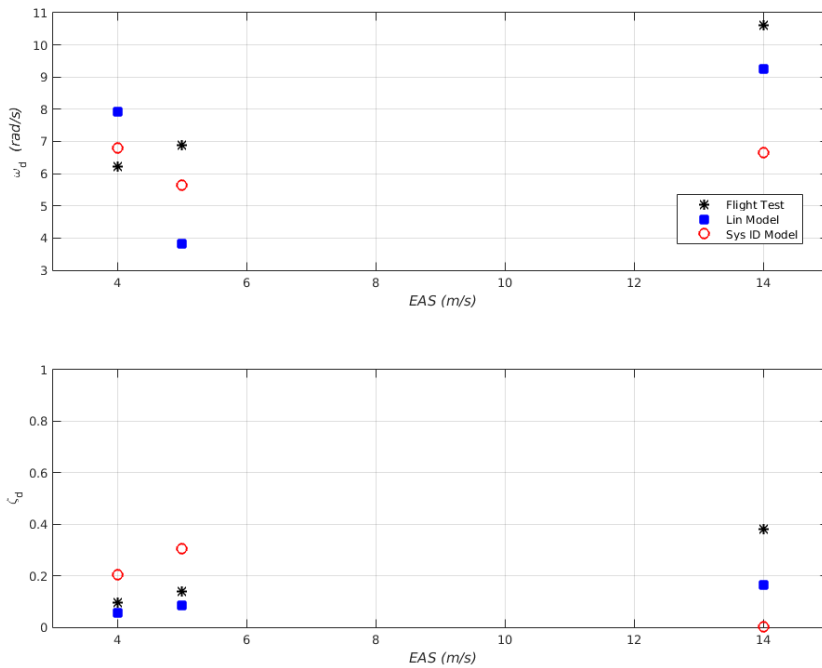


FIGURE 6.6: Effect of Airspeed on Dutch Roll Characteristics - All models.

- At $EAS = 14\text{m/s}$, the identified model characteristics are very different from the flight test characteristics, with 37% difference in frequency and 38% difference in damping ratio. The MLE algorithm did not converge to the right model for various reasons, but most notably the atmospheric gusts changing the instantaneous airspeed readings.

It would be desirable to expand this analysis by performing more flight testing at airspeeds in the 6DoF model flight envelope.

6.2.4 Roll Mode

The valid Roll mode tests were carried at different airspeeds, thus the parameter estimation discussion will focus only on the effect of the airspeed on the Roll mode characteristics. Recalling the state space representation equation of the Roll mode as in Equation 6.4, Table 6.11 presents the parameter estimates of the mode at all tested airspeeds, the standard error, the percentage error and the 95% confidence interval on each estimate.

$$\begin{bmatrix} \dot{p} \\ \dot{\phi} \end{bmatrix} = \begin{bmatrix} l_p & 0 \\ 1 & 0 \end{bmatrix} \begin{bmatrix} p \\ \phi \end{bmatrix} + \begin{bmatrix} l_{\delta_a} & l_{\delta_r} \\ 0 & 0 \end{bmatrix} \begin{bmatrix} \delta_a \\ \delta_r \end{bmatrix} \quad (6.4)$$

Figure 6.7 shows the response in roll rate for the Roll mode test at EAS = 18 m/s, for both the flight test data and the identified model⁹. It is noticeable that the maximum amplitude of the innovation is 16.6% of the maximum amplitude of the measured p-response. Also, both the measured p-response and the identified model p-response have comparable time constants and amplitudes. At this airspeed, the identified model is a very suitable representation of the real aircraft.

	Parameter	Estimate	Std Error	% Error	95% Confidence Interval
4 m/s	l_p	-100.9	0.060	0.1	[-101.027 , -100.789]
	l_{δ_a}	-11.40	0.556	4.9	[-12.511 , -10.286]
	l_{δ_r}	544.2	0.000	0.0	[544.213, 544.213]
18 m/s	l_p	-5.623	0.314	5.6	[-6.251 , -4.995]
	l_{δ_a}	-0.596	0.030	5.1	[-0.657 , -0.536]
	l_{δ_r}	-254.7	0.000	0.0	[-254.739, -254.739]

TABLE 6.11: Roll mode Parameter Estimates.

The Roll mode parameters present the lowest percentage errors and narrow 95% confidence intervals. This is because the roll mode reduced order model not only has very few parameters to identify at once but also is based only on two states.

Table 6.12 presents the effect of airspeed on the roll mode time constant for the flight test data, the 6DoF linearised model and the identified model.

	EAS (m/s)	Test Data	6 DoF Linearised Model	Identified Model
Time Constant (s)	4	0.24	0.010	0.016
	18	0.28	0.018	0.010

TABLE 6.12: Effect of Airspeed on Roll mode Characteristics - All models.

⁹Similar figure for the other airspeeds are in Appendices.

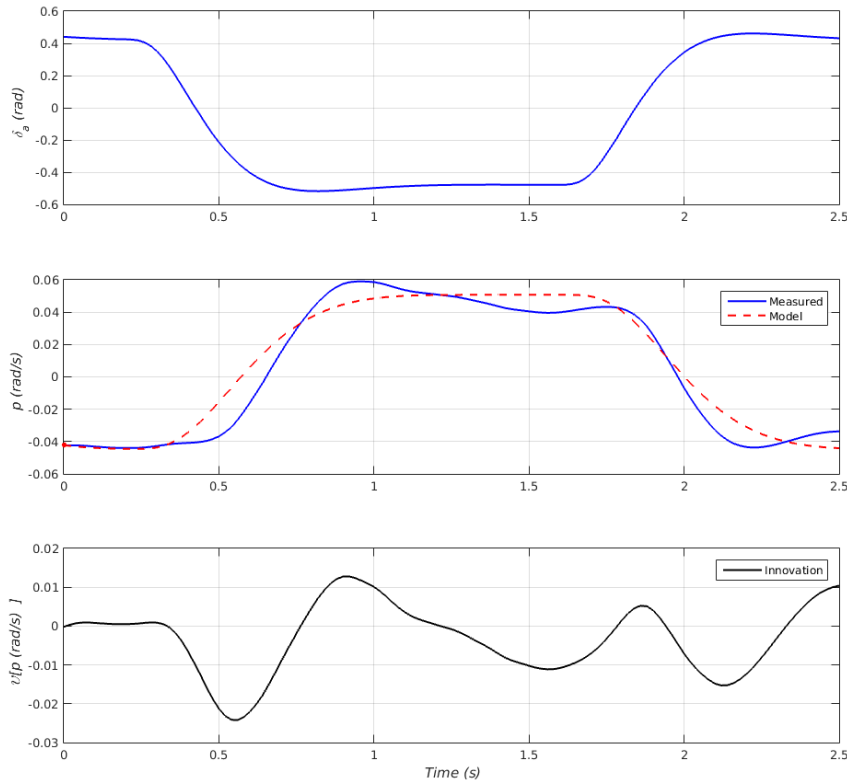


FIGURE 6.7: Roll mode Flight Test data and Identified Model p-response.

The data from Table 6.12 shows that:

- During the flight test, the input in aileron was not instantaneous from the trimmed position to the step, thus the technique¹⁰ used to compute the time constant of the flight test data is not adequate and gives time constants that are greater than the actual value of the roll mode time constant.
- The 6DoF linearised model is not valid at EAS = 4 m/s as this airspeed is out of the flight envelope of the model.

The system identification methodology presented in this thesis is thus adequate when identifying the Roll mode of the aircraft.

¹⁰Time Constants estimation technique.

6.2.5 Full Lateral Model (3-2-1-1 δ_a)

No convergent solution has been found for any of the valid full lateral tests. This is explained by the fact that despite the relatively small number of parameters to estimate, the high number of states in the model could not be fit simultaneously. Also, the instrumentation was not accurate enough, especially in airspeed readings, thus made the model even more difficult to identify.

It is recommended to either use a better airspeed sensor, fly in no wind condition or use the wind tunnel where no gust is expected. These precautions will allow to perform better parameter estimates for the full lateral model.

Chapter 7

Models Validation

This chapter presents the validation of both the full non linear 6DoF model and the System Identification model obtained within this thesis. It consists of using independent flight test data, which has not been used for the formulation of the System Identification model development and compare it to the models results. A statistical analysis of the innovations (difference between the flight test data and the models outputs) is carried out. A comparison on the mean and standard deviation of the innovations is made and is used for discussion.

7.1 Short Period Pitching Oscillations (SPPO)

The test used for validation of the SPPO models is a test at $c g_0$ and 6m/s EAS. Figure 7.1 presents the response in pitch rate of the SPPO for the validation test, the identified model at $c g_0$ and the 6DoF model, with the innovations for both models.

It appears that both the 6DoF model and the identified model are good matches to the validation test data. It was impossible to extract the frequencies and damping ratios of the validation flight test and the 6DoF response as at least one overshoot after the input is required when using the maximum slope graphical technique. The validation analysis is thus done only on the innovations. The maximum innovation of the 6DoF model is 40% of the maximum amplitude of the validation test data while the maximum innovation of the identified model is 19% of the maximum amplitude of the validation test data.

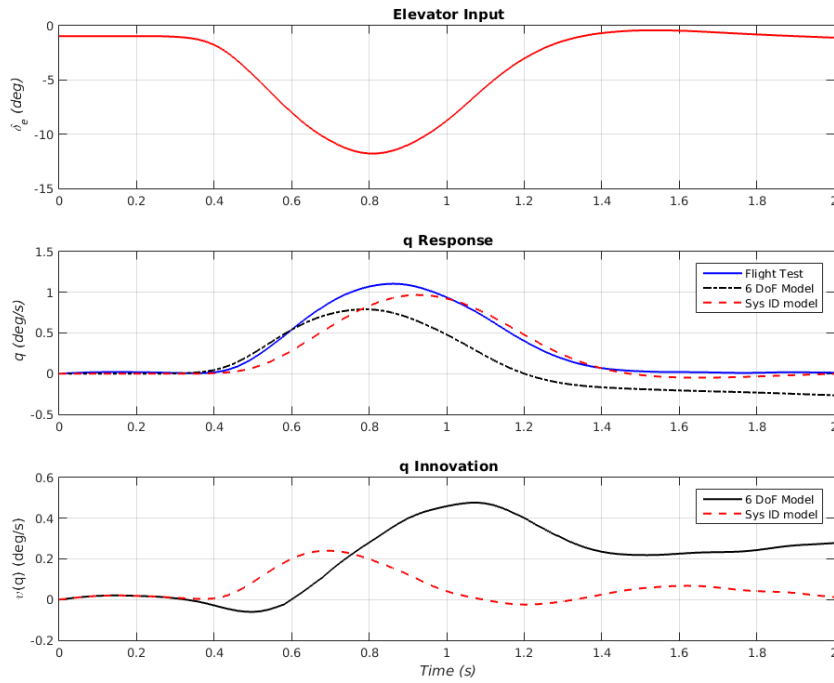


FIGURE 7.1: SPPO Validation q-Response.

The statistical analysis is done on the innovations and Figure 7.2 presents the histograms of the innovations of both the 6DoF model and the identified model. A normal distribution has been fitted on both histograms and the mean values and standard deviations are summarised in Table 7.1.

	6 DoF Model	Identified Model
Mean (deg/s)	0.198	0.059
Standard Deviation (deg/s)	0.164	0.073

TABLE 7.1: SPPO q-Innovations Statistical Characteristics.

From Figure 7.2, it appears that a normal distribution is a good fit to the histogram for the identified model but not necessary for the non linear 6DoF model (a noticeable number of counts are far from the mean value of the innovation). This means that the full non-linear model fails to capture some of the inner dynamics of the aircraft. In addition, from Table 7.1, it is noticeable that the 6DoF model innovations, assuming the normal distribution is an acceptable fit, have a mean value further from zero when compared to the identified model and a standard deviation much higher (124% higher).

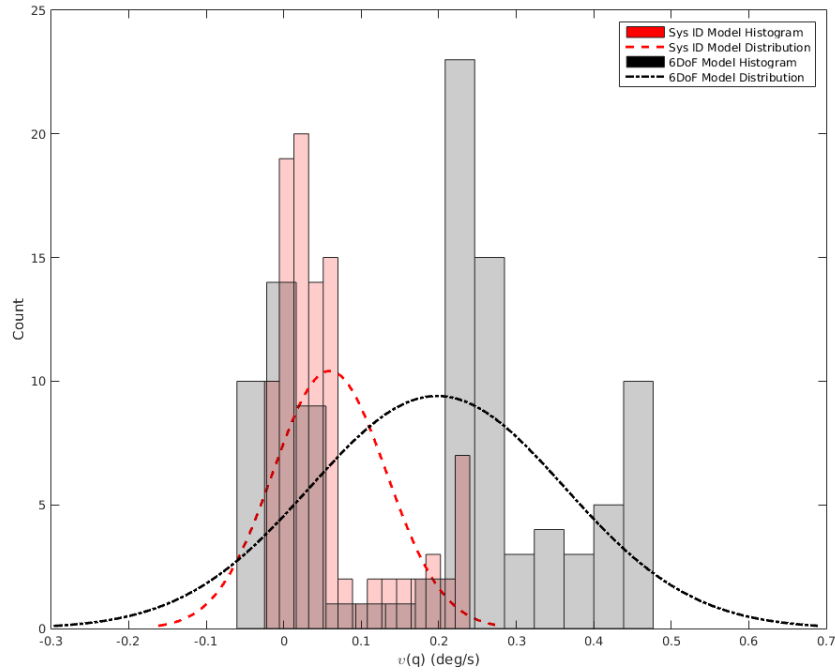


FIGURE 7.2: SPPO q-Innovations Histograms.

With such characteristics, the SPPO identified model is validated, while the 6DoF model is an acceptable approximation but would require additional work otherwise may fail to capture some of the real aircraft dynamics.

7.2 Dutch Roll

The test used for validation of the Dutch Roll models is a test at $c g_0$ and 5m/s EAS. Figure 7.3 presents the response in yaw rate of the Dutch Roll for the validation test, the identified model and the 6DoF model, with the innovations for both models.

It appears that both the 6DoF model and the identified model are good matches to the validation test data. However, the full non-linear 6DoF model response during the input is not a second order response. This could be explained by the fact that the pilot input is not a perfect series of doublets and the non linearities included in the model are responsible for the flattered portions of r-response. Also, the 6DoF model has overall higher amplitudes than the validation test response.

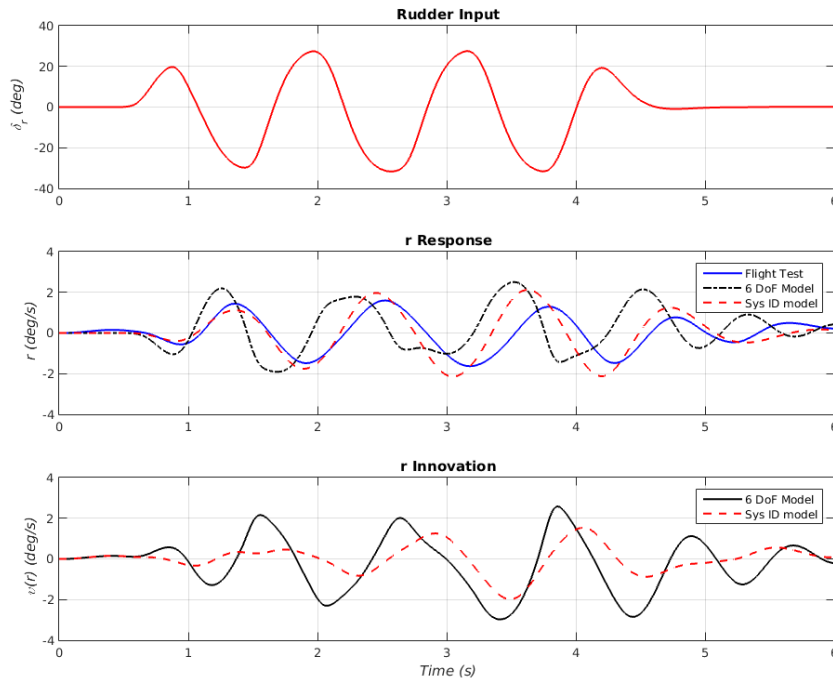


FIGURE 7.3: Dutch Roll Validation r-Response.

The modal characteristics of the validation test, full non linear response and identified model are in Table 7.2.

	Flight Test	6 DoF Model	Identified Model
Frequency (rad/s)	6.75	7.13	5.65
Damping Ratio	0.103	0.155	0.306

TABLE 7.2: Dutch Roll Validation Modal Characteristics.

The frequencies of the 6DoF model and the identified model are 5% higher and 16% lower than the validation test one respectively. Also, the damping ratio are 50% and 197% higher respectively¹. Thus, in terms of modal characteristics, the 6DoF represents better the flight test data. However, from Figure 7.3 the innovations of the 6DoF model have a much higher amplitude than the identified model. The maximum innovation of the 6DoF model is 139% of the maximum amplitude of the validation test data while the maximum innovation of the identified model is 90% of the maximum amplitude of the validation test data. Thus, in terms of innovations amplitude, the identified model is a better fit to the validation data.

¹These percentages are high partly because of the low value of the damping ratio.

It should also be noted that due to the difference in frequencies, the test and the models are out of phase. This could be an explanation to the relatively high innovations amplitude.

Figure 7.4 presents the histograms of the innovations of both the 6DoF model and the identified model. A normal distribution has been fitted on both histograms and the mean values and standard deviations are summarised in Table 7.3.

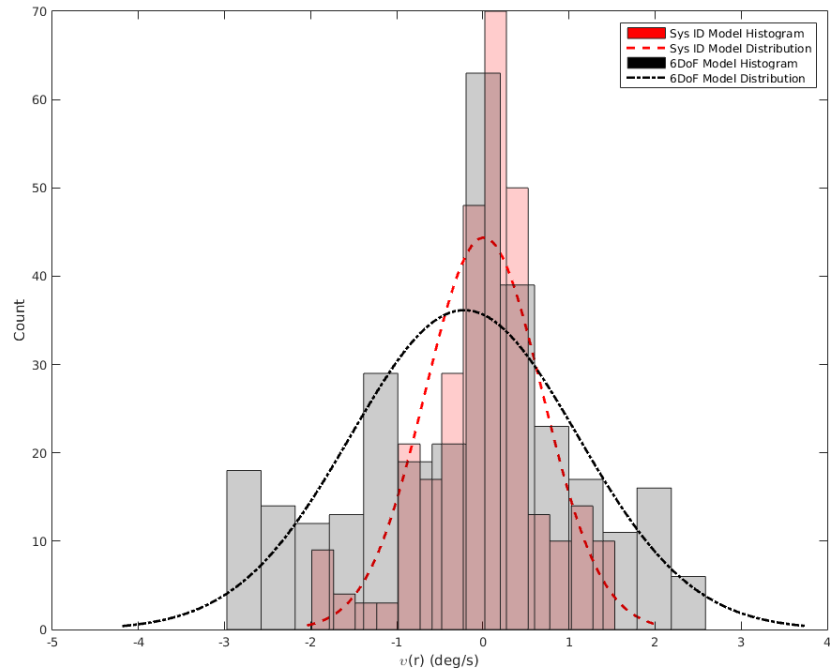


FIGURE 7.4: Dutch Roll r-Innovations Histograms.

	6 DoF Model	Identified Model
Mean (deg/s)	-0.216	0.010
Standard Deviation (deg/s)	1.318	0.679

TABLE 7.3: Dutch Roll r-Innovations Statistical Characteristics.

From Figure 7.4, it appears that normal distributions are good fits to both histograms. Both models capture well the dynamics of the aircraft system. The difference between the models and the flight test data could thus been attributed to random external physical phenomena. Also, Table 7.3 shows that both models innovations have mean values very close to zero. The 6DoF model innovations have a higher standard deviation when compared to the identified model innovations.

Thus in terms of innovations mean values and standard deviation, the identified model is a better fit to the validation data.

The validation of the Dutch Roll highlighted that for validation, more than one criteria should be investigated. Focusing only on the frequencies and damping ratios may lead to incorrect validation as the amplitudes may not be of the same scale. Also, the sole analysis of the innovations does not highlight the difference in frequency which leads to responses to be out of phase, hence higher innovations. The analysis of the mean value and standard deviation of the innovations helps examine the nature of the innovations but does not tell anything about the accuracy in terms of modal characteristics of the models.

Both models are acceptable approximations to the aircraft Dutch Roll dynamics.

7.3 Roll Mode

The test used for validation of the Roll mode models is a test at $c g_0$ and 4m/s EAS. Figure 7.5 presents the response in roll rate of the Roll mode for the validation test, the identified model and the 6DoF model, with the innovations for both models.

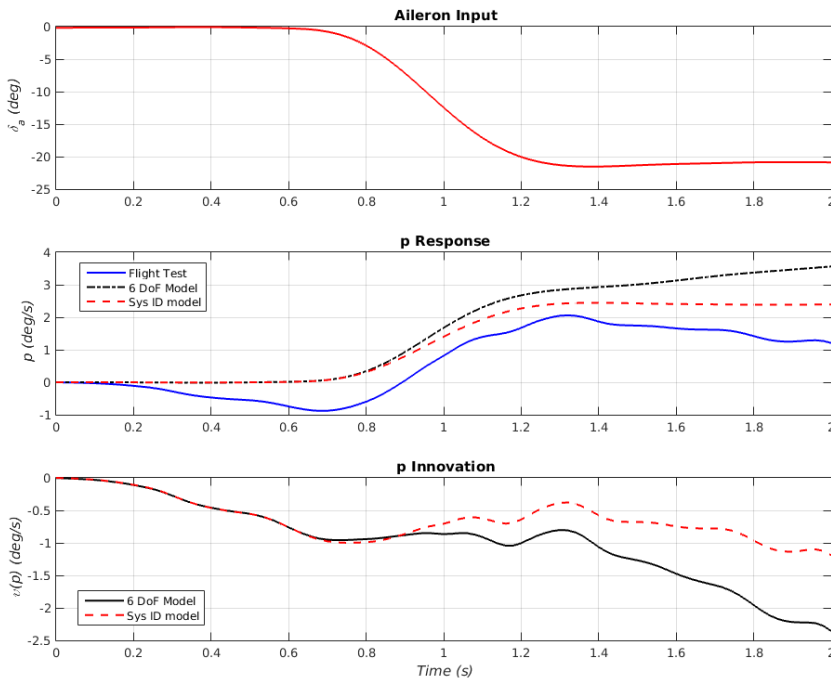


FIGURE 7.5: Roll Mode Validation p-Response.

It appears that both the 6DoF model and the identified model are acceptable matches to the validation test data. Yet, it should be noted that before the test input, the roll rate of the flight test data is decreasing. This means the aircraft was not adequately trimmed during this test². This creates high discrepancies in the roll rate responses in terms of magnitude but the trends qualitatively look similar. Quantitatively, the modal characteristics of the validation test, full non linear response and identified model are in Table 7.4.

	Flight Test	6 DoF Model	Identified Model
Time Constant (s)	0.18	0.15	0.016

TABLE 7.4: Roll Mode Validation Modal Characteristics.

The values for the time constant of the flight test data and the 6DoF model are obtained with the use of a graphical method³. This method is valid with a step input while in our case, we have a ramp. Thus, those values are not accurate. However, using the same method for both the flight test data and the 6DoF model, the obtained time constants are similar (16% difference).

Figure 7.6 presents the histograms of the innovations of both the 6DoF model and the identified model. A normal distribution has been fitted on both histograms and the mean values and standard deviations are summarised in Table 7.5.

	6 DoF Model	Identified Model
Mean (deg/s)	-0.967	-0.638
Standard Deviation (deg/s)	0.616	0.314

TABLE 7.5: Roll Model p-Innovations Statistical Characteristics.

From Figure 7.6, it appears that normal distributions are good fits to both histograms. Both models capture well the dynamics of the aircraft system. The difference between the models and the flight test data could thus be attributed to random external physical phenomena. From Table 7.3, both models innovations have non-zero mean values, due to the fact that the aircraft was not adequately trimmed during the flight test, but the standard deviations of the innovations are

²It is the only validation test that was "acceptable".

³The time constant method.

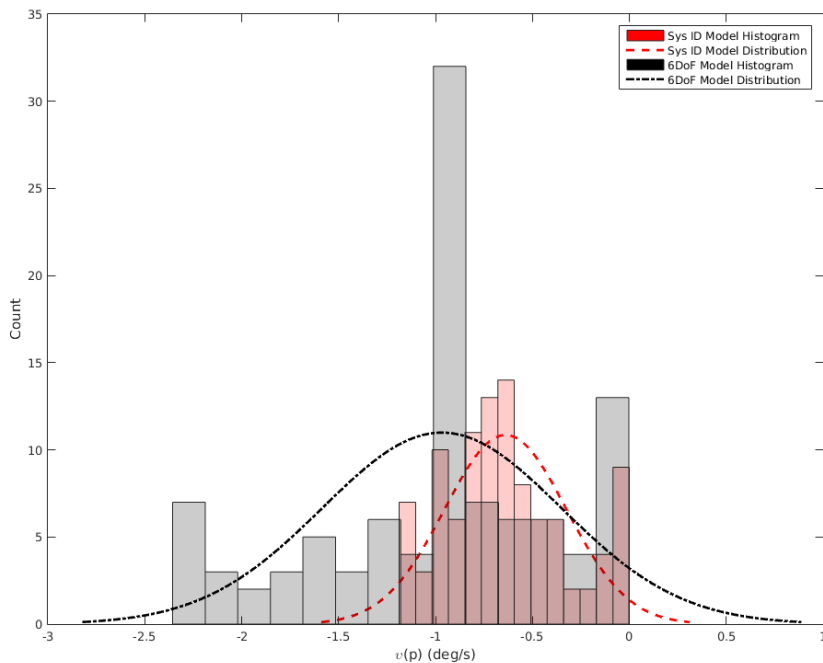


FIGURE 7.6: Roll Mode r-Innovations Histograms.

relatively small. The identified model innovation have a smaller standard deviation than the 6DoF model. It is then a better approximation to the real aircraft.

Both models are a good representation of the real aircraft roll model dynamics and are thus validated.

7.4 Phugoid

The test used for validation of the Phugoid models is a test at cg_0 and 5m/s EAS. Figure 7.7 presents the response in pitch rate of the Phugoid for the validation test, the identified model at cg_0 and the 6DoF model, with the innovations for both models.

It appears that both the 6DoF model and the identified model are good matches to the validation test data. The identified model is the full longitudinal dynamics model developed in previous chapters. Despite the fact that when estimating its parameters, this model presented great discrepancies when compared to the flight test data (3-2-1-1 δ_e input), qualitatively as shown in Figure 7.7, its q-response is very comparable to the Phugoid validation test data. This could be explained as

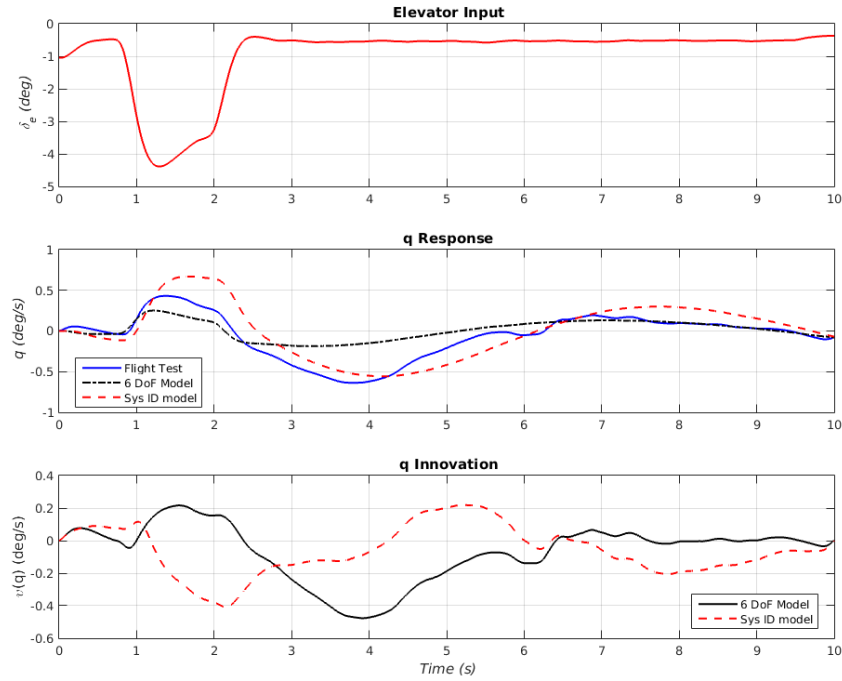


FIGURE 7.7: Phugoid Validation q-Response.

the Phugoid validation test is not as complex as the pseudo 3-2-1-1 δ_e that was used when estimating the parameters and the response is a second order response to a step input.

Quantitatively, the modal characteristics of the validation test, full non linear response and identified model are in Table 7.6.

	Flight Test	6 DoF Model	Identified Model
Frequency (rad/s)	1.300	0.928	0.888
Damping Ratio	0.142	0.122	0.189

TABLE 7.6: Phugoid Validation Modal Characteristics.

The frequencies and damping ratios of the two models are very comparable to the characteristics of the validation test data, with 28% and 31% difference in frequency for the 6DoF model and the identified model respectively. The difference in damping ratio is 14% and 33% respectively. The 6DoF is a better fit to the validation data when considering only modal characteristics.

The difference between the validation data and the full 6DoF model damping ratio can be explained by the omission of the fuselage in the flight dynamics modelling. Indeed the drag has a great impact on the Phugoid damping ratio. The aerodynamic coefficients have been obtained without the fuselage, thus the drag coefficient of the 6DoF model is less important than the real aircraft. Also, the absence of viscous drag in the VLM modelling could be a cause of this discrepancies.

Regarding the innovations, Figure 7.8 presents the histograms of the innovations of both the 6DoF model and the identified model. A normal distribution has been fitted on both histograms and the mean values and standard deviations are summarised in Table 7.7.

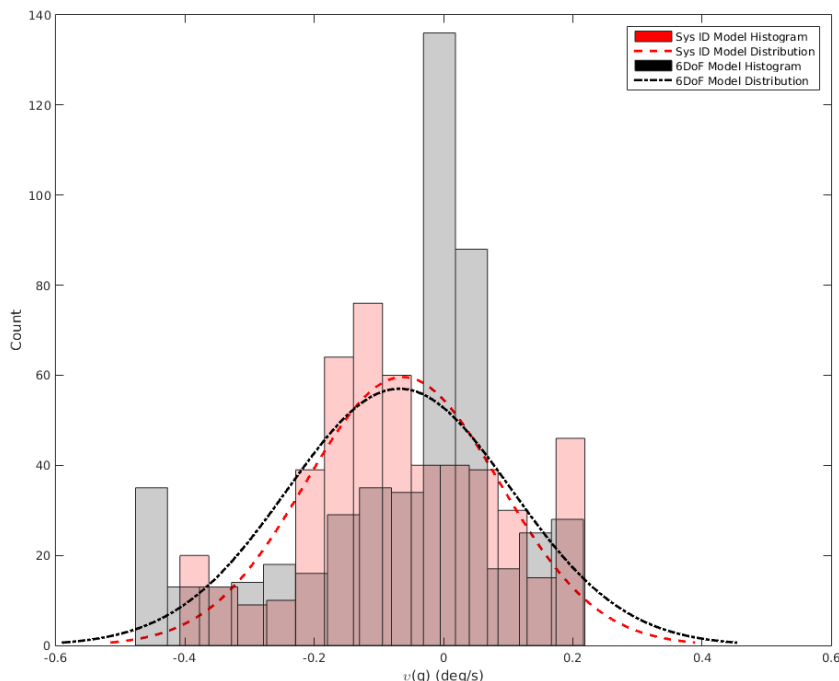


FIGURE 7.8: Phugoid q -Innovations Histograms.

	6 DoF Model	Identified Model
Mean (deg/s)	-0.068	-0.063
Standard Deviation (deg/s)	0.173	0.150

TABLE 7.7: Phugoid q -Innovations Statistical Characteristics.

Figure 7.8, shows that normal distributions are good fits to both histograms. The two models are good representations of the dynamics of the aircraft. The difference

between the models and the flight test data could then been due to random external physical phenomena. In addition, Table 7.7 shows that the mean values of the two distributions are very close to zero and very similar. Also, the standard deviations are relatively small when compared to the amplitude of the q-responses.

The two models are good approximations to the Phugoid dynamics of the aircraft and are thus validated.

Chapter 8

Conclusion & Suggestions

8.1 Aim and Objectives Achievement

8.1.1 Aim Achievement

The aim of this thesis has been achieved, instrumentation, modelling of a 6 Degrees of Freedom model and System Identification of the Easystar II aircraft, followed by validation of all models.

8.1.2 Instrumentation Objectives Achievement

The aircraft has been appropriately instrumented for the system identification and models validation.

- Different electronic boards have been considered for the instrumentation of the aircraft, and the 3DR Pixhawk has been selected for this mission. This is mainly due to its ease of use, its inboard Inertial Measurement Unit with acceptable sampling rates and its vast online community ready to help with any related problem.
- All components of the instrumentation have been put together and calibrated if required.
- The PWM (Pulse-Width Modulation) signals from the electronic board have been accordingly converted into control surfaces deflections and motor thrust.

- The download of the logged data has been facilitated with a user-friendly script with a Graphic User Interface.

8.1.3 Modelling Objectives Achievement

The aircraft has been modelled as a non-linear 6DoF model into Simulink.

- The airframe geometry has been modelled in AVL, and the aerodynamic coefficients computed.
- The mass properties of the airframe have been obtained with an XFLR5 model and a MATLAB routine has been used to compute the mass properties of the aircraft, including all instrumentation, motor, servos and Electronic Speed Controllers (ESC).
- The 6DoF model has been developed within MATLAB/Simulink, trimmed, decoupled and linearised.
- A discussion on the effect of airspeed and CG position on the linearised model modal characteristics has been carried out.

8.1.4 System Identification Objectives Achievement

A System Identification for aircraft applications based on the Maximum Likelihood Estimation (MLE) methodology has been developed and implemented. The reduced order models appeared to be remarkably good approximations of the flight test data, while the full order models were less accurate representations. The full lateral model has not been identified as the MLE algorithm did not produce a suitable solution.

- The model structure has been postulated and determined.
- The Experimental framework has been defined and a testing plan designed.
- The data analysis methodology defined and implemented.
- The MLE parameter estimation algorithm has been implemented making use of SIDPAC (System Identification Programs for Aircraft)[26].

- A model validation methodology have been defined.
- The flight test has been successfully carried out with the help of a RC-plane test pilot and a student flight test engineer.
- The flight test data has been processed and filtered.
- The model parameters have been estimated and the model state space representation matrices built.
- A discussion on the accuracy of the identified models have been carried out, alongside with the linearised 6DoF model.
- A discussion on the effects of the airspeed and centre of gravity position on the parameter estimates and modal characteristics of the identified models have been carried out. The results have been compared with the linearised 6DoF model and flight test data and further discussed.

8.1.5 Validation Objectives Achievement

The full non-linear 6DoF model and the identified models have been validated. The reduced order models have been validated as expected, and the identified full longitudinal model, despite its apparent poor representation of the aircraft dynamics when performing the parameter estimates has been validated for Phugoid dynamics.

- The models have been validated using independent validation flight test data.
- A discussion on the modal characteristics of the models compared to the validation flight data have been carried out.
- A discussion on the statistical characteristics (arithmetic mean value and standard deviation) of the errors between the validation flight test data and the model responses have been carried out.

8.2 Personal Research Outcomes

After the completion of this thesis, several results have been obtained:

- An instrumented aircraft, ready to be used for further flight testing.
- VLM models of the aircraft, with a discussion on the limitations of the VLM modelling.
- A 6DoF model of the aircraft that could be used for further research (Controller design, real time parameter estimation, ect...), with a discussion on its limitations and the impact of airspeed and CG position on its model characteristics.
- A user friendly data processing script for the 3DR Pixhawk.
- A System Identification Methodology for fixed wing aircraft applicable to other similar aircraft.
- A user friendly fixed wing aircraft parameter estimation script.
- A validation methodology based on both modal characteristics and innovations statistical analysis.
- Identified reduced order models and full longitudinal models (validated), with a discussion on their accuracy and the effects of CG position and Airspeed on their modal characteristics.

Those outcomes can be used for further investigation of the Easystar II or other similar fixed wing aircraft.

8.3 Main Difficulties

The main difficulties encountered during this project can be summarised as:

- The hardware implementation was difficult, as I was new to electronics.
- The binding between the RC Transmitter and the RC receiver on-board the aircraft was weak and led to two crashes.
- The difficulties the pilot encountered trimming the aircraft, especially during windy days compelled us to reject a great number of tests.
- The poor quality of the airspeed readings led to poor parameter estimates.

8.4 Improvements and Suggestions for Future Work

Further improvements could be done to the work presented in this thesis.

8.4.1 Instrumentation Improvements

The instrumentation based on the Pixhawk used in this thesis records the air data and the control deflections and thrust at a frequency of 10Hz while recording all other states at 50Hz. Improvements can be made here by manually programming the Pixhawk or getting into its parameters to set the sampling frequency at 50Hz for all readings. Also, the airspeed sensor used in this thesis is not as precise as expected and made the parameter estimation more difficult. A different one could be used to get better airspeed readings. An angle of attack boom could also be fitted to the aircraft nose, in order to have more accurate values of the angle of attack and sideslip angles, but this may affect the aircraft dynamic characteristics. Ultimately, an automation of the in-flight inputs could be implemented, in order to always have control surfaces deflections as required by the testing plan.

8.4.2 Modelling Improvements

Adnan Asif (MSc Aerospace Dynamics student at Cranfield University in 2014-2015) developed a CAD model of the Easystar II for his thesis. Using this to obtain the mass properties of the aircraft would improve the accuracy of the 6 DoF model. Also, a CFD analysis of the aircraft could be carried out in order to obtain the more accurate values of the aerodynamic coefficients, including the viscous drag. In addition, the flight envelope in terms of airspeed of the 6DoF model should be extended as the aircraft was flown at speeds slightly lower than the ones initially expected. Also, the aircraft motor has not been modelled and could be added to the presented work in the future.

8.4.3 System Identification Improvements

It would be suitable to use the wind tunnel testing methodology presented in this thesis and conduct wind tunnel testing on the aircraft for the system identification.

Not only gusts and atmospheric disturbances are not expected in a wind tunnel but instantaneous wind speed could be obtained from the wind tunnel instrumentation. Also, a different method could be used for the parameter estimation and compared to the results presented in this thesis. Additionally, when estimating the full longitudinal and lateral parameters, it may be suitable not to use any a priori value for some of the parameters. In this thesis some of the parameters were considered known from the reduced order models to save computational time.

8.4.4 Validation Improvements

The validation could be done for all CG positions and airspeeds, with independent data sets. In this thesis due to the lack of quality test data for validation, only one data set has been used to validate the models regarding each mode.

Appendix A

6DoF Model SIMULINK Blocks

A.1 Overall Equations of Motion Subsystem

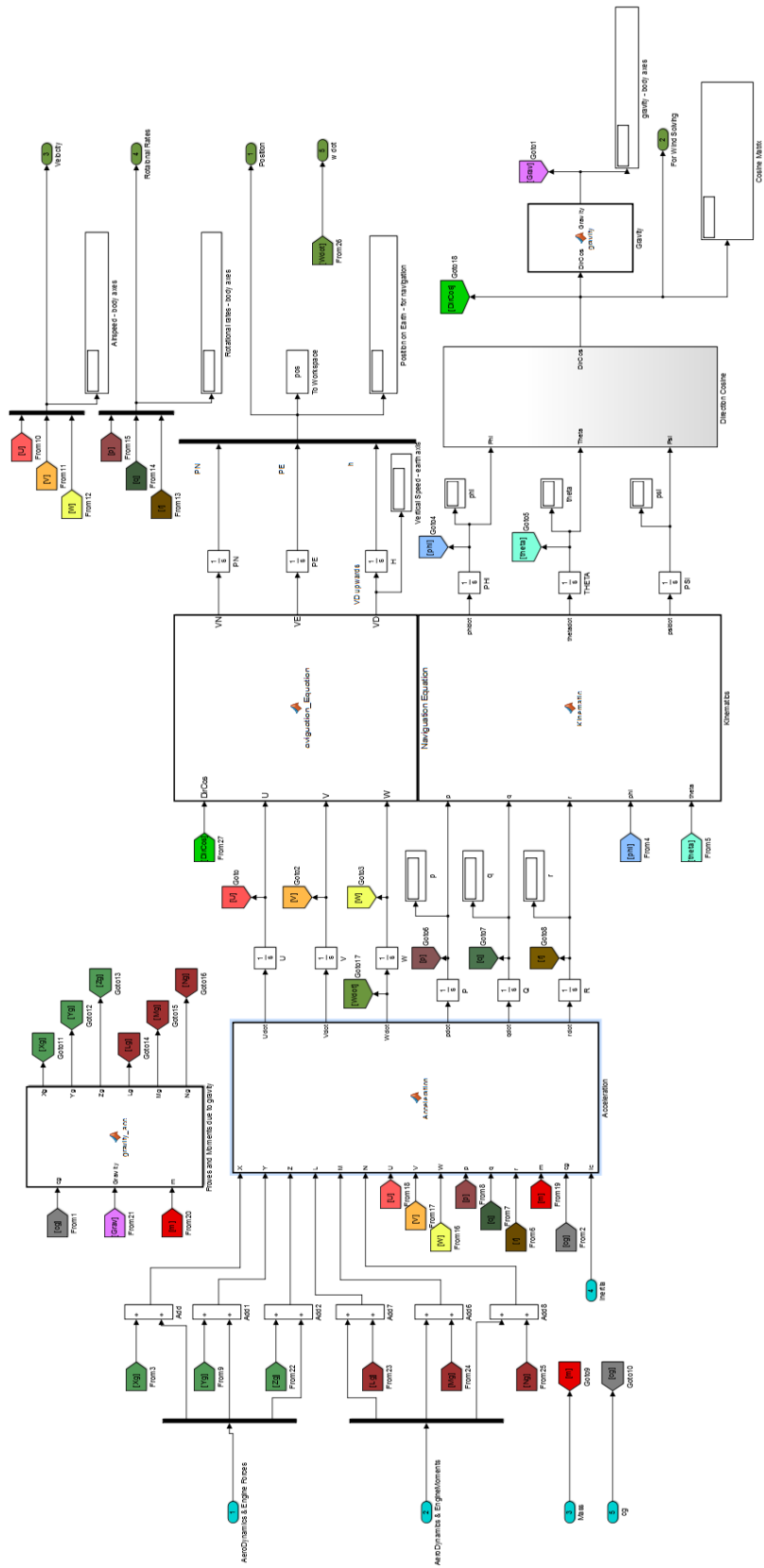


FIGURE A.1: Equations of Motion Subsystem.

A.2 Overall 6 DoF Simulation Model

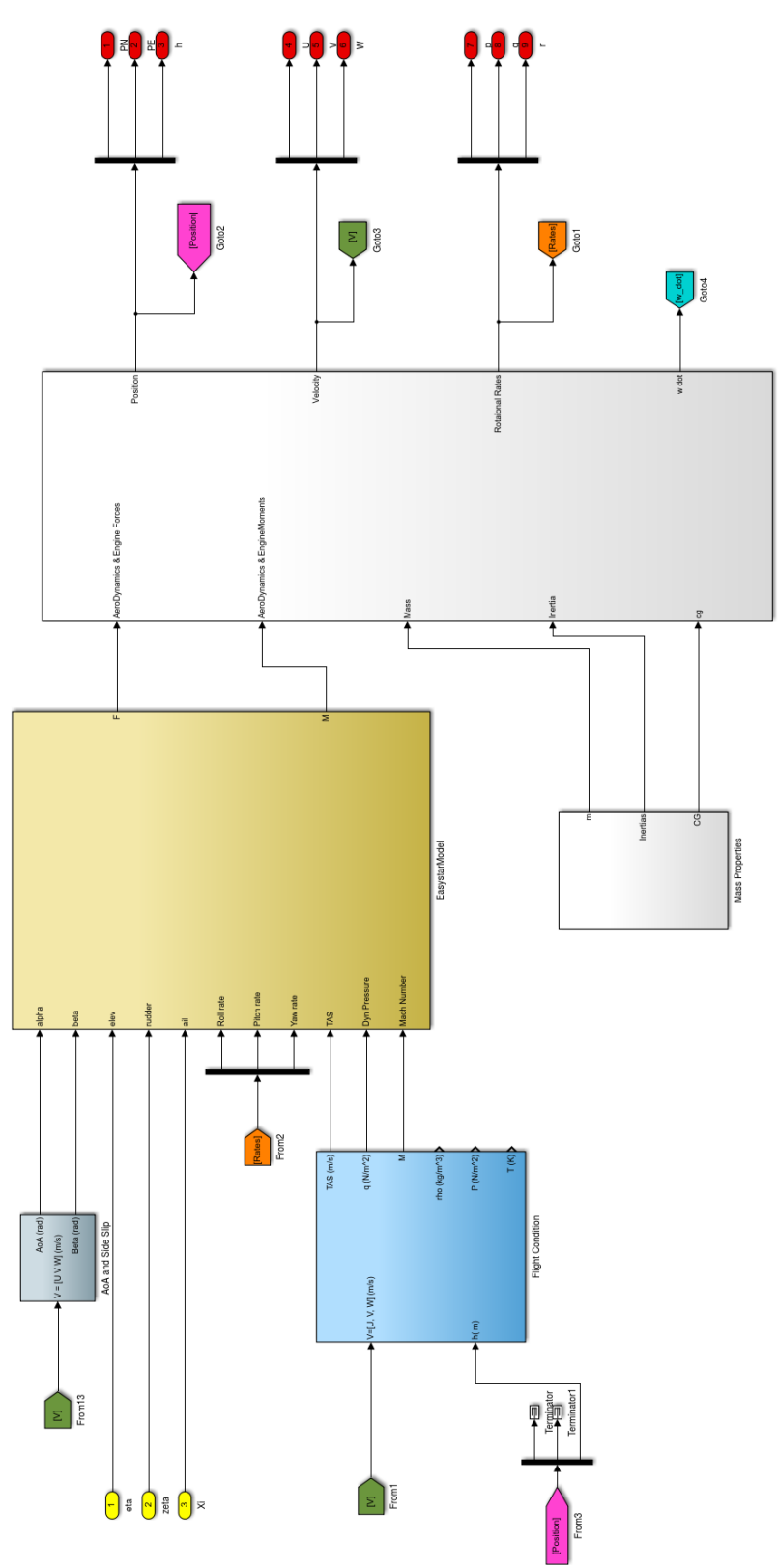


FIGURE A.2: Overall 6 DoF Simulation Model.

Appendix B

Graphical User Interfaces

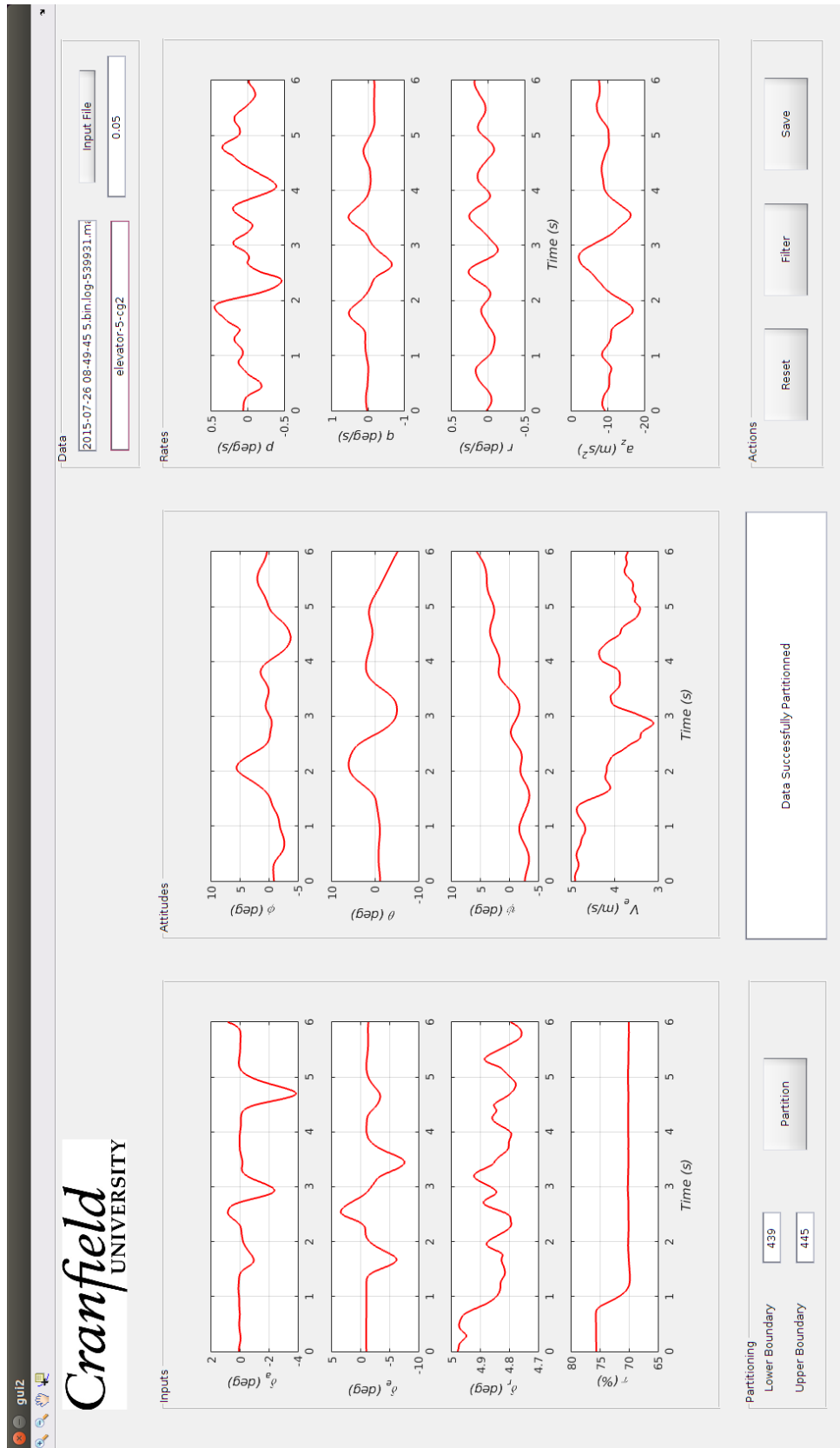


FIGURE B.1: Data Analysis Graphic User Interface.

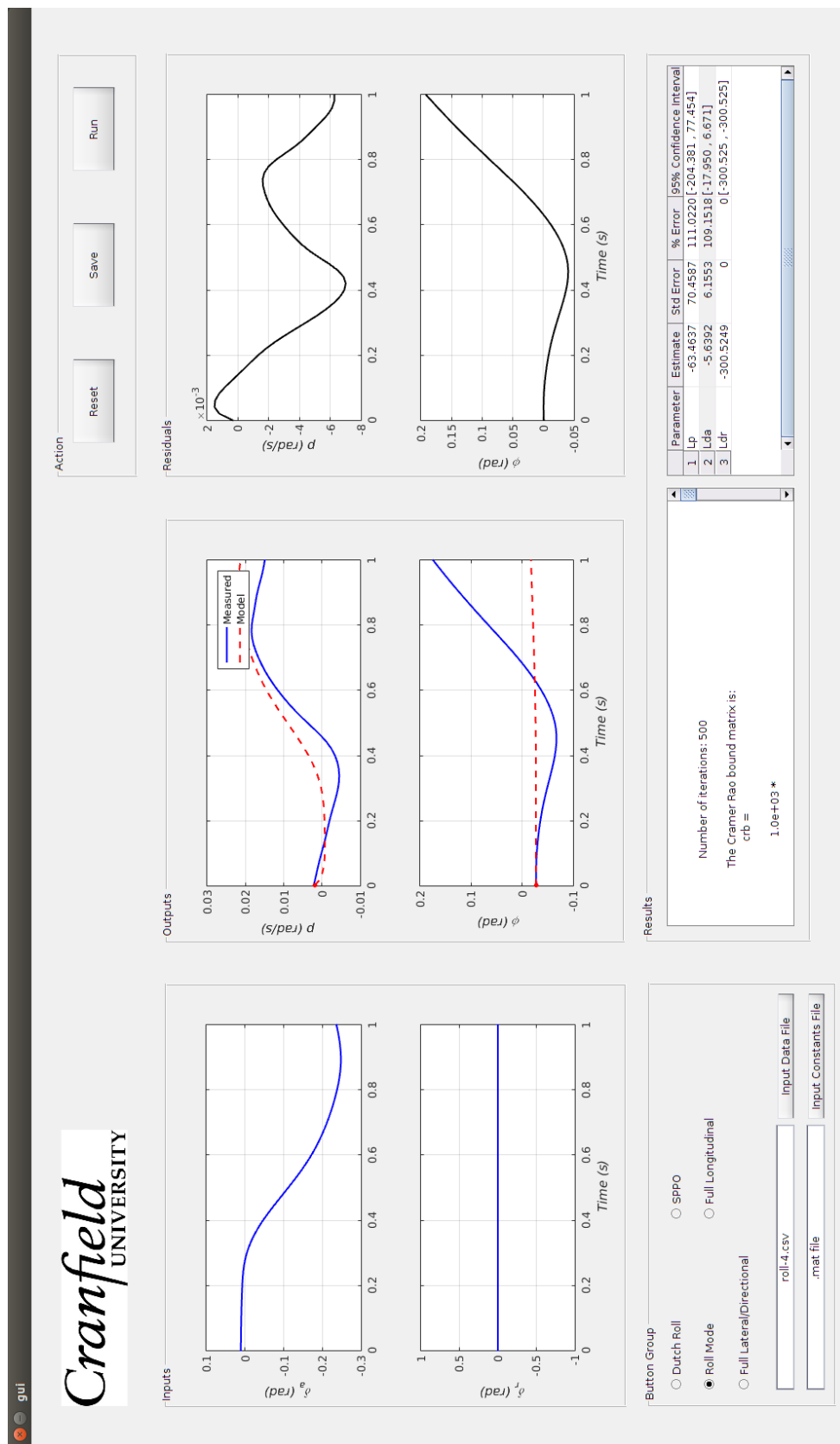


FIGURE B.2: MLE Parameter Estimation Graphic User Interface.

Appendix C

System Identification Results

	cg_0	cg_1	cg_2	cg_3
CG Position (% of MAC)	11.70	17.19	24.35	25.46

TABLE C.1: Centre of Gravity Positions.

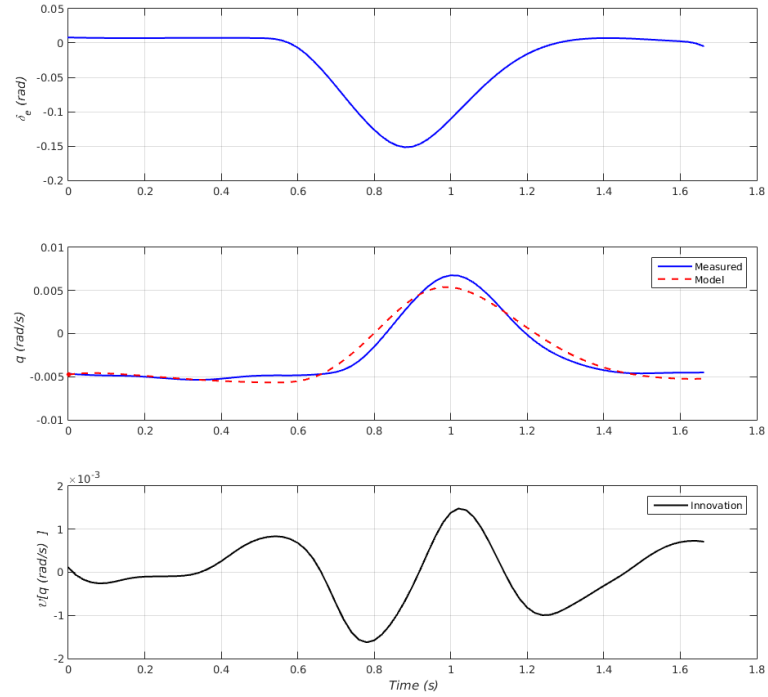
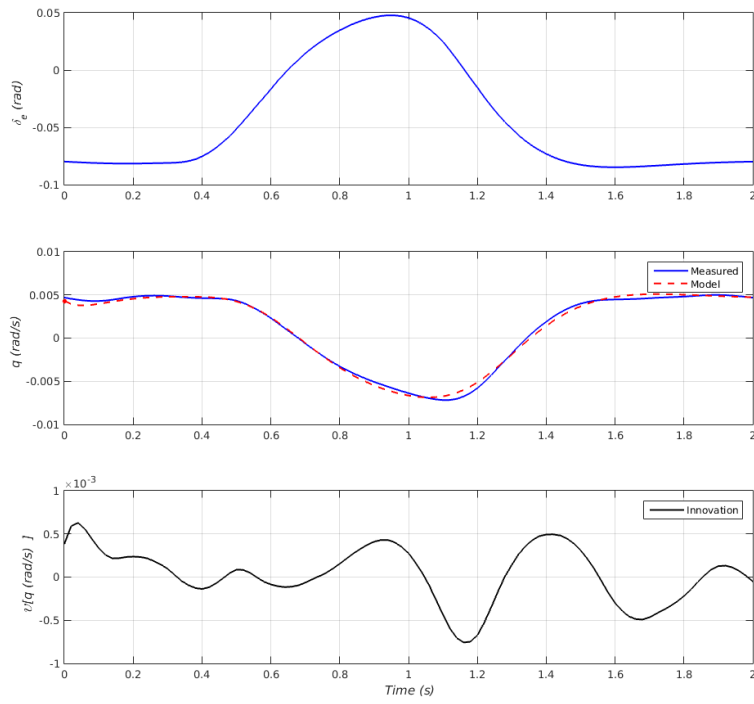
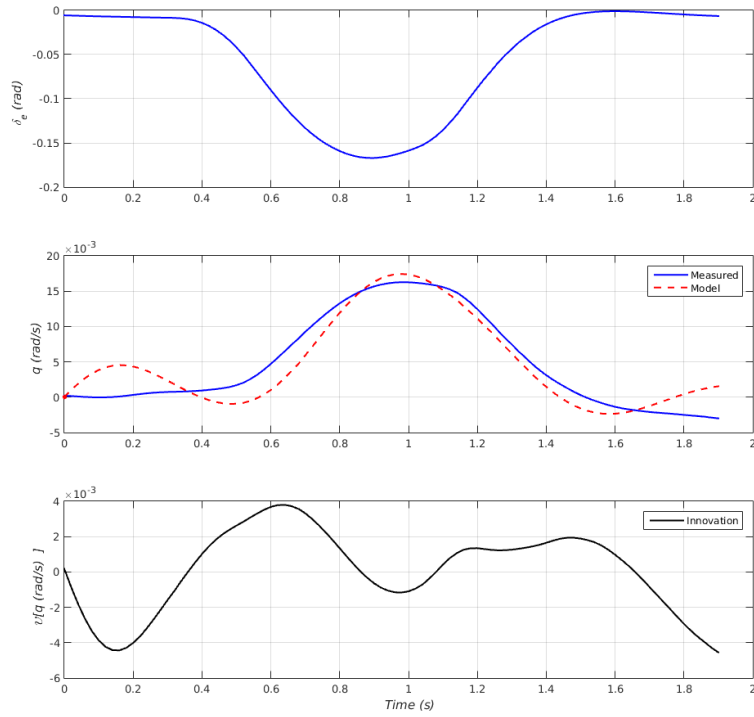
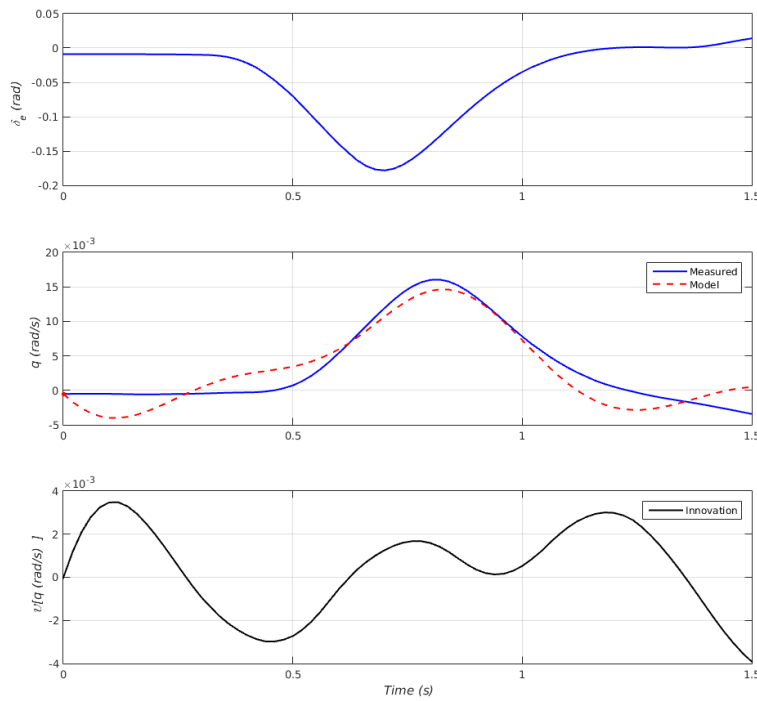
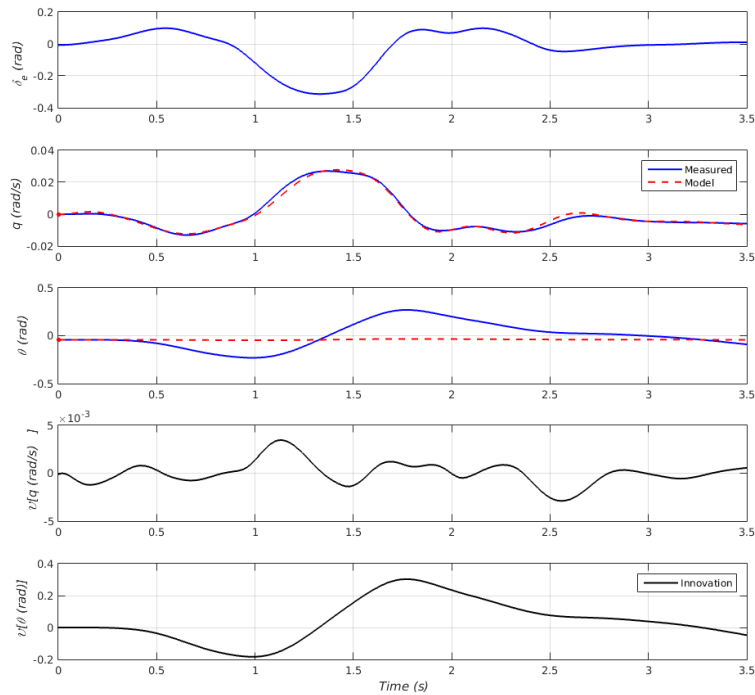
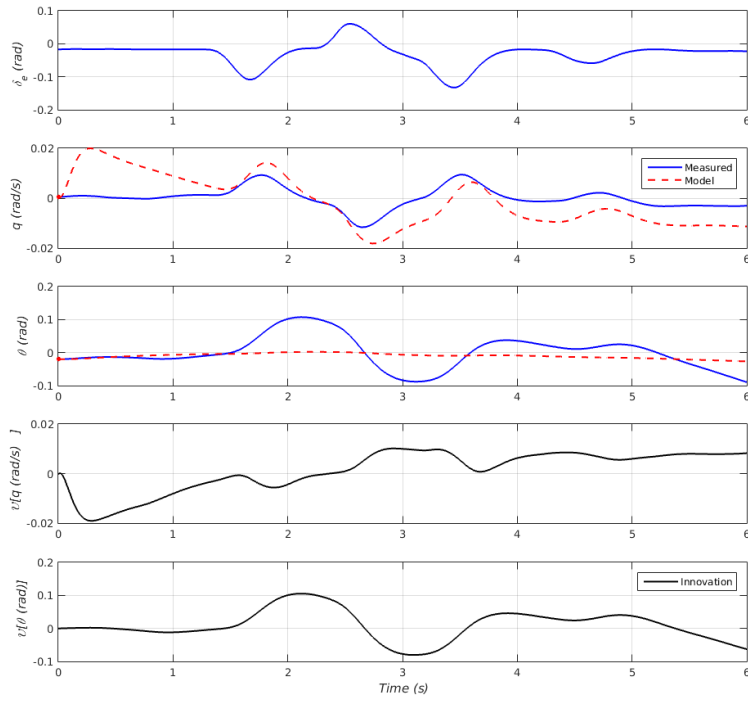
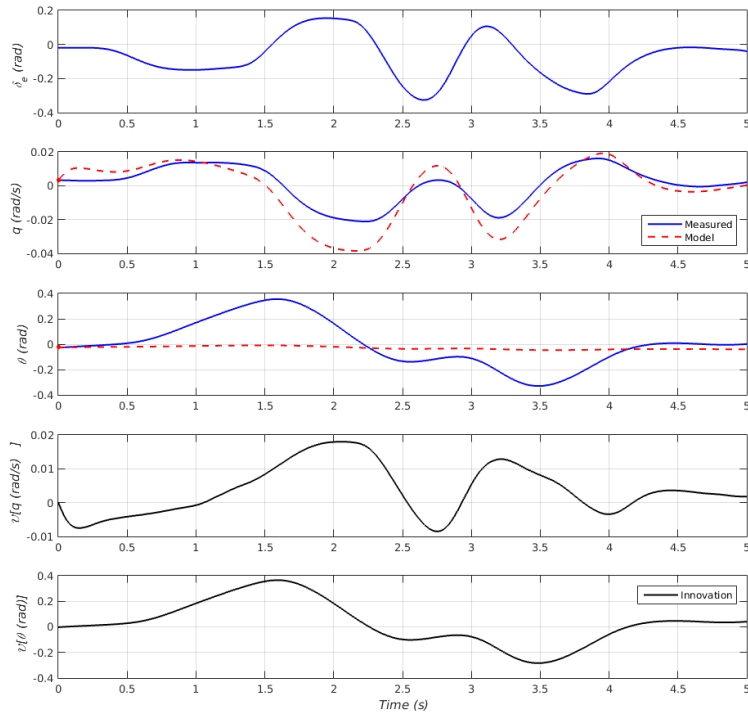
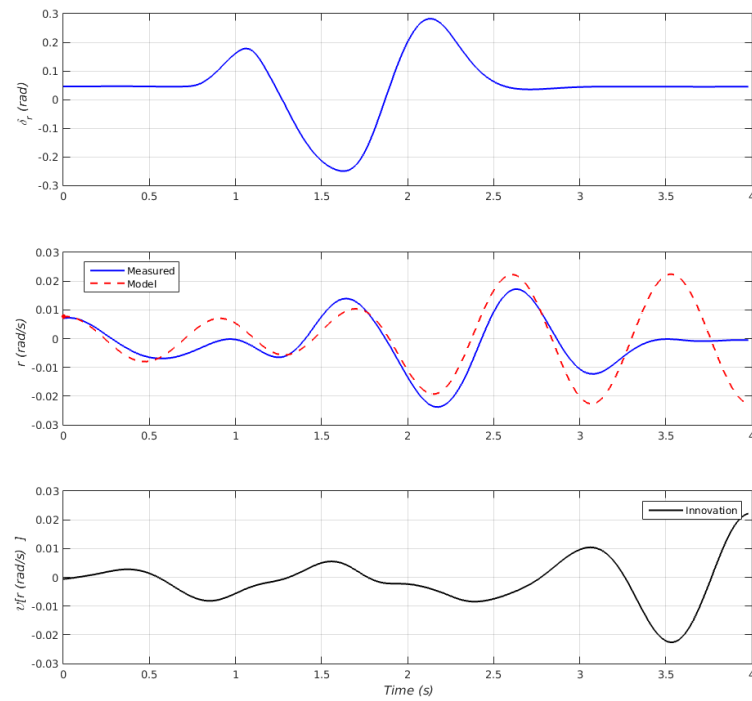
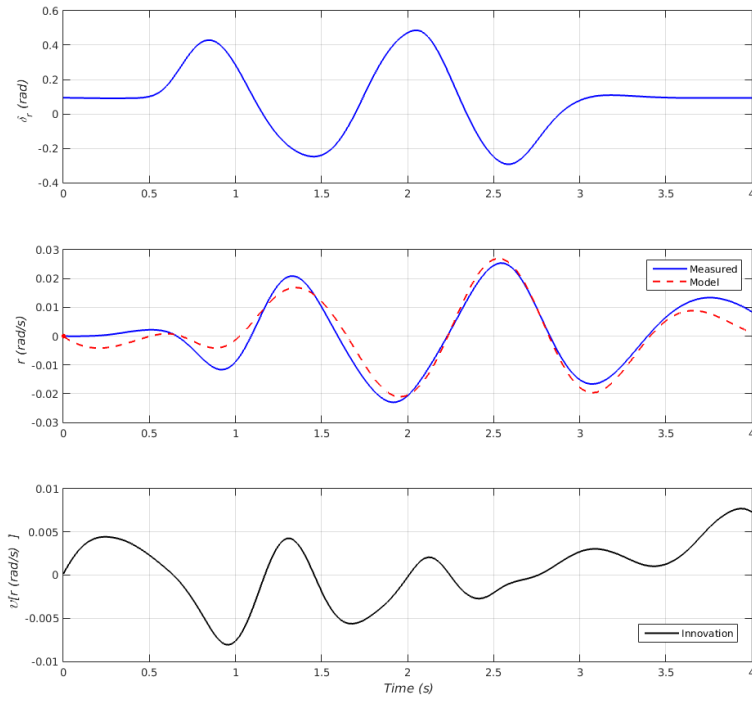


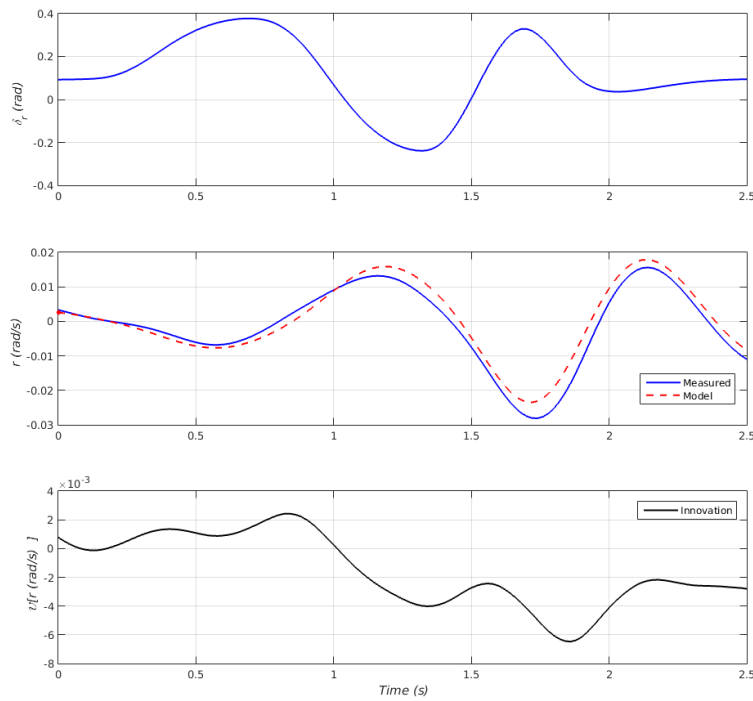
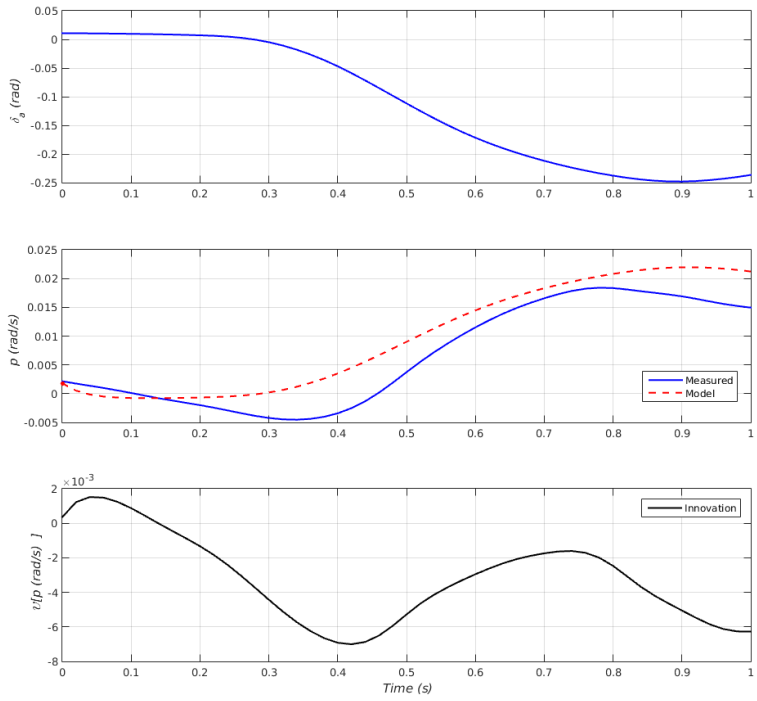
FIGURE C.1: SPPO - CG = cg_2 ; EAS = 5m/s

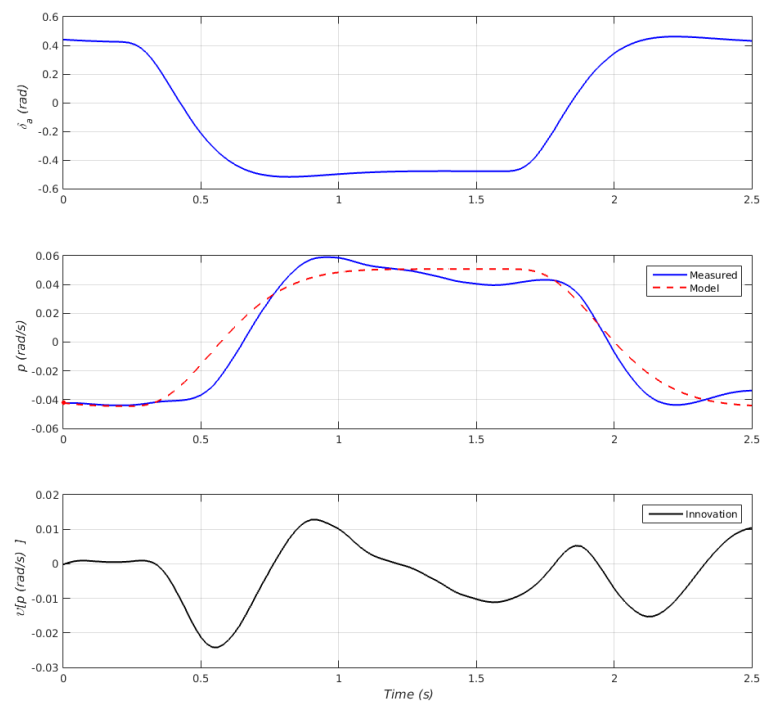
FIGURE C.2: SPPO - CG = $c g_0$; EAS = 4m/sFIGURE C.3: SPPO - CG = $c g_1$; EAS = 4m/s

FIGURE C.4: SPPO - CG = $c g_1$; EAS = 4m/sFIGURE C.5: Full Longitudinal - CG = $c g_1$; EAS = 4m/s

FIGURE C.6: Full Longitudinal - CG = $c g_0$; EAS = 5m/sFIGURE C.7: Full Longitudinal - CG = $c g_0$; EAS = 6m/s

FIGURE C.8: Dutch Roll - CG = cg_3 ; EAS = 14m/sFIGURE C.9: Dutch Roll - CG = cg_0 ; EAS = 5m/s

FIGURE C.10: Dutch Roll - CG = $c g_0$; EAS = 4m/sFIGURE C.11: Roll Mode - CG = $c g_0$; EAS = 4m/s

FIGURE C.12: Roll Mode - CG = cg_3 ; EAS = 18m/s

Bibliography

- [1] Intel website. Intel Edison. Company Communication, March 2015. URL <http://www.intel.com/content/www/us/en/do-it-yourself/edison.html>.
- [2] 3DR website. 3DR Pixhawk. Company Communication, March 2015. URL https://store.3drobotics.com/products/3dr-pixhawk?taxon_id=42.
- [3] XBee website. XBeeTM/XBee-PROTM OEM RF Modules User Manual, Product Manual v1.xAx - 802.15.4 Protocol, For OEM RF Module Part Numbers: XB24-...-001, XBP24-...-001. Product Manual, March 2015.
- [4] Wong D.R., Q. Ou, M. Sinclair, Y. J. Li, X. Q. Chen, and A. Marburg. Unmanned Aerial Vehicle Flight Model Validation Using On Board Sensing and Instrumentation. Technical report, Department of Mechanical Engineering University of Canterbury, 2008.
- [5] P. Thomas. *Tools and Techniques for the Low Cost Flight Testing of Unmanned Aerial Vehicles*. PhD thesis, Cranfield University, 2010.
- [6] C. L. Bottasso, D. Leonello, A. Maffezzoli, and F. Riccardi. A procedure for the identification of the inertial properties of small size uavs. In *48th AIAA Aerospace Sciences Meeting Including the New Horizons Forum and Aerospace Exposition*, Milan, Italy, 2009. XX AIDAA Congress.
- [7] M. Cook. *Flight Dynamics Principles*. Elsevier Aerospace Engineering Series, 2007.
- [8] A. Cooke. Air Vehicle Modelling ad Simulation. Lecture Notes, February 2015.
- [9] Q. Mauviel. Development and Validation of a Miniature Air Vehicle Model. Master's thesis, Cranfield University, August 2012.

- [10] Sparkfun website. Intel Edison IMU. Company Communication, March 2015.
URL <http://www.sparkfun.com/products/13033>.
- [11] InvenSense website. MPU 9150 IMU. Company Communication, March 2015.
URL <http://www.invensense.com/mems/gyro/mpu9150.html>.
- [12] 3DR website. Pixhawk Airspeed Sensor Kit. Company Communication, March 2015. URL <http://store.3drobotics.com/products=pixhawk-airspeed-sensor-kit>.
- [13] T9 HobbuSport website. N2 Industries Airspeed Sensor Kit. Company Communication, March 2015. URL <http://www.t9hobbysport.com/n2-industries-airspeed-frsky-smart-port-sensor>.
- [14] X.Q. Chen, D. R. Wong Q. Ou, Y. J. Li, M. Sinclair, and A. Marburg. *Flight Dynamics Modelling and Experimental Validation for Unmanned Aerial Vehicles, Mobile Robots - State of the Art in Land, Sea, Air, and Collaborative Missions*. XiaoQiChen (Ed.), Canterbury, New Zealand, 2009.
- [15] J.R. Raol, G. Girija, and J. Singh. *Modelling and Parameter Estimation of Dynamic Systems*. IET, 2004.
- [16] T. M. Kier. Comparison of Unsteady Aerodynamic Modelling Methodologies with respect to Flight Loads Analysis. *Collection of Technical Papers - AIAA Atmospheric Flight Mechanics Conference*, 1:616–629, 2005.
- [17] J. D. Anderson. *Fundamentals of Aerodynamics*. McGraw-Hill, 2007.
- [18] S. Hedman. Vortex Lattice Method for Calculation of Quasi Steady State Loadings on Thin Elastic Wings. Technical Report 105, Aeronautical Research Institute of Sweden, October 1965.
- [19] Halder A., Agarwal V., R. Garhwal, and M. Sinha. Determination of Inertial Characteristics of a High Wing Unmanned Air Vehicle. *Institution of Engineers (India) Journal - Aerospace*, 89:3 – 8, 2008.
- [20] Zadeh L. A. From Circuit Theory to System Theory. *Proceedings of the IRE*, 50:856 – 865, 1962.
- [21] V. Klein and A. Morelli. *Aircraft System Identification*. AIAA Education Series, 2006.

- [22] H. Guimeno. Flight Data Acquisition System and Parameters Estimation for a Small UAV. Master's thesis, Cranfield University, August 2012.
- [23] A. J. Steer. An analysis of the Flight Dynamics of a Second Generation SST Aircraft. Technical report, COA Report, October 1999.
- [24] O. D. G. Castillo and E. H. Londner. UAV Flight Testing with an Airborne Sonic anemometer IMU and GPS. In *28th AIAA Applied Aerodynamics Conference*, Chicago, Illinois, 2010. AIAA.
- [25] Bianchi G and R. Sorrentino. *Electric Filter Simulation and Design*. McGraw-Hill Professional, 2007.
- [26] E. A. Morelli. System Identification Programs for Aircraft (SIDPAC). In *AIAA Atmospheric Flight Mechanics Conference*, Monterey, CA, August 2002. AIAA.